國 立 交 通 大 學

生物科技研究所
碩士論文

利用飽和定點突變方法研究酵母菌氧化鯊烯環化酵素內的假設活性區胺基酸對於催化環化/重組反應的影響

Site-Saturated Mutagenesis Approach to Investigate the Putative Active-Site Residues from *Saccharomyces cerevisiae* Oxidosqualene-Lanosterol Cyclase that Influences the Cyclization/Rearrangement Reactions

研 究 生：李文暄

指導教授：吳東昆 博士

中華民國 九十六年七月

Site-Saturated Mutagenesis Approach to Investigate the Putative Active-Site Residues from *Saccharomyces cerevisiae* Oxidosqualene-Lanosterol Cyclase that Influences the Cyclization/Rearrangement Reactions

研究生：李文暄　　Student: Wen-Hsuan Li

指導教授：吳東昆 博士　　Advisor: Dr. Tung-Kung Wu

國 立 交 通 大 學

生物科技研究所

碩士論文

A Thesis

Submitted to Department of Biological Science and Technology

College of Science

National Chiao Tung University

in partial Fulfillment of the Requirements

for the Degree of

Master

in

Biological Science and Technology

July, 2007

Hsinchu, Taiwan, Republic of China

中華民國九十六年七月

利用飽和定點突變方法研究酵母菌氧化鯊烯環化酵素內的假設活性區胺基酸對於催化環化/重組反應的影響

學生：李文暄　　指導教授：吳東昆　博士

國立交通大學　生物科技研究所碩士班

摘要

在酵母菌以及哺乳類動物中，氧化鯊烯環化酵素(OSC)催化(3*S*)-2,3-氧化鯊烯((3*S*)-2,3-oxidosqulaene)進行環化/重組反應而產生羊毛硬脂醇。這個複雜的環化/重組反應的機制包含了氧化鯊烯上的環氧基(epoxide)被質子化而起始環化反應以及一連串的氫化基、甲基的重組和最後高度專一性的去質子化步驟。我們利用飽和定點突變的方法來探討酵母菌中氧化鯊烯環化酵素的兩個胺基酸, Tyr99 以及 Trp443 的功能以及在酵素催化反應的過程中所扮演的角色。在 OSC^{Tyr99} 的功能性分析中,當其殘基被突變成某些帶極性側鏈的胺基酸時可以有功能性補充的作用而支持其氧化鯊烯環化酵素(OSC)被突變的酵母菌存活下來，並且形成產物的多樣性。經由產物的分析我們分離出了之前未被發表過兩個新的三環碳陽離子中間產物，分別是(13α*H*)-isomalabarica-14*Z*,17*E*,21-trien-3β-ol 以及 (13α*H*)-isomalabarica-14*E*,17*E*,21-trien-3β-ol。 經由實驗結果我們推測 Tyr99 在環化機制中可能是穩定椅形-船型(chair-boat)結構所形成的 6-6-5 三環馬可尼可夫碳-14 陽離子(6-6-5 tricyclic Markovnikov C-14 cation)以及控制接下來碳-15 脫氫反應的立體化學(stereochemical)。在分子模擬的分析中，Tyr99 相對於碳-陽離子的空間位置不同於 His234 和 Phe445，進而影響了酵素與其碳陽離子中間體之間的反應位向和靜電作用因此導致反應最後選擇不同位置進行去質子化的結果。而量子力學的計算結果顯示出酵素催化反應裡所產生的種種效應都對在三環馬可尼可夫碳陽離子的去質子化步驟中立體化學特性有重大影響。另一方面，關於 OSC^{Trp443} 的飽和定點突變分析中，其中兩個突變，Trp443Ala 以及 Trp443Lys 同時產生了兩個單環的產物 achilleol A 和

camelliol C。而 achilleol A 和 camelliol C 這兩個單環產物証明了其生成是由於不完整的環化反應被迫終止在碳-10 而形成碳陽離子中間體，再經由不同位置的去質子化反應所造成。綜合產物比例以及分子模擬的分析，推測 OSC^{Trp443} 的功能可能是在於影響受質反反應前的摺疊構形以及穩定環氧基被質子化隨即 A 環形的中所產生的碳陽離子。最後，我們的實驗結果可以說明藉由飽和定點突變方法以及產物分離/分析的實驗可以更深入了解氧化鯊烯環化酵素的結構、功能以及機制之間的關係。

Site-Saturated Mutagenesis Approach to Investigate the Putative Active-Site Residues from *Saccharomyces cerevisiae* Oxidosqualene-Lanosterol Cyclase that Influences the Cyclization/Rearrangement Reactions

Student: Wen-Hsuan Li Advisor: Dr. Tung-Kung Wu

Institute of Biological Science and Technology

Naitonal Chiao Tung Unversity

Abstract

Oxidosqualene-lanosterol cyclase (ERG7) catalyzes the cyclization/rearrangement of (3*S*)-2,3-oxidosqualene to lanosterol in yeast and mammals. The complex cyclization/rearrangement reaction mechanism consists of initial epoxide protonation, four successive cationic cyclizations, four consecutive hydride or methyl group rearrangements, and a final highly specific deprotonation step. Site-saturated mutagenesis experiments were carried out on the Tyr99 and Trp443 positions of OSC in *Saccharomyces cerevisiae* to investigate their putative functional role in the catalytic cyclization. For functional analysis of OSC^{Tyr99}, some polar side-chain group substitutions genetically complemented yeast viability and produced spatially related product diversity. Product isolation and characterization revealed two novel tricyclic intermediates, (13α*H*)-isomalabarica-14*Z*,17*E*,21-trien-3β-ol and (13α*H*)-isomalabarica-14*E*,17*E*,21-trien-3β-ol, for the first time. These results suggested that the functional role of the Tyr99 in affecting both the chair-boat 6-6-5 tricyclic Markonikov C-14 cation stabilization and the stereochemistry of the protons at the C-15 position for subsequent deprotonation reaction. Homology modeling analysis, results revealed that Tyr99 residue is located spatially differently from that of His234 and Phe445 to the common C-14 cation which

affects the orientation or electrostatic interaction between the enzyme and its cationic intermediate, and results in abstracting of a proton from a different position or orientation. The quantum mechanical calculation results suggested that the energetics of stereochemical control during the tricyclic Markovnikov cation deprotonation step could be affected by the inclusion of these enzymatic effects. The site-saturated mutagenesis applying on the OSC^{Trp443} revealed that two truncated monocyclic intermediates, achilleol A and camelliol C, were concomitantly produced from the Trp443Ala and Trp443Lys mutants. The formation of achilleol A and camelliol C were identified as evidence for premature truncation of C-10 cationic intermediates following the proton abstraction from different position. The product profile coupling with homology modeling analysis showed that the functional role of Trp443 of OSC might influence the substrate prefolding and stabilizing the epoxide protonation and A-ring formation. Finally, these results further exemplify the potential of site-saturated mutagenesis coupled with product isolation/characterization in elucidating the structure-function-mechanism relationships of the oxidosqualene cyclase.

謝　誌

忙碌而充實的、充滿酸甜苦辣的兩年研究生活，在完成這份論文後即將劃下句點。在這段時間裡，所有我遇到的人、事、物，都帶來很大的衝擊，讓我成長、也讓我改變了許多。這短短的兩年在我人生中扮演著關鍵性的時期，這段日子也是我受到最多幫助的時候。要感謝的人太多了，可是我還是要一一列出來:

感謝吳東昆老師: 謝謝您在兩年前給我機會,願意讓沒有生科背景的我加入這間正在成長茁壯的實驗室。在這裡我學習獨立思考的能力，養成積極的處事態度，十分感謝您在這兩年研究上的指導。從老師身上我也學到許多做人做事的道理，對我的人生有很大的啟發。

感謝袁俊傑老師、林敬堯老師、刁維光老師: 謝謝您們在百忙之中抽空審閱、修改我的論文、親臨指導我的口試,並且不吝惜的給予許多寶貴的建議,使我收穫良多。

感謝清華大學貴儀中心的彭菊蘭小姐在 NMR 光譜分析上的幫忙。

感謝程翔學長: 謝謝你在這段時間裡所有的幫助，沒有你，我的實驗會很不順利，我的論文也不會完整。謝謝你像大哥哥一樣關心我的實驗、我的生活。你真的是一位不可多得的好學長。

感謝媛婷學姊: 在我剛進來對所有都很陌生的時候，謝謝妳總是很有耐心、不厭其煩的教導我、給我鼓勵，也感謝那段有妳陪伴熬夜通銀染的日子。

感謝已經畢業的美婷學姊在我初入實驗室時，教我很多實驗的技巧，也分享許多她的碩班的心得以及在最後口試前的加油打氣。

感謝實驗室的博班學長們，晉豪學長:謝謝你在 GC-MS 的幫助，還有幫我解決很多電腦上的問題。文鴻、晉源、裕國學長:謝謝你們在這段日子裡像大哥哥般的照顧，讓我覺得在這間實驗室的女生都很幸福，跟你們一起打球、跑步也很開心。

Thanks to my lovely friend, Mili: you are so kind and cute. Thanks for your concern, listening, and being my English teacher. I'll always miss you.

感謝一起奮鬥的同窗好友，OSC 組的好搭檔，晧宇:你懂得很多，跟你一起討論實驗很開心，也謝謝你在實驗上的幫忙; 大景、怡親:跟你們一起熬夜做實驗、吃宵夜、寫論文的日子很開心，謝謝你們常常鼓勵我、還有一起搞笑。

感謝即將升上碩二的學弟妹: 文祥、采婷、小高，謝謝你們在過去一年裡所有的幫助。也謝謝 2007 年剛加入 Wu lab 的夥伴: 聖慈、禕婷、天昶、亦諄在口試其間的幫忙。

感謝我最親愛的家人:老爸、老媽、老妹修惠，謝謝你們的支持，讓我可以在這個遠離家鄉、高消費水準的新竹，無後顧之憂的完成我的學業，有你們的我真的很幸福。也感謝時常關心我的摯友: 俊涵、嘉珮、姿穎、康康、莉芬姊、君如。

感謝一路走來始終如一的繹翔：很多時候、很多事，如果沒有你真的不知該怎麼度過，你給了我好多也教了我好多，謝謝你。

感謝上天賜給我的這一切，感謝所有曾經幫助過我的人，希望將來我可以有機會回報。

Table of Contents

List of Figures

List of Tables

Chapter 1: Introduction

1.1 Triterpenoids and sterol biosynthetic pathways

Terpenoids are ubiquitous in all forms of life. This family of natural products encompasses an enormous variety of chemical structures and equally diverse array of biological functions. Triterpenoids usually have a tetracyclic or pentacyclic core structure designated as A, B, C, D (and E) rings, with the $C_{30}H_{50}O$ formula (1) (Fig. 1.1). However, monocyclic, bicyclic, tricyclic, and hexacyclic triterpenoids have also been isolated from various sources.[1-3] Although sterols and steroids are subsets of triterpenoids, having the same general ring structure and biosynthetic origin, different transformations such as alkylations or methylations are occurred in either the ring structure or sidechain. Sterols are characterized by the presence of an alcohol moiety at C-3 position and are usually found in membranes. Oxidosqualene (2) is converted to the different triterpene skeletons in various organisms. Lanosterol (3) is the first cyclized intermediate product in the biosynthesis of cholesterol (4) in animals and ergosterol (5) in fungi. The lanosterol equivalent in plants is cycloartenol (6). The direct cyclization of squalene (7) via squalene-hopene cyclase leads to the production of bacterial sterol surrogates such as diplopterol (8). [1]

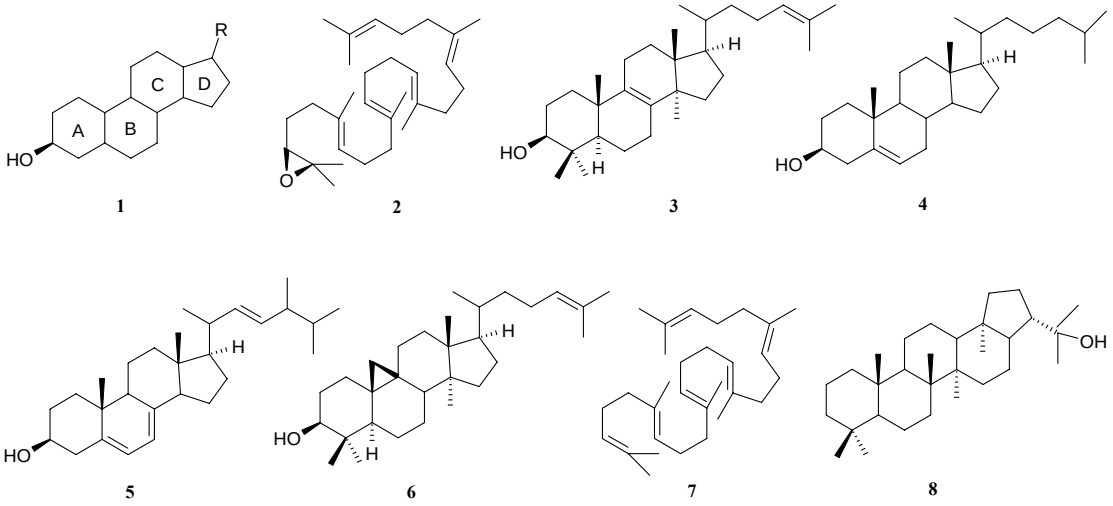

Figure1.1 Examples of triterpenoid structures

Sterols are vital constituents of cell membranes. Cholesterol is the plasma membrane sterol in animals and also serves as the metabolic precursor of steroid including estrogens and androgens. In plants, campesterol, stigmasterol, and β–sitosterol are the most common sterol components of membranes. In bacteria, sterols are usually absent, but some bacteria and protozoan produce pentacyclic triterpenes such as hopene and 3-deoxytriterpenoids which are regarded as sterol surrogates in these organisms.[1] As each of these compounds serves an indispensable role, it is evident why a complete understanding of the enzymes directing their biosynthesis is necessary.

In general, the sterol biosynthetic pathway is from acetyl-CoA initially converted to isoprene units, which is subsequently condensed to form a linear molecule with 30 carbons, squalene, that cyclized to form hopene by squalene-hopene cyclase in bacteria. Squalene epoxidase is responsible for the epoxidation of squalene to 2,3-oxidosqualene which is further converted to lanosterol, the first cyclized precursor leading to cholesterol and ergosterol in animals or fungi via oxidosqualene cyclase, the product of the *ERG7* gene (Fig. 1.2).

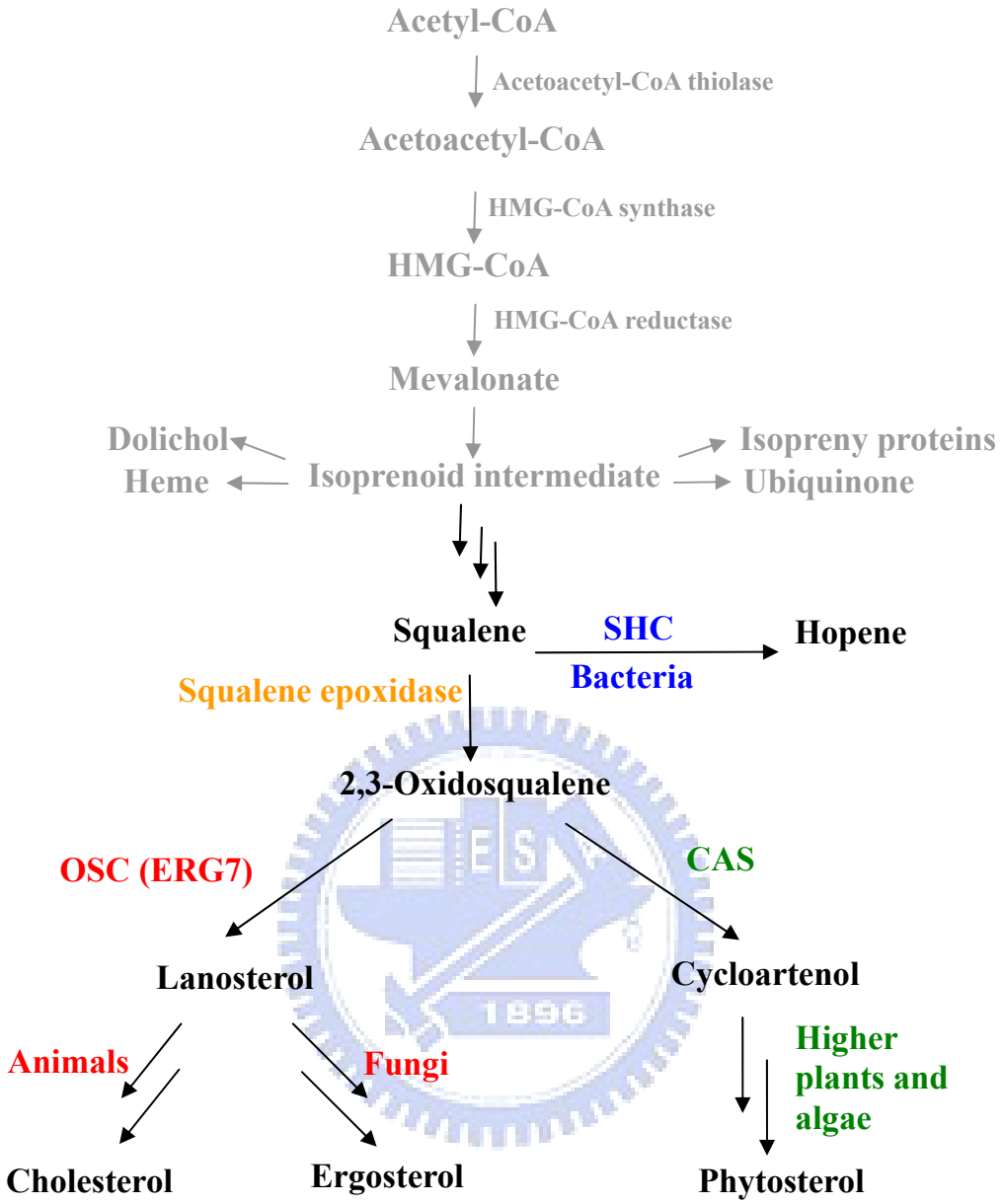

Figure 1.2 Outline of sterol biosynthetic pathway.

One of the most relevant triterpene derivatives is cholesterol. Current treatments for the hypercholesterolemia was targeting at the step catalyzed by HMG-CoA reductase, which is the rate-limiting step in the early part of the pathway. However, this reaction is not the first committed step in the biosynthesis of cholesterol. Mammals require HMG-CoA reductase for the biosynthesis of isoprenoid intermediates, and its inhibition can not only effect the cholesterol pathway, but also a variety of other pathways including

protein prenylation as well as ubiquinone and dolichol biosynthesis.[4,5] Among the downstream of cholesterol biosynthesis, cyclization of lanosterol for example via oxidosqualene cyclase toward the hypercholesterolemia, might provide insight of the development of a safer, more effective treatment.

1.2 The overview of oxidosqualene cyclase family

1.2.1 Products specificity

Oxidosqualene cyclases (OSCs) are a unique family of eukaryotic enzymes that catalyze the cyclization of acyclic (*3S*)-2,3-oxidosqualene into over 100 cyclic triterpene alcohols ($C_{30}H_{50}O$) and triterpene diols ($C_{30}H_{52}O_2$) identified in nature.[3] The cyclization of oxidosqualene and squalene to polycyclic triterpenoids has fascinated and captivated scientists for more than fifty years.

These polyolefin are stereoselectively cyclized and skeletally rearranged in a single enzyme-catalyzed reaction to yield tetracyclic and pentacyclic triterpenoids including hopene (6-6-6-6-5 pentacycles) in bacterial, lanosterol (6-6-6-5 tetracycles) in animals and fungi, cycloartenol (6-6-6-5 tetracycles), lupeol (6-6-6-6-5 pentacycles) and β–amyrin (6-6-6-6-6 pentacycles) in higher plants (Fig. 1.3).[3]

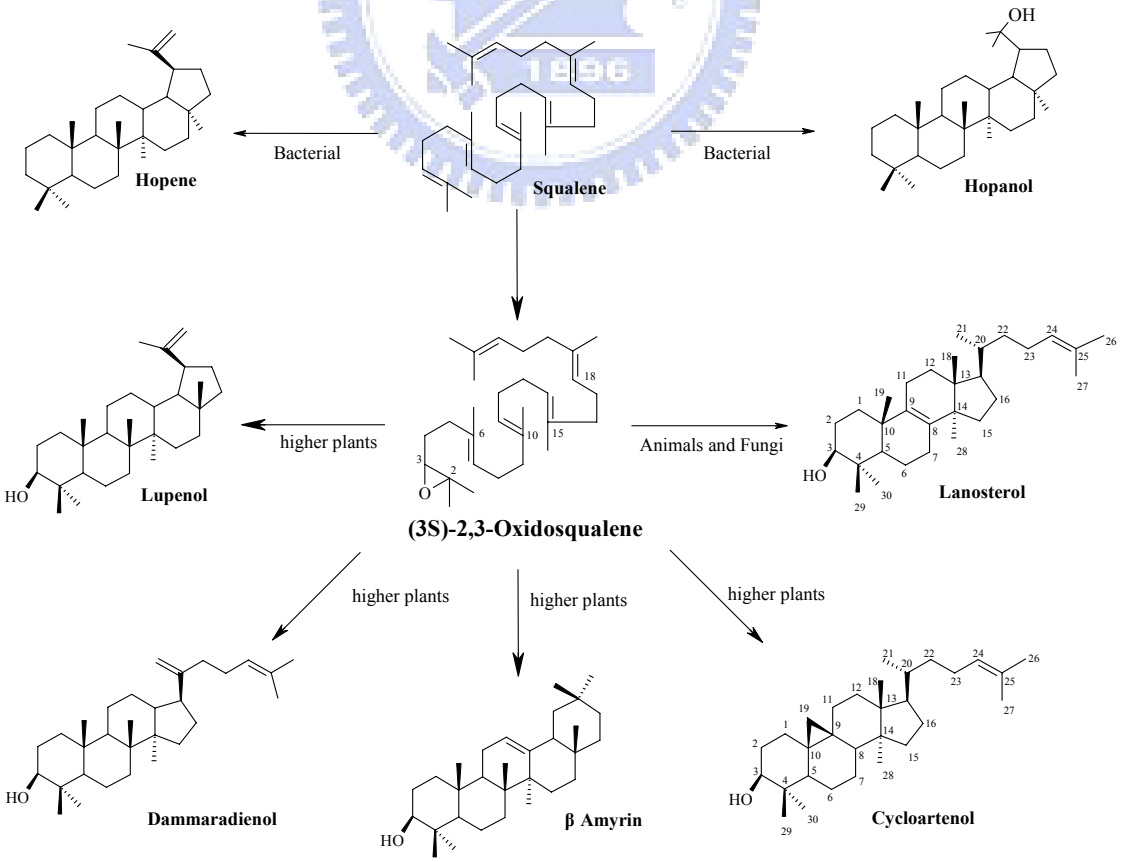

Figure 1.3 The product specificity of the cyclase is species-dependent

1.2.2 Substrate conformation and cyclization

The cyclization of oxidosqualene reaction is initiated by epoxide protonation, followed by cation-olefin mediated cyclization, hydride/methyl group rearrangement, and terminated either by deprotonation or water addition.[1] These enzymes catalyze what are possibly the most complex multiple-steps chemical transformations found in nature. As many as sixteen bonds are broken and sixteen new bonds formed in the course of cyclization.[6] In addition, these enzymes display remarkable regiospecificity and stereoselectivity during the reaction. In some case, several different stereocenters are established in the product molecule.[6] Furthermore, the chemical transformations catalyzed by oxidosqualene cyclase proceed through highly reactive cationic intermediates. The short-lived cation intermediates are protected and stabilized within the active site cavity of the oxidosqualene cyclases. Despite being surrounded by numerous nucleophiles, either form the amino acid sidechains or from the protein backbone, these cations are not quenched prematurely.[7]

The different substrate prefolded conformation results in different intermediate cations formation. The species-dependent cyclization products can be grouped into two types, protosterol and dammarenyl cation. The conformation of the two major intermediate cations is different at the formation of B-ring. In protosterol cation pathway, a six-membered B-ring boat form was produced, whereas the chair form six-membered B-ring was found in the dammarenyl cation pathway (Fig. 1.4).[1]

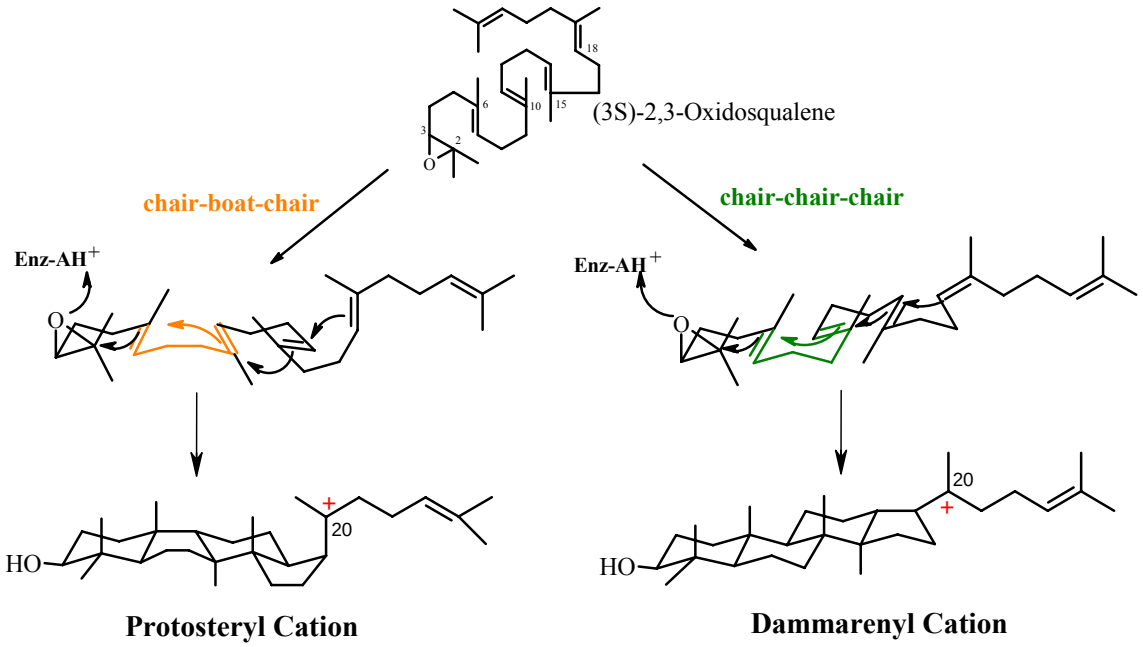

Figure1.4 Cyclization of oxidosqualene to the protosteryl and dammarenyl cations

The protosteryl cation contains A/B-*trans*, 9/10-*syn*, B/C-*trans* ring junction stereochemistry, requiring the substrate to adopt the energically less favorable chair-boat-chair conformation.[8-12] It is accepted that "chair-boat-chair" conformation of the substrate, oxidosqualene, is triggered to give a protosterol C-20 cation, following a series of 1,2-methyl and hydride shifts and final a different position proton elimination to yield either lanosterol or cycloartenol. On the other hand, the "all-chair" dammarenyl cation conformation undergoes similar rearrangement or ring expansion and final elimination to give dammaradienol, lepenol, α-amyrin or β-amyrin via different cation intermediates (Fig. 1.5).[6]

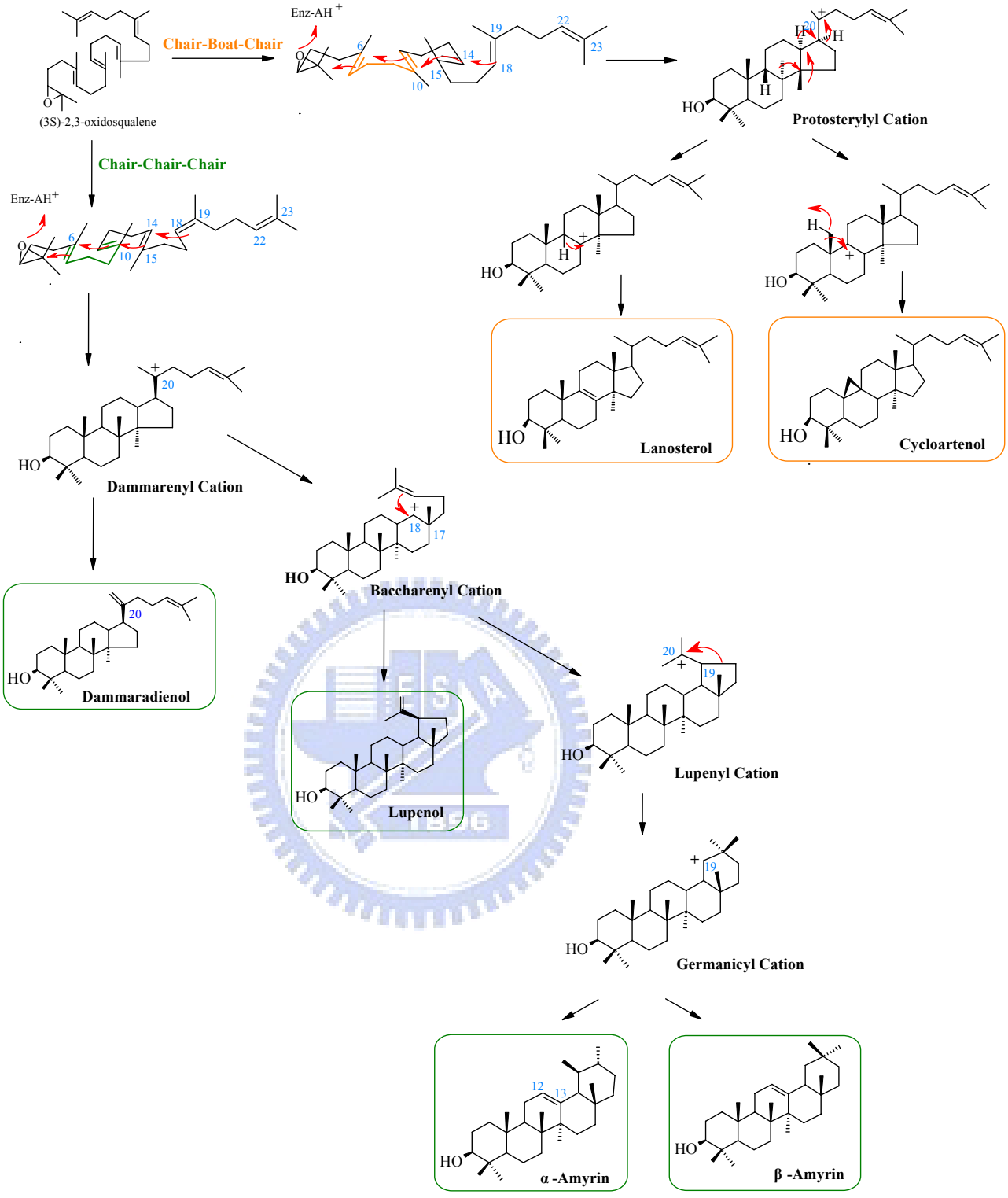

Figure1.5 Mechanism of cyclization of 2,3-oxidosqualene to complexly cyclic products via different cation intermediates.

1.2.3 The historic hypothetical models based on the OSC cyclization mechanism

Insight into the cyclization of lanosterol came when Rittenberg and Bloch used previously published isotopic data, along with new data of their own to show how the carbons of cholesterol could be derived from squalene in 1937-1942.[13-14] In 1953, Woodward and Bloch first proposed a hypothesis concerning the course of cyclization of squalene followed by rearrangement to lanosterol.[15] However, the isotopic feeding experiment showed that the oxidosqualene rather squalene was the direct precursor of lanosterol. Afterward, the mechanistic and evolutionary aspects have elicited intense chemical and biochemical interest.

Bloch and Cornforth also used the isotopic feeding experiments to obtain the shifts of 1,2-methyl and hydride during lanosterol formation.[16-17] Furthermore, Corey and van Tamelen demonstrated the more detail intermediates information during lanosterol biosynthesis in the enzyme active site via many substrate analogue compounds feeding experiments.[18-20] Further, Barton proved that OSC in eukaryote only accepted the (3*S*)- and not the (3*R*)-enantiomer of oxidosqualene as a substrate.[21]

Lots of theoretical models of the cyclization mechanism have also been proposed in the absence of the information about the enzyme itself. Ourisson proposed the essential elements for enzyme-catalyzed cyclization/rearrangement reaction. An acidic site, a basic site, and many nucleophilic cations stabilizing sites are highly conserved in the cyclases. The cyclase enzymes might be derived from a common ancestor, primitive squalene cyclase to oxidosqualene cyclase in higher organisms. This hypothesis opened an evolutionary study of these cyclase enzymes.[22-24]

In the light of substrate specificity and stereochemistry, Johnson proposed a model for the cyclization mechanism in 1987 (Fig. 1.6).[25-26] This model supposes that the acid residues on the active site provide proton for epoxide group of oxidosqualene or

double-bond of squalene to initiate the reaction and subsequently proceed the cation-olefin polycyclization. A key concept in this model, which is proposed that a number of anionic sites in the cyclase enzyme would guide the cation generation and the formation of the proper ring system.[27]

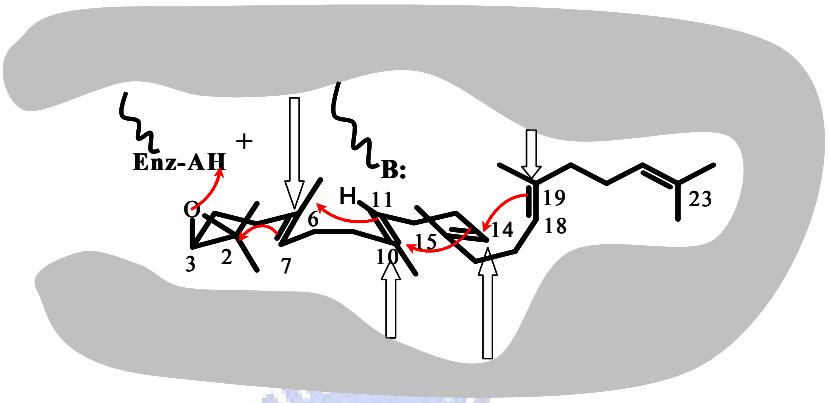

Figure 1.6 Johson model for ocidosqualene cyclization.

The unusual large amounts of tyrosines or tryptophans are highly conserved in most oxidosqualene cyclase known to date.[28] In 1992, this finding has led Griffin to propose an aromatic hypothesis for cyclase active site. In the aromatic hypothesis model, the "π-cation interaction" could be performed via the electron-rich indole of tryptophans, phenol group of tyrosine, or phenylalanine residues in the manner (Fig. 1.7). In such a model, aromatic residues play the role of the anions group just like in the Johnson *et al*. mechanism.

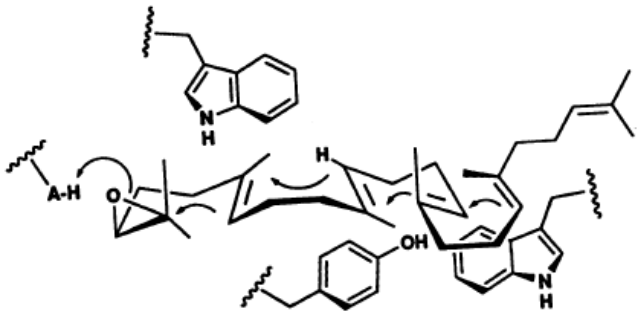

Figure 1.7 Griffin's hypothesis model for involvement of aromatic residues in cyclization of OS to protosteryl cation

1.2.4 Oxidosqualene-lanosterol cyclase (OSC)

The formation of lanosterol, the required precursor of cholesterol in vertebrates and ergosterol in fungi, is catalyzed by oxidosqualene-lanosterol cyclase (or lanosterol synthase), the protein encoded from *ERG7* gene (EC 5.4.99.7). The oxidosqualene cyclase gene was initially isolated from *C. albicans* by complementation of an *ERG7* mutation in *S. cerevisiae*.[29] This ERG7 gene contains an open reading frame encoding a 731-amino acid, 83kDa protein.

In order to understand the structure-function relationships of oxidosqualene cyclase-catalyzed reactions, both chemical and molecular biological studies have significantly contributed mechanistic insights into the oxidosqualene cyclase-catalyzed cyclization/rearrangement cascade. For example, cloning, sequencing, and site-directed mutagenesis studies of putative oxidosqualene cyclase genes have facilitated understanding of cyclase evolution and analysis of product diversity determining factors, perhaps the single most remarkable feature of cyclase enzymes.

Detailed studies with nonnatural substrates have established the overall pathways of the enzymatic reactions involving: 1) binding of the polyolefinic substrate in a pre-folded conformation, 2) initiation of the reaction by protonation of a double bond (squalene) or an epoxide (2,3-oxidosqualene), 3) ring formation, 4) skeletal rearrangement by 1,2-methyl and hydride shifts, 5) termination by deprotonation or addition of water.[30]

Crystallization and structural characterization of the membrane protein SHC from *Alicyclobacillus acidocaldarius* have provided a detailed model for determination of the substrate entrance channel and catalytically important active-site residues.[2, 31-32]

In 2004, Thoma *et al*. have succeeded in determining the long-awaited structure of human OSC in complex with the reaction product lanosterol and it provided an important additional snapshot of the triterpene polycyclization cascades (Fig. 1.8a).[33]

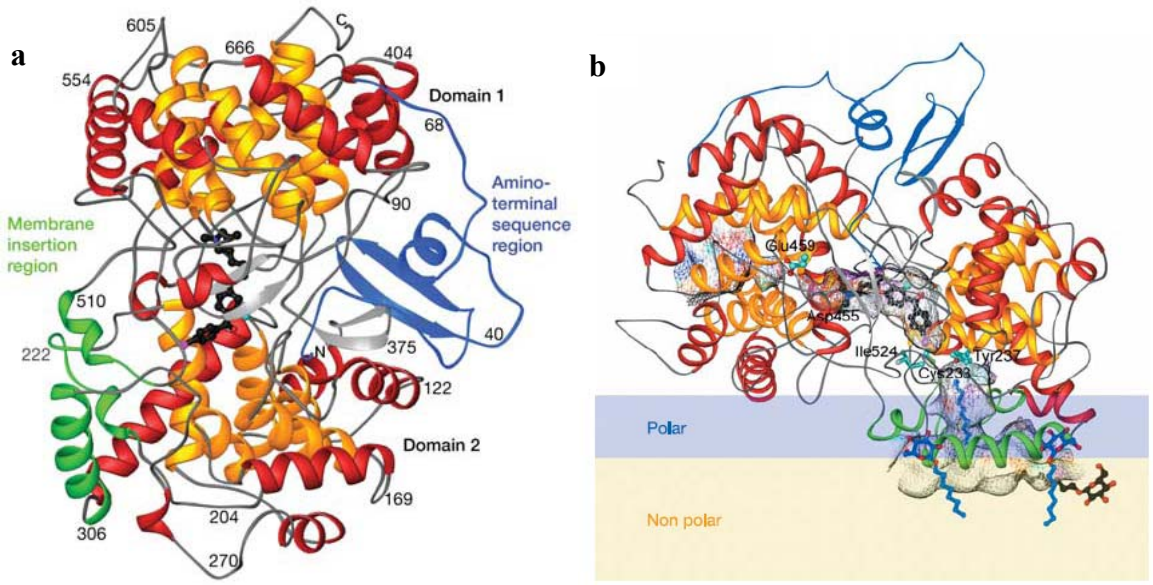

Figure 1.8 Crystal structure of human OSC (a) Ribbon diagram of human OSC. The C and N termini and several sequence positions are labeled. The inner barrel helices are colored yellow. The bound inhibitor, Ro48-8071 (black), indicates the location of the active site. (b) The orientation of OSC relative to one leaflet of the membrane, Ro 48-8071 bind in the certral active-site cavity.[33]

Base on the observation of crystal structure of monotopic membrane protein human OSC, the membrane-inserted surface consists of a plateau in 25Å diameter and a channel that leads to the active-site cavity. This channel is supposed to allow the substrate oxidosqualene to enter the hydrophobic active site but a constriction site separates it from the active-site cavity. Either the sidechain conformation change in the residues Tyr237, Cys233, and Ile524, or the strained loops rearrangement from 516-524 or 697-699 would lead the substrate passing the constricted site of the channel then enter into the enzyme active site. (Fig. 1.8b).

Cyclization mechanism:

The catalytic mechanism for the cyclization reaction of (3*S*)-2,3-oxidosqualene to lanosterol involved several steps and a series of discrete conformationally rigid, partially cyclized carbocationic intermediates. The formation of lanosterol is initiated in the pre-chair-boat-chair conformation of 2,3-oxidosqualene from an initial protonation of the epoxide moiety by Asp455 (in human OSC numbering). Protonation of this epoxide ring would trigger a cascade of ring-forming reactions to the protosterol cation formation. Skeletal rearrangement of this intermediate cation through a series of 1,2-hydride and 1,2-methyl group would shift the cation to the C-8 (lanosterol numbering) cation production, and a final deprotonation step would lead to the product lanosterol generation (Fig. 1.9).

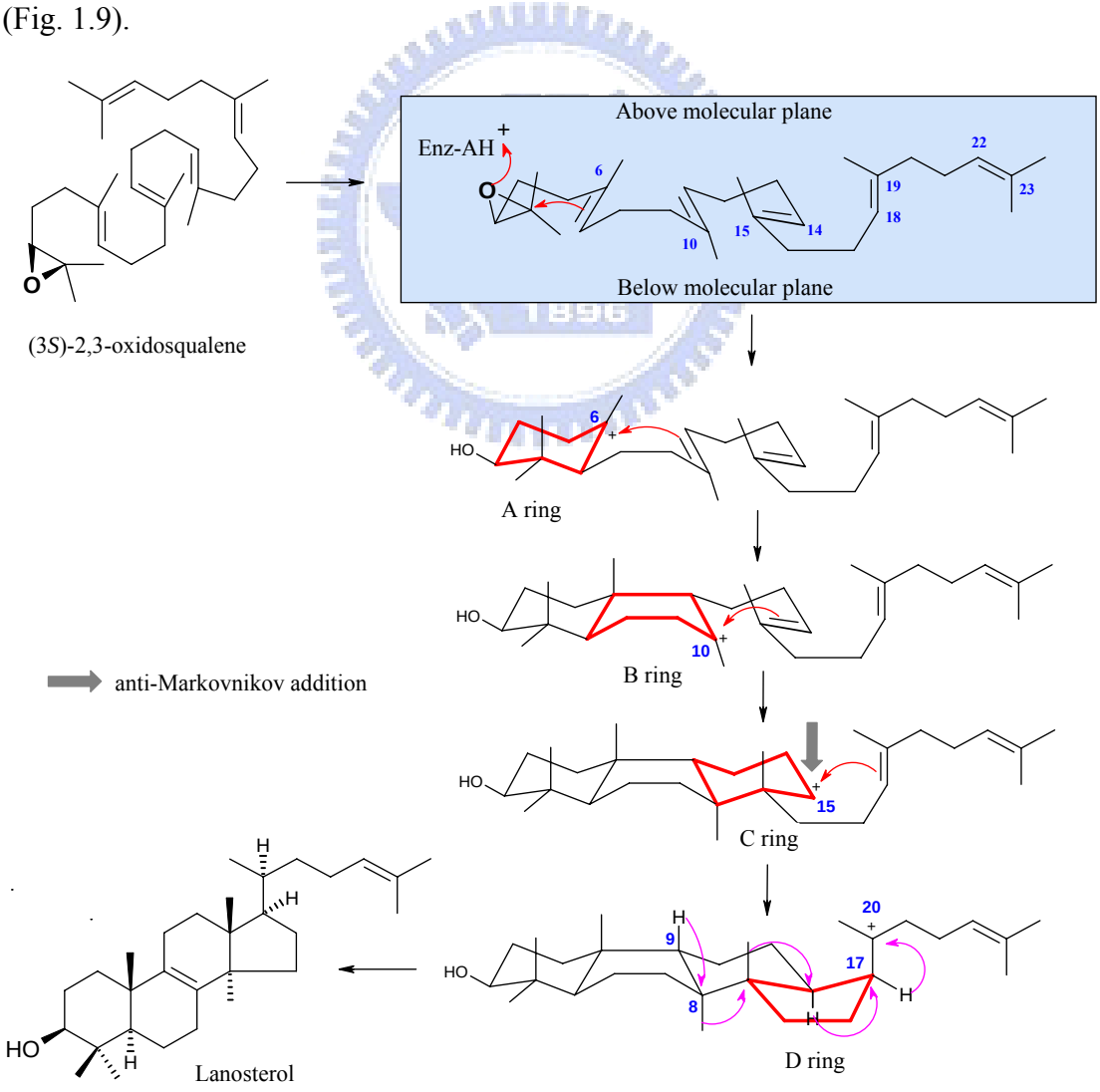

Figure 1.9 Mechanism of cyclization 2,3-oxidosqualene to lanosterol.

Initiation

In early work to predict the catalytically important residues, Corey *et al*. set a series of alanine scanning site-directed mutations of the highly conserved amino acids from *S. cerevisia*e ERG7. Complementation experiment results showed that His146, H234, and Asp456 were the catalytically essential residues. From this, a model was proposed that the protonated His146 would increases the acidity of Asp456 which acts as the proton donor for initiating cyclization.[34-35] In parallel, the X-ray structure of humanOSC also showed that Asp455 (Asp456 of *S. cerevisiae* ERG7) is hydrogen-bonding to Cys456 and Cys533, and it contributes to the required acidity for the protonation of epoxide. And then Asp455 can be reprotonated from a H-bonding network of bulk solvent (Fig. 1.10).[30,33] Based on experimental and theoretical studies it is widely accepted that initiation reaction was happening via the protonation and the following concerted A ring was also carried out.[36-40]

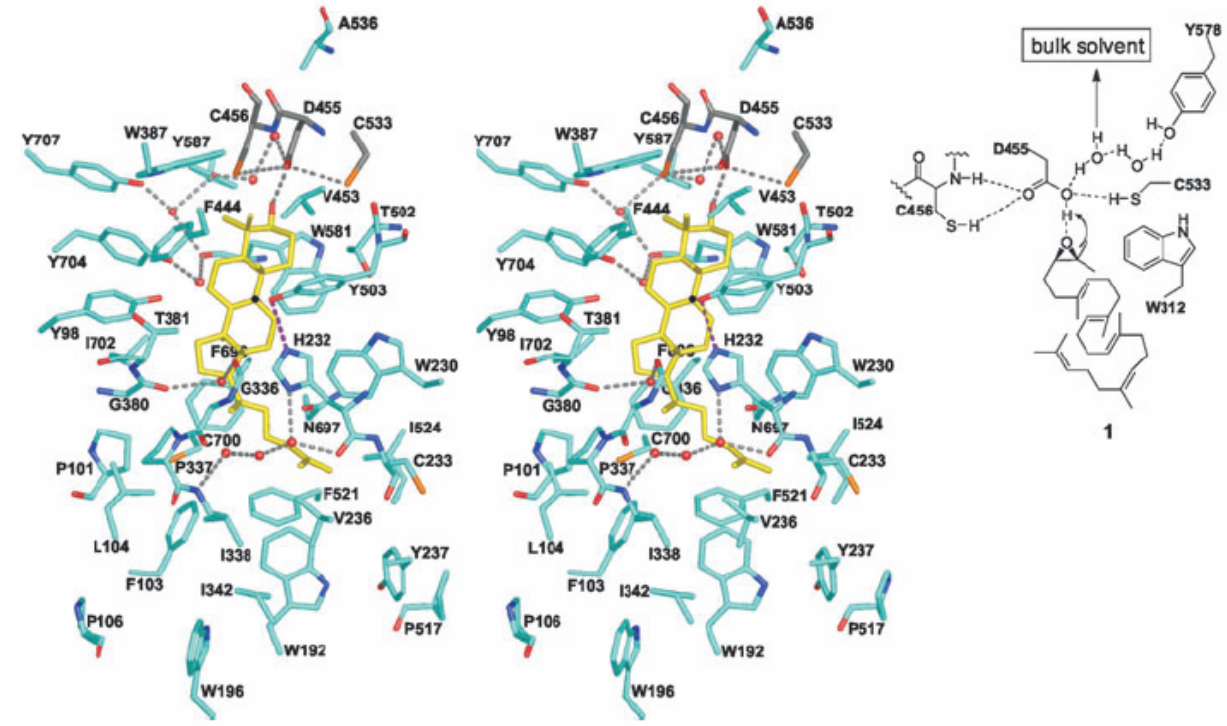

Figure 1.10 H. sapiens OSC (turquoise) with lanosterol (yellow): polar residues around catalytic acid Asp455, polar interactions, and hydrogen-bonding network.

Ring formation

In early studies about the B-ring formation, Matsuda *et al*. found that Val454 is strictly conserved in the *S. cerviase* OSC and the corresponding residue Ile481 in *A. thaliana* cycloartenol synthase was also considered as a catalytically important residue. A series of Val454 mutants were substituted as the hydrophobic residues in decreasing the amino acid side chain size of steric bulk from isopropyl to methyl or hydrogen (Phe, Leu, Ile, Ala and Gly). The Ala and Gly mutants allow the monocyclic products formation. It was suggested that steric bulk contributed from the valine side chain might participate in prefolding of the oxidosqualene especially in the Δ^{10} olefin condensation in the B-ring formation.[41] On the basis of X-ray crystallographic analysis of human OSC structure, Thomal *et al*. suggested that highly conserved aromatic residues Trp387, Phe444, and Trp581 (which corresponds to Trp390, Phe445, and Trp 583 of *S. cerevisiae* ERG7) stabilize the intermediate tertiary cation at C-6 and C-10 through cation-π interaction. However, generation of truncated tricyclic and altered deprotonation products from the Phe445 site-directed mutagenesis from *S. cerevisiae* provides an evidence that Phe445 might affect the cationic stabilization at the C-14 position for C-ring formation and also at C-8/C-9 position for final deprotonation.[42]

Moreover, the induction of the energetically unfavorable boat conformation of the B-ring is thought to be generated via the optimally positioned Tyr98 (Tyr99 of *S. cerevisiae* ERG7) pushing the methyl group at C-8 (lanosterol numbering) below the molecular plane of oxidosqualene (Fig. 1.11).

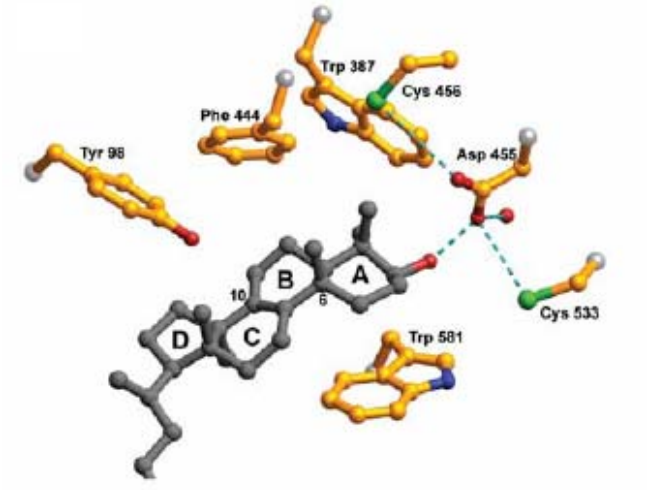

Figure 1.11 Trp387, Phe444 and Trp581 are able to stabilize the cyclization intermediates cation C-6 and C-10 through cation-π interaction. Catalytic Asp455 is activated by Cys456 and Cys533. The Tyr 98 side chain contributes the energetically unfavorable boat conformation of B-ring.

The concept of C-ring closure with subsequent ring expansion was initially suggested by Corey *et al*. based on the finding that the cyclization of 20-oxaoxidosqualene by the OSC of *S. cerevisiae* yields not only the expected 6-6-6-5 product but 6-6-5 fused-ring product additionally (Fig. 1.12).[2, 30, 43]

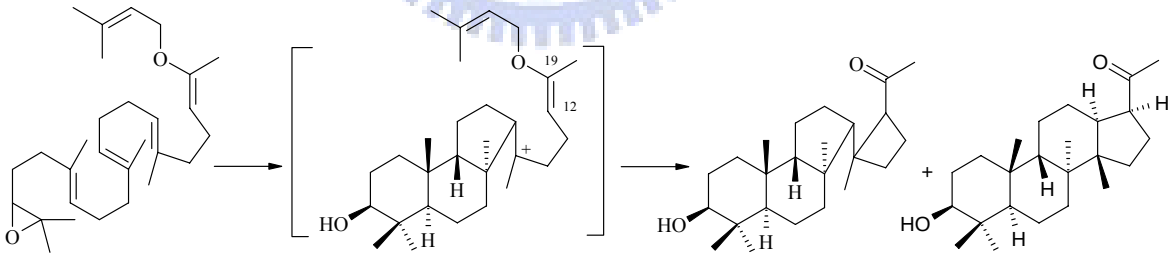

Figure 1.12 Substrate analogues and products catalyzed by *S. cerevisiae* OSC which are suggestive of a five-membered C-ring intermediate.

Observations of numerous partially cyclized 6-6-5 and 6-6-6-5 side products arising from the substrate-analogue studies have been considered to support the relevance of the C-14 cation intermediate and also provided further evidence for a five-membered C-ring closure (Markovnikov) followed by subsequent ring expansion. Steric pressure through the enzyme, however, might only play a secondary role for the prefolded C-ring conformation

formation, because the energetically favorable chair conformation is required for the C-ring formation.[7] Computational studies also provides further support for the 6-6-5 to 6-6-6 rearrangement pathway.[37] In addition, Thoma *et al*. showed that side chains of His232 and Phe696 (His234 and Phe699 in *S. cerevisiae* ERG7) are situated in well position for stabilizing the anti-Markovnikov secondary cation at C-14 with π–cation interactions during C-ring formation through the X-ray crystallographic analysis of human OSC protein.

Rearrangement and deprotonation

Due to the lack of an aromatic residue like Trp169 in SHC for stabilizing the long-lived secondary cation at C-17 for the six-membered E-ring cyclization of hopene, the end of OSC cyclization cascade is stopped at the formation of the five-membered D- ring. Skeletal rearrangement through 1,2-shift of hydride and methyl substituents (Fig. 1.9) convert the protosterol cation to lanosterol C-8 or C-9 cation. It was confirmed that the high π–electron density in the enzyme active site could stabilize the positive charge intermediate during the rearrangement. Thus, the enzyme's role in skeletal rearrangement is thought to shift equilibrium between the protosteryl cation toward carbocations at the C-8 and C-9 position of lanosteryl cation.[7, 33]

After skeletal rearrangement to C-8 and C-9 lanosterol cation the cyclization is terminated by proton removement. In the deprotonation step, OSC displays the specific catalytic selectivity for lanosterol synthesis which is the most thermodynamic stable deprotonation product (Saytzeff product) with a tetrasubstituted double bond. Thomal's group confirmed that His 232 (H234 in *S. cerevisiae* ERG7) is the only basic residue in the proximity to the termination site,[2,7, 34-35] and His232 would also form a hydrogen bond with the hydroxy group of Tyr503 (Tyr510 in *S. cerevisiae* ERG7), which is in a better position to accept the proton from C-9 of the lanosterol cation than His232 itself. The

interpretation of His232 and Tyr 503 as the catalytic base dyad in OSC was supported by site-directed mutagenesis data (Fig. 1.13): 1) The site-saturated mutagenesis experiments of His234 residue in *S. cerevisiae* ERG7 generated multiple triterpene products including protosta-20,24-dien-3β-ol, protosta-12,24-diene-3β-ol and parkeol from various ERG7^{His234x} mutants[44-45] and 2) the ERG7^{Tyr510Ala} mutant in *S. cerevisiae* formed parkeol.[46,47] By the same token, the functional analysis of Trp232 in *S. cerevisiae* ERG7 illustrated that Trp232 might play a catalytic role in the influence of rearrangement process and determination of deprotonation position but does not intervene in the cyclizaiotn steps (Fig. 1.13).[48]

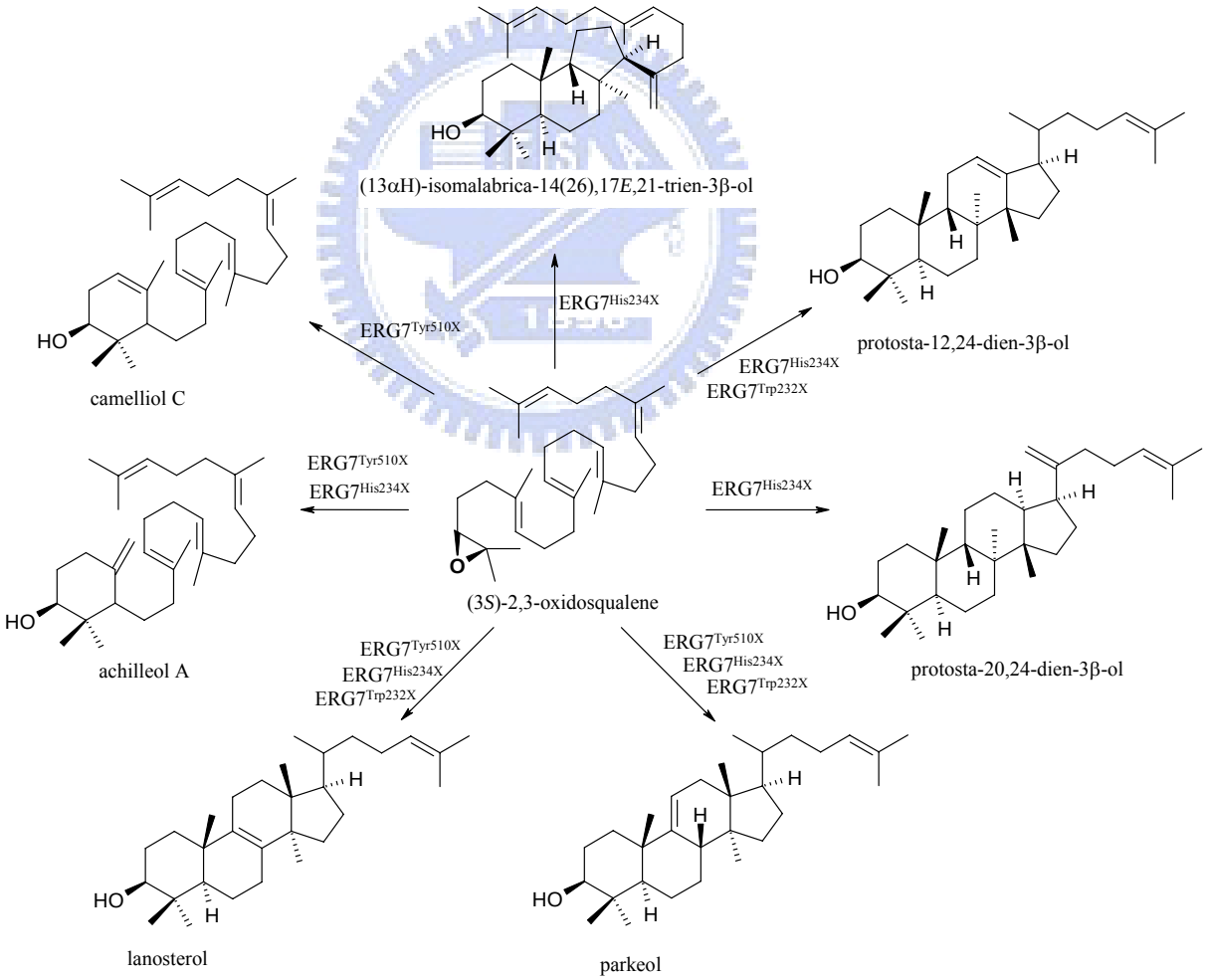

Figure 1.13 The products diversity from site-saturated mutant of His234, Tyr510 and Trp232.

1.2.5 Cycloartenol synthase (CAS)

Cycloartenol synthase (EC 5.4.99.8, from *Arabidopsis thaliana*) is a protosteryl-type oxidosqualene cyclase that initially cyclizes oxidosqualene to the protosteryl cation intermediate and then mediates a series of hydride and methyl shifts to form the C-9 cation intermediate. In the final step of the reaction, cycloartenol synthase induces cyclopropyl ring formation via abstracting a proton form C-19 to form cycloartenol. This reaction is very similar to that catalyzed by oxidosqualene-lanosterol cyclase. All steps in cycloartenol and oxidosqualene-lanosterol cyclase are identical with the exception of the final deprotonation reaction. Cycloartenol synthases form the cyclopropyl ring and abstract a proton from C-19, whereas lanosterol synthases remove a different proton and form lanosterol (Fig. 1.14).

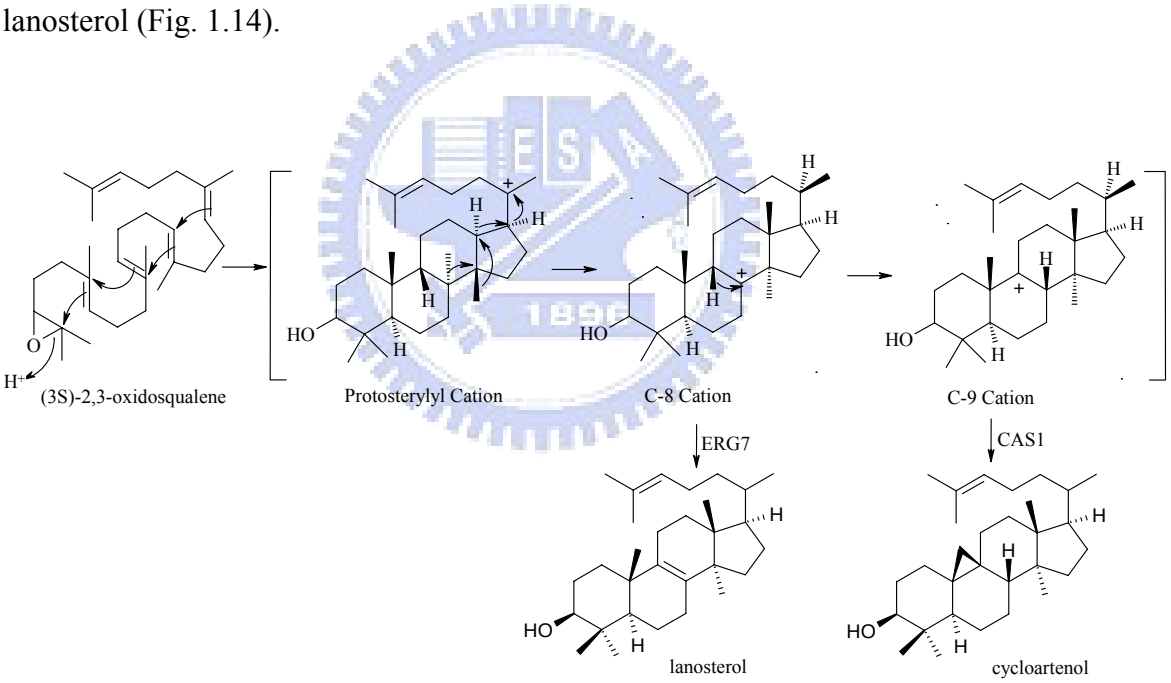

Figure 1.14 Cyclization of oxidosqualene by oxidosqualene-lanosterol cyclase and cycloartenol synthase.

Furthermore, because the cyclopropyl ring formation in the cycloartenol biosynthesis is thermodynamically unfavorable relative to the lanosterol formation, some of amino acid differences are probably specifically required for inducing cyclopropyl ring formation and excluding the formation of more energetically favored products by the cycloartenol

synthase.

Regarding the previous mutagenesis studies in cycloartenol synthase, Tyr410, His477, and Ile481 are catalytically important residues in *Ath*CAS1.[6, 49-52] These residues are strictly conserved in cycloartenol synthase, but in animal or fungal oxidosqualene-lanosterol cyclase maintain Thr, Cys or Gln, and Val at the corresponding positions (Fig. 1.15). These residues synergize to promote the cycloartenol biosynthesis, and mutations at these positions would allow the lanosterol formation.

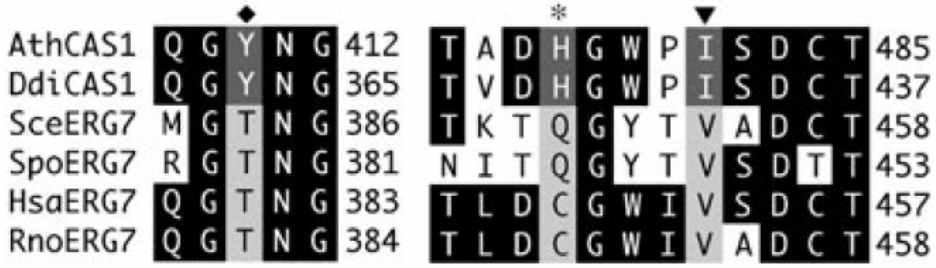

Figure 1.15 Conservation pattern between CAS1 and ERG7. Tyr410 (◆), His477 (∗) and Ile481 (▼) are strictly conserved in CAS1; Thr, Cys or Gln, Val is conserved at the corresponding position in ERG7.

Ile481 is conserved in all cycloartenol synthase, whereas Val is present in oxidosqualene-lanosterol synthase (Fig. 1.15). The Ile481 γ-methyl might promote cycloartenol formation by preventing the rotation of the intermediate cation through steric interactions with C-2 and the two axial methyl groups at the A- ring. Removing the γ-methyl group with an Ile481Val mutation resulted in 25% lanosterol production in addition to cycloartenol and parkeol. Besides, Ile481 may also be involved in assisting for the proper substrate folding as well as cyclization reaction. Mutation of Ile481 to smaller residues (Ala and Gly) has led to achilleol A and camelliol C production (Fig. 1.16 and Tab. 1.1).[49]

Tyr410 and His 257 participate in an H-bonding network positioned near the C-19 methyl group for deprotonation reaction.[51] Tyr410 is present in all cycloartenol synthase,

but animal and fungal oxidosqualene-lanosterol synthase maintain Thr at the corresponding position (Fig. 1.15). The *Ath*CAS1 Tyr410Thr mutant forms 65% lanosterol along with 9β-lanosta-7,24-dien-3β-ol and parkeol (Fig. 1.16 and Tab. 1.1). Removing the aromatic ring of Tyr410 decreases the steric bulk above the intermediate cation. Because the hydroxyl group in Thr is closer to the α–carbon then in Tyr, the polar groups of Tyr410Thr, Tyr532, and His257 were repositioned in the Tyr410Thr mutant. This combination of steric and electronic changes abolishes the cycloartenol synthesis and allows deprotonation of C-8/C-9 lanosterol cation to form lanosterol, parkeol and 9β-lanosta-7,24-dien-3β-ol.[50]

His477 is not in the active site, but is a second-sphere residue that affects the product profile through interactions with the side chain of Tyr410.[51] His477 is strictly conserved in the known cycloartenol synthase, whereas oxidosqualene-lanosterol synthases maintain either Gln or Cys (Fig. 1.15). The *Ath*CAS1 His477Gln mutant has the polar functionality moved toward C-11 and consequently resulting in more parkeol production than lanosterol. *Ath*CAS1 His477Asn mutant forms lanosterol by positioning the basic group near the C-9/C-8, but also produced parkeol due to close enough to C-11.[52]

The double mutant of CAS I481V/ Y410T formed lanosterol more accurately than either single mutant. However the triple mutant (His477Asn/Gln Ile481Val Tyr410Thr) didn't promote the lanosterol synthesis because the hydroxyl group of Thr positioned too far to interact with the amide group of Asn or Gln residues. The His477Asn Ile481Val double mutant is the most accurate example for the enzyme mutation to generate lanosterol.[52] (Tab. 1.1)

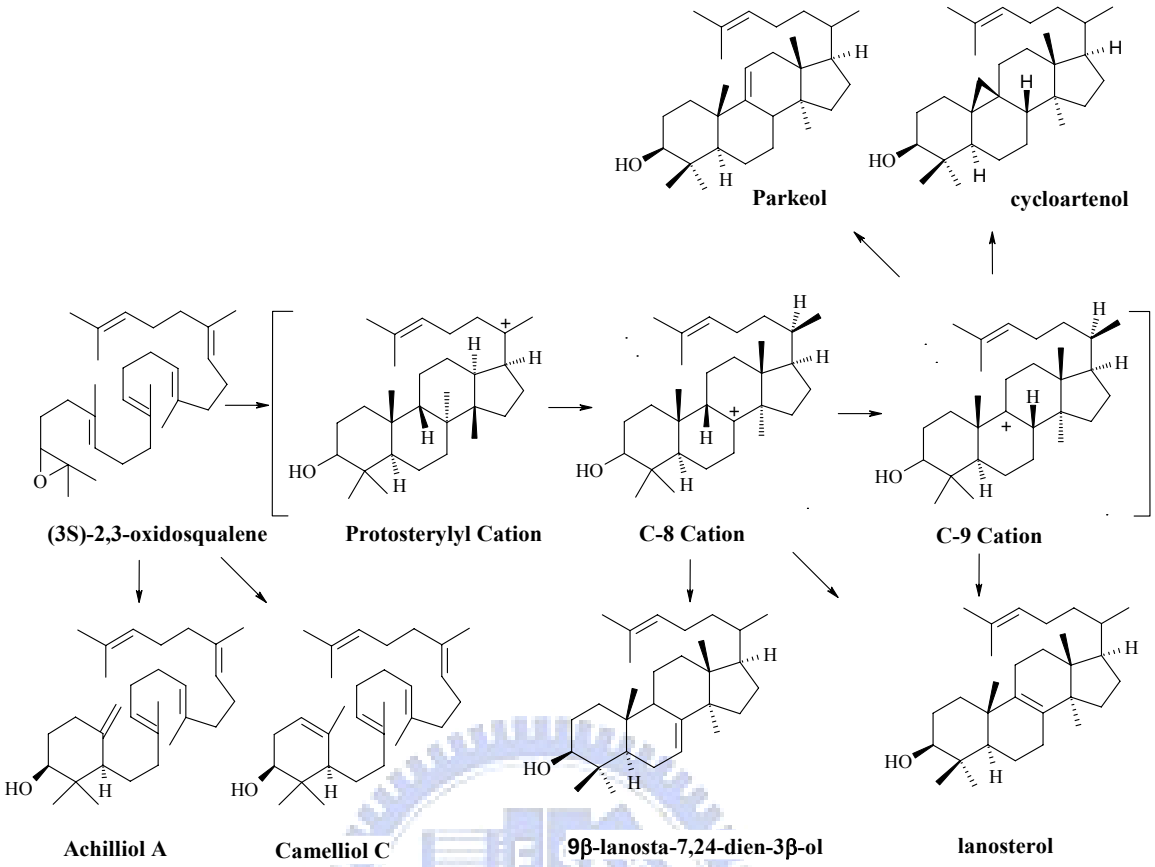

Figure 1.16 Products formed by cycloartenol synthase mutants.

*Ath*CAS1 mutants	Cycloartenol	Lanosterol	Parkeol	9ß-Δ7-Lanosterol	Achilleol A	Camelliol C
CAS1^{I481}	99	-	1	-	-	-
CAS1^{I481L}	83	1	16	-	-	-
CAS1^{I481V}	55	24	21	-	-	-
CAS1^{I481A}	12	54	15	-	13	6
CAS1^{I481G}	17	23	4	-	44	12
CAS1^{Y410T}	-	65	2	33	-	-
CAS1^{Y410C}	-	75	-	24	1	-
CAS1^{H477N}	-	88	12	-	-	-
CAS1^{H477Q}	-	22	73	5	-	-
CAS1$^{I481V/\ Y410T}$	-	78	< 1	22	-	-
CAS1$^{I481V/\ H477N/\ Y410T}$	-	78	-	22	-	-
CAS1$^{I481V/\ H477Q/\ Y410T}$	-	78	-	22	-	-
CAS1$^{I481V/\ H477N}$	-	99	1	-	-	-
CAS1$^{I481V/\ H477Q}$	-	94	6	-	-	-

Table 1.1 Product profiles of *A. thaliana* cycloartenol synthase Ile481, Tyr410 and His477 mutants.

1.2.6 Squalene-hopene cyclase (SHC)

In bacteria, sterols are usually absent, but some bacteria and protozoans produce pentacyclic triterpenes which are regarded as sterol surrogates in these organisms.[1] The prokaryotic squalene-hopene cyclases (SHCs) catalyze a stereochemically and mechanistically simpler process than the eukaryotic oxidosqualene cyclase did. SHCs convert squalene into the pentacyclic hopene skeleton by adopting an all pre-chair conformation leading to C-22 hopanyl cation, then undergoes a deprotonation step to form hopene or alternatively the nucleophilic attack by water molecule to afford hopenol (Fig. 1.17). However, the skeletal rearrangement is not generally observed in the catalytic pathways of SHCs.

Furthermore, the bacteria SHCs displayed very low substrate specificity. They can cyclize not only the natural substrate, but also both enantiomers of oxidosqualene, and regular polyprenols. In contrast, the eukaryotic OSCs have a rigorous substrate specificity as they do not accept intact squalene or its (*3R*)-oxidosqualene, and cyclize specifically the (*3S*)-oxidosqualene.[1-2]

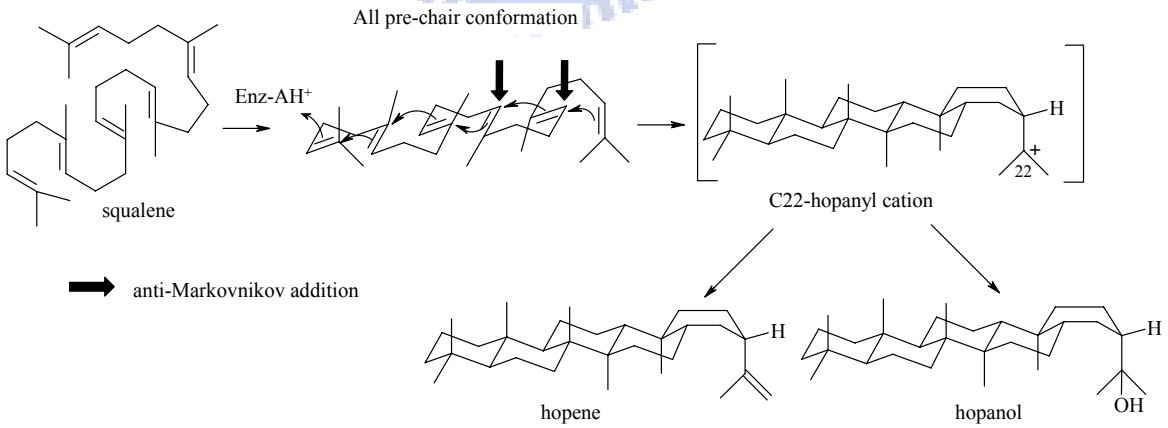

Figure 1.17 Polycyclization Mechanism of squalene by prokaryotic squalene-hopene cyclase (SHC).

In 1997, Wendt *et al.* reported the X-ray analysis of *A. acidocaldarius* SHC, which is the first three-dimensional crystal structure among the many know triterpene synthase, revealing an α–helix-rich dumbbell-shaped homodimer containing a large central cavity as the putative active site.[31,53-55]

Squalene-hopene cyclase is a dimeric membrane protein, and it penetrates but does not completely pass through the bacterial membrane. Substrate squalene, embedded in the membrane, enters the cyclase active site through a hydrophobic channel connecting with the membrane surface. A nonpolar "plateau" flanked the channel entrance in the vicinity of α-helix 8, would likely comprise the membrane association motif (Fig. 1.18).

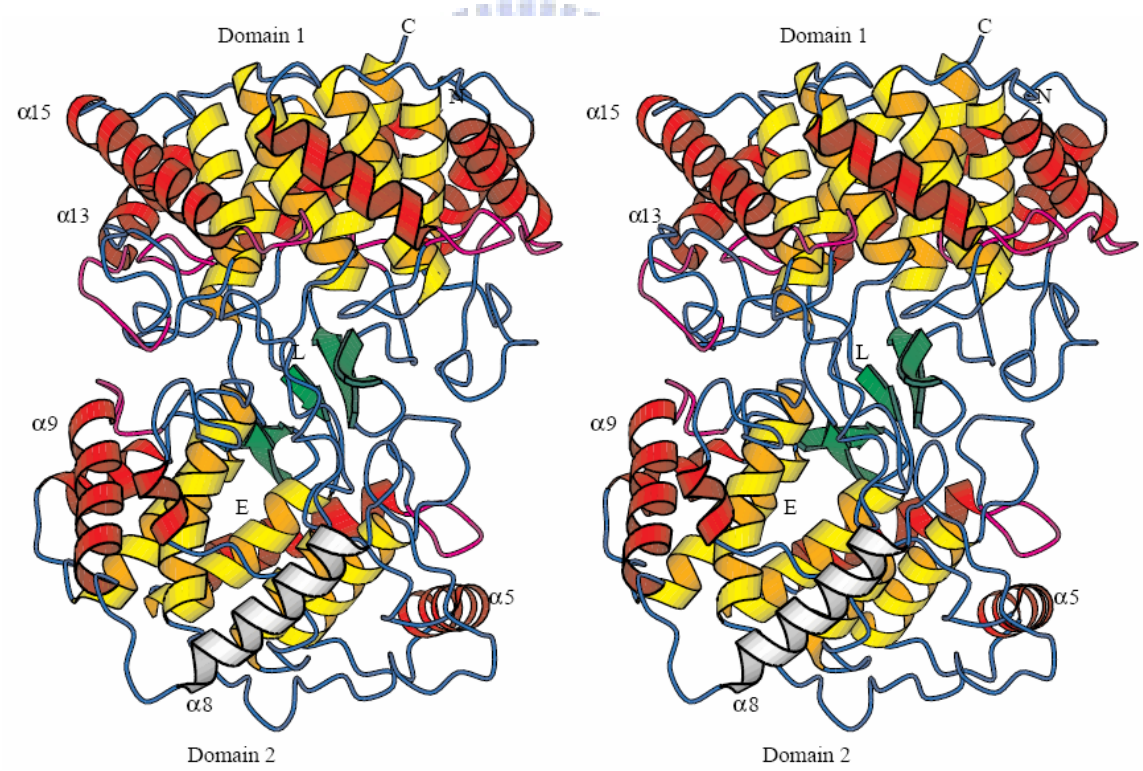

Figure 1.18 Overall structure of *A. acidocaldarius* squalene-hopene cyclase (SHC). N and C: NH2- and COOH-termini; L: the position of the competitive inhibitor LDAO; E: the entrance of the active site channel; Color code: internal (yellow) and external (red) barrel helices; β structure (green); QW-motifs (purple); and helix α-8 in the suggested membrane-binding region (white).[31]

In 1996, Poralla's group reported the mutagenesis of the short amino acid sequence from Asp374 to Ala379 (the DXDDTA motif) of *A.acidicaldarius* SHC. The polycyclization reaction is triggered via proton attack on the terminal double bond of squalene, donated by the DXDDTA motif.[53,56-57] Wentd *et al.* have proposed that Asp376 acts as proton donor on the terminal double bond to initiate the polycyclization and that H451 would enhance the acidity of Asp376. A negative countercharge on the hydrogen bond pair Asp374:Asp377 resides in an appropriate position to stabilize the C2 and C6 cations (squalene numbering). Three hydrogen bonds connecting Asp376 with bulk solvent would lead reprotonation while the cyclizing cation migrates away from the catalytic acid (Fig. 1.19).[2,30]

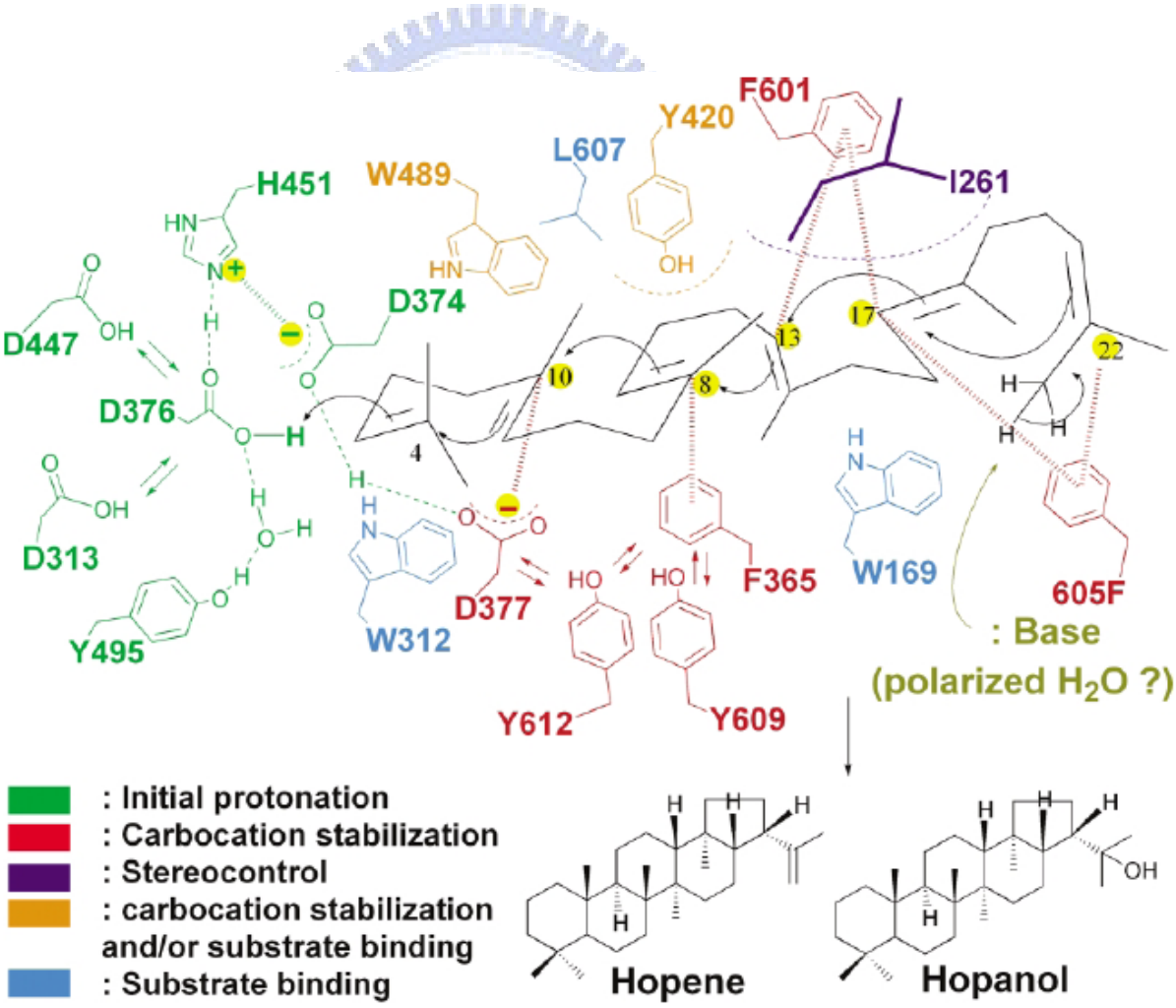

Figure 1.19 The placements and functions of crucial amino acids inside the central cavity of SHC.[54]

Crystal structures of SHC coupled with the site-directed mutational data have provided a wealth of mechanism information between the active site residues and the substrate.[2] The residues of Trp312 and Trp169 were suggested for binding with substrate, but Wendt *et al*. proposed these two residues could be assigned for the stabilization of C-4 cation and C-13 cation (hopene numbering) via cation-π interaction (Fig. 1.19).[2,55] The function of Tyr420 is likely to be assigned for stabilization of the C-8 cation despite Tyr609 being positioned around the C-8 cation (Fig. 1.19). Because mutating Tyr420 to Ala and Gly afforded bicyclic and tricyclic product, Tyr420 may additionally play a structural role in the folding process of the hopene skeleton in B- or C-ring formation.[53] Trp489 has been proposed to work for stabilizing the C-10 cation through cation-π interaction during A-ring formation.[54]

Phe605 seems well positioned to stabilize the terminal cation resulting form E-ring formation in SHC, and it is supported by the conservation of Phe605 among all known squalene cyclase as well as the absence of this residue in the OSC, where only four rings are formed.[55]

For the terminal cyclization reaction, the hopanyl cation is then quenched by the putative water molecule that either deprotonates C23 or adds to C23 as a hydroxyl group. Based on molecular dynamics simulations, Reinert *et al.* suggested that the cyclizing squalene contracts from both sides towards its center. The water molecule has never been observed in any SHC structure, indicating that it has no defined binding site. However, after the hopenyl cation has been formed, there is enough space in the cavity to accommodate a hydrogen-bonding water network which is in turn fixed by Glu45 and Gln262.[58]

1.3 The amino acid sequence alignment of (oxido-)squalene cyclase

Although *S. cerevisiae* and human OSC and SHC only shared sequence identity of about 40%, the catalytic cyclization reactions by SHC or OSC family show enormously similar structural and stereochemical control and parallel mechanism. High product specificity in cyclases is believed to be achieved through several factors: (1) by enforcing substrates to occupy prefolded conformations, (2) by progression of reaction via rigidly held, partially cyclized carbocationic intermediates, and (3) by stabilization of intermediate carbocations by cation-π interactions of frequently occurring aromatic residues in the active site, thus preventing early truncation of the cyclization cascade by deprotonation or nucleophilic addition of solvent molecules.[7]

During the past decade, advances in molecular biology, molecular modeling, and protein crystallography have provided enormous information for understanding this remarkable cyclization. Especially, X-ray structural information of SHC and human OSC examined a perspective view of the active site, coupling with site-directed mutagenesis, many of functional important residues had been identified.

In order to understand a consequence of functional, structural, or evolutionary relationships between the cyclases sequence, we used Clustal W to produce multiple sequence alignment of the following enzymes: *H. sapoens* OSC: P48449, *S. cerevisiae* OSC: P38604, *A. thaliana* CAS: P38605, *A. acidocaldarius* SHC: P33247, which were identified from Protein Data Bank (PDB) in NCBI (Fig. 1.20).

```
Hs_OSC          MTEGTCLRRRGGPYKTEPATDLGR--WRLNCERGR--------QTWTYLQDERAGREQTG 50
At_CAS          -MWKLKIAEGGSPWLRTTNNHVGRQFWEFDPNLGTPEDLAAVEEARKSFSDNRFVQKHSA 59
Sc_OSC          -MTEFYSDTIG---LPKTDPRLWR---LRTDELGR--------ESWEYLTPQQAANDPPS 45
Aa_SHC          ----------------------------------------------MAEQLVEAP-- 9

Hs_OSC          LEAYALGLDTKNYFKDLP----------KAHTAFEGALN-GMTFYVGLQAED-GHWTGDY 98
At_CAS          DLLMRLQFSRENLISPVLPQVKIEDTDDVTEEMVETTLKRGLDFYSTIQAHD-GHWPGDY 118
Sc_OSC          TFTQWLLQDPK-FPQPHPERNK----HSPDFSAFDACHN-GASFFKLLQEPDSGIFPCQY 99
Aa_SHC          -------------------------------AYARTLDRAVEYLLSCQKDE-GYWWGPL 36

Hs_OSC          GGPLFLLPGLLITCHVARIP---LPAGYREEIVRYLRSVQL-PDGGWGLHIEDKSTVFGT 154
At_CAS          GGPMFLLPGLIITLSITGALNTVLSEQHKQEMRRYLYNHQN-EDGGWGLHIEGPSTMFGS 177
Sc_OSC          KGPMFMTIGYVAVNYIAGIE---IPEHERIELIRYIVNTAHPVDGGWGLHSVDKSTVFGT 156
Aa_SHC          LSNVTMEAEYVLLCHILDRVD----RDRMEKIRRYLLHEQR-EDGTWALYPGGPPDLDTT 91

Hs_OSC          ALNYVSLRILGVGPDDPD--LVRARNILHKKGGAVAIPSWGKFWLAVLNVYSWEGLNTLF 212
At_CAS          VLNYVTLRLLGEGPNDGDGDMEKGRDWILNHGGATNITSWGKMWLSVLGAFEWSGNNPLP 237
Sc_OSC          VLNYVILRLLGLPKDHPV--CAKARSTLLRLGGAIGSPHWGKIWLSALNLYKWEGVNPAP 214
Aa_SHC          IEAYVALKYIGMSRDEEP--MQKALRFIQSQGGIESSRVFTRMWLALVGEYPWEKVPMVP 149

Hs_OSC          PEMWLFPDWAPAHPSTLWCHCRQVYLPMSYCYAVRLSAAEDPLVQSLRQELYVEDFASID 272
At_CAS          PEIWLLPYFLPIHPGRMWCHCRMVYLPMSYLYGKRFVGPITSTVLSLRKELFTVPYHEVN 297
Sc_OSC          PETWLLPYSLPMHPGRWWVHTRGVYIPVSYLSLVKFSCPMTPLLEELRNEIYTKPFDKIN 274
Aa_SHC          PEIMFLGKRMPLNIYEFGSWARATVVALSIVMSRQPVFPLPERARVP--ELYETDVPPRR 207

Hs_OSC          WLAQRNNVAPDELYTPHSWLLRVVYALLN-----LYEHHHS-AHLRQRAVQKLYEHIVAD 326
At_CAS          WNEARNLCAKEDLYYPHPLVQDILWASLHKIVEPVLMRWPG-ANLREKAIRTAIEHIHYE 356
Sc_OSC          FSKNRNTVCGVDLYYPHSTTLNIANSLVV-----FYEKYLRNRFIYSLSKKKVYDLIKTE 329
Aa_SHC          RGAKGG----------GGWIFDALDRALHG-----YQKLSVHPFRRAAEIRALDWLLERQ 252

Hs_OSC          DRFTKSISIGPISKTINMLVRWYVDGPASTAFQEHVSRIPDYLWMGLDGMKMQGTNGSQI 386
At_CAS          DENTRYICIGPVNKVLNMLCCWVED-PNSEAFKLHLPRIHDFLWLAEDGMKMQGYNGSQL 415
Sc_OSC          LQNTDSLCIAPVNQAFCALVTLIEEGVDSEAFQRLQYRFKDALFHGPQGMTIMGTNGVQT 389
Aa_SHC          AGDGSWGGIQPP-WFYALIALKILDMTQHPAFIKGWEGLELYGVELDYGGWMFQASISPV 311

Hs_OSC          WDTAFAIQALLEAGGHHRPEFSSCLQKAHEFLRLSQVPDNPP-DYQKYYRQMRKGGFSFS 445
At_CAS          WDTGFAIQAILATN--LVEEYGPVLEKAHSFVKNSQVLEDCPGDLNYWYRHISKGAWPFS 473
Sc_OSC          WDCAFAIQYFFVAGLAERPEFYNTIVSAYKFLCHAQFDTECV---PGSYRDKRKGAWGFS 446
Aa_SHC          WDTGLAVLALRAAG---LPADHDRLVKAGEWLLDRQIT--VPGDWAVKRPNLKPGGFAFQ 366
```

```
Hs_OSC          TLDCGWIVSDCTAEALKAVLLLQEKCP-HVT-EHIPRERLCDAVAVLLNMRNPD----GG 499
At_CAS          TADHGWPISDCTAEGLKAALLLSKVPK-AIVGEPIDAKRLYEAVNVIISLQNAD----GG 528
Sc_OSC          TKTQGYTVADCTAEAIKAIIMVKNSPVFSEVHHMISSERLFEGIDVLLNLQNIGSFEYGS 506
Aa_SHC          FDNVYYPDVDDTAVVVWALNTLR------LPDERRRRDAMTKGFRWIVGMQSSN----GG 416

Hs_OSC          FATYETKRGGHLLELLNPSEVFGDIMIDYTYVECTSAVMQALKYFHKRFPEHRAAEIRET 559
At_CAS          LATYELTRSYPWLELINPAETFGDIVIDYPYVECTSAAIQALISFRKLYPGHRKKEVDEC 588
Sc_OSC          FATYEKIKAPLAMETLNPAEVFGNIMVEYPYVECTDSSVLGLTYFHKYF-DYRKEEIRTR 565
Aa_SHC          WGAYDVDNTSDLPNHIPFCDFG--EVTDPPSEDVTAHVLECFG-------SFGYDDAWKV 467

Hs_OSC          LTQGLEFCRRQQRADGSWEGSWGVCFTYGTWFGLEAFACMGQTYRDGTACAEVSRACDFL 619
At_CAS          IEKAVKFIESIQAADGSWYGSWAVCFTYGTWFGVKGLVAVGKTLKN---SPHVAKACEFL 645
Sc_OSC          IRIAIEFIKKSQLPDGSWYGSWGICFTYAGMFALEALHTVGETYEN---SSTVRKGCDFL 622
Aa_SHC          IRRAVEYLKREQKPDGSWFGRWGVNYLYGTGAVVSALKAVGIDTRE----PYIQKALDWV 523

Hs_OSC          LSRQMADGGWGEDFESCEERRY--LQSAQSQIHNTCWAMMGLMAVRHPDIEAQ--ERGVR 675
At_CAS          LSKQQPSGGWGESYLSCQDKVYSNLDGNRSHVVNTAWAMLALIGAGQAEVDRKPLHRAAR 705
Sc_OSC          VSKQMKDGGWGESMKSSELHSY--VDSEKSLVVQTAWALIALLFAEYPNKEVI--DRGID 678
Aa_SHC          EQHQNPDGGWGEDCRSYEDPAY--AGKGASTPSQTAWALMALIAGGRAESEAAR--RGVQ 579

Hs_OSC          CLLEKQLPNGDWPQENIAG-VFNKSCAISYTSYRNIFPIWALGRFSQLYPERALAGHP    732
At_CAS          YLINAQMENGDFPQQEIMG-VFNRNCMITYAAYRNIFPIWALGEYRCQVLLQQGE---    759
Sc_OSC          LLKNRQEESGEWKFESVEG-VFNHSCAIEYPSYRFLFPIKALGMYSRAYETHTL----    731
Aa_SHC          YLVETQRPDGGWDEPYYTGTGFPGDFYLGYTMYRHVFPTLALGRYKQAIERR------    631
```

Figure 1.20 Nucleic acid sequence alignment of OSC, CAS, SHC genes. Abbreviations Hs, At, Sc, and Aa stand for *H. sapoens*, *A. thaliana*, *S. cerevisiae*, *A. acidocaldarius*, respectively. Dashed lines indicate the gap introduced for better alignment.

QW motif

Squalene and oxidosqualene cyclase shared a characteristic sequence repeat, $[(K/R)(G/A)X_{2\text{-}3}(F/Y/W)(L/I/V)_3X_3QX_{2\text{-}5}GXW]$.[59] This repeat typically occurs five times in oxidosqualene cyclase and up to eight times in the squalene-hopene cyclase (Fig. 1.21). The high conservation of this repeat throughout the triterpene cyclases has led to a hypothesis that the conserved and unusual rich aromatic amino acids may be involve in the

stabilization of carbocationic intermediates. Such an arrangement has made Poralla to suggest that QW motifs may act to stabilize the transient carbocationic intermediates.[60]

However, the X-ray analysis of the SHC showed that QW motifs are not located in the active-site cavity but rather at the surface of the enzyme. These conserved amino acid residues of the repeats form an complicated network of hydrogen-bonding and hydrophobic interactions that connect the α-barrel helices. Wendt *et al*. proposed that this arrangement might reinforce the cyclases against an unusually high energy, released during the process of pentacyclic ring formation from acyclic squalene.[31]

OSC (H.S.)	QW6	79	NGMTFYVGLQAEDGHW	94
OSC (S.c.)	QW6	79	NGASFFKLLQEPDSGIF	95
SHC (A.a.)	QW6	17	RAVEYLLSCQKDEGYW	32
CAS (A.t.)	QW6	99	RGLDFYSTIQAHDGHW	114
OSC (H.S.)	QW5	127	EIVRYLRSVQLPDGGW	142
OSC (S.c.)	QW5	127	ELIRYIVNTAHPVDGGW	143
SHC (A.a.)	QW5c	63	KIRRYLLHEQREDGTW	78
CAS (A.t.)	QW5	139	EMRRYLYNHQNEDGGW	164
SHC (A.a.)	QW5b	243	RALDWLLERQAGDGSW	258
SHC (A.a.)	QW5a	335	KAGEWLLDRQITVPGDW	363
SHC (A.a.)	QW4	402	KGFRWIVGMQSSNGGW	417
OSC (H.S.)	QW3	561	TQGLEFCRRQQRADGSW	577
OSC (S.c.)	QW3	568	IAIEFIKKSQLPDGSW	583
SHC (A.a.)	QW3	470	RAVEYLKREQKPDGSW	485
CAS (A.t.)	QW3	591	KAVKFIESIQAADGSW	606
OSC (H.S.)	QW2	614	RACDFLLSRQMADGGW	629
OSC (S.c.)	QW2	617	KGCDFLVSKQMKDGGW	632
SHC (A.a.)	QW2	518	KALDWVEQHQNPDGGW	533
CAS (A.t.)	QW2	640	KACEFLLSKQQPSGGW	655
OSC (H.S.)	QW1	672	RGVRCLLEKQLPNGDW	687
OSC (S.c.)	QW1	675	RGIDLLKNRQEESGEW	690
SHC (A.a.)	QW1	576	RGVQYLVETQRPDGGW	591
CAS (A.t.)	QW1	702	RAARYLINAQMENGDF	718

Figure 1.21 Aligned QW motifs of squalene and oxidosqualene cyclase. Abbreviations Hs, Aa, Sc, and At stand for *H. sapoens*, *A. acidocaldarius*, *S. cerevisiae*, *A. thaliana*, respectively.

1.4 Research goal

Oxidosqualene cyclases are key enzymes in sterol biosynthesis. They catalyzed the stereoselective cyclization and precise skeletal rearrangement of (*3S*)-2,3-oxidosqualene to lanosterol in mammals and fungi and to cycloartenol in algae and higher plant. Complexity, efficiency, and high stereoselectivity of cyclase catalyzed reactions make them prime examples for studying multiple enzyme functions and interesting tools in synthetic chemistry. To provide insight into the catalytic mechanism, functional role of specific residues, and mutation-induced product specificity/diversity profile, many experimental data were reported such as substrate analogues, site-specific mutagenesis coupled with product characterization. Due to the large size and membrane-bound nature of OSCs, three-dimensional structural information is still not available except the SHC from *A. acidocaldarius* and human OSC.[31, 33]

The identification for the crystal structure of human OSC provided us a wealthier perception of the enzymatic OS cyclization and attracted us and other researchers to elucidate how the putative active site residues impact cyclization/rearrangement outcome or product specificity and diversity. Nevertheless, the important residues involved in stereo- or rigio-specific control of these product profiles are still far from being fully understood.

The catalytic importance of the Tyr98 residue of the human OSC was inconspicuous until the recent crystal structure of the protein was reported. In view of crystal structures from bacterial SHC and human OSC, it shows that human OSC has an inserted amino acid above and a deleted residue below the molecular plane of 2,3-oxidosqualene, thus preventing the methyl group at C10 to be located above the molecular plane and avoiding the substrate to adopt the energetically favored chair conformation.[7] Further, it was suggested that the Tyr98 of the human OSC positioned spatially to enforce the

energetically unfavorable boat form of oxidosqualene for lanosterol B-ring formation through pushing the methyl group at C-8 (lanosterol numbering) below the molecule plane.[33] However, there is no experimental data to characterize and validate the functional role of Tyr98, as the above-mentioned hypothesis.

The Tyr99 residue of *S. cerevisiae* oxidosqualene-lanosterol cyclase (ERG7) corresponds to the Tyr98 residue in the human OSC. The multiple sequence alignment revealed that the Tyr99 residue of ERG7 is highly conserved in both the oxidosqualene-lanosterol cyclase and oxidosqualene-cycloartenol synthase, but different substituted amino acids were noticed for β–amyrin synthase and lupeol synthase. Also, a one-residue insertion proximal to the Try99 position of ERG7 was observed specifically for oxidosqualene-lanosterol cyclase from *S. cerevisiae*, *Trypanosoma brucei*, and *T. cruzi*, but not for mammalian oxidosqualene-lanosterol cyclase. According to these observations, we suppose that Tyr99 residue of *S. cerevisiae* ERG7 may play a different functional role than it of human OSC.

In this thesis, the functional role of the Tyr99 position in the ERG7-catalyzed cyclization/rearrangement cascade and product profile of the cyclase was further substantiated, via generation of the site-saturated mutants of $ERG7^{Y99X}$ and characterization of the product profiles.

On the other hand, in the previous studies of oxidosqualene-cycloartenol synthase (*A. thaliana* CAS) mutations, a series of amino acid residues sequence, ^{469}AWPFSTADHGWPI^{481}, was found within an upstream region of the putative active site. Detailed analysis of the mutations indicated that this region is involved in either protein evolution or crucial determination of the cyclization/rearrangement cascade in cyclase product diversity.[61] Therefore, a series of amino acid residues, ^{441}GAWGFSTKTQGYT^{453} (corresponding to the region Ala469-Ile481 of CAS) within *S. cerevisiae* ERG7, were subjected to both alanine-scanning mutagenesis and plasmid shuffle selection for

identification of possible residues involved in the complementation of cyclase-deficient yeast strains.[62] The complementation results are showed in Fig. 1.22. Several inactive mutations were identified, including Trp443Ala, Phe445Ala and Lys448Ala mutations, which failed to complement the cyclase deficiency. The functional roles of Phe445 of ERG7 has been characterized and the mutational-induced product profiles has been determined through site-directed mutagenesis.[62]

In order to further understanding the functional role of the Trp443, the effects of substitutions of Trp443 with other 19 essential amino acid residues in the catalytic activity and the product profiles were investigated. A series of saturated mutagenesis were constructed and the product profiles characterizations were also carried out in this thesis. My experimental flowchart is illustrated in Figure 1.23.

Mutation	Complementary results: CBY57 (ERG7△::LEU2)
Wild-Type	+
Negative control	−
Gly441Ala (pFHCOSCRS-13)	+
Trp443Ala (pFHCOSCRS-12)	−
Gly444Ala (pFHCOSCRS-11)	+
Phe445Ala (pFHCOSCRS-10)	−
Ser446Ala (pFHCOSCRS-9)	+
Thr447Ala (pFHCOSCRS-7)	+
Lys448Ala (pFHCOSCRS-6)	−
Thr449Ala (pFHCOSCRS-5)	+
Gln450Ala (pFHCOSCRS-4)	+
Gly451Ala (pFHCOSCRS-3)	+
Tyr452Ala (pFHCOSCRS-2)	+
Thr453Ala (pFHCOSCRS-1)	+

Figure 1.22 The complementary results of 12 Alanine mutants (amino acid sequence 441-453 of *S. cerevisiae* ERG7)

Experimental flowchart

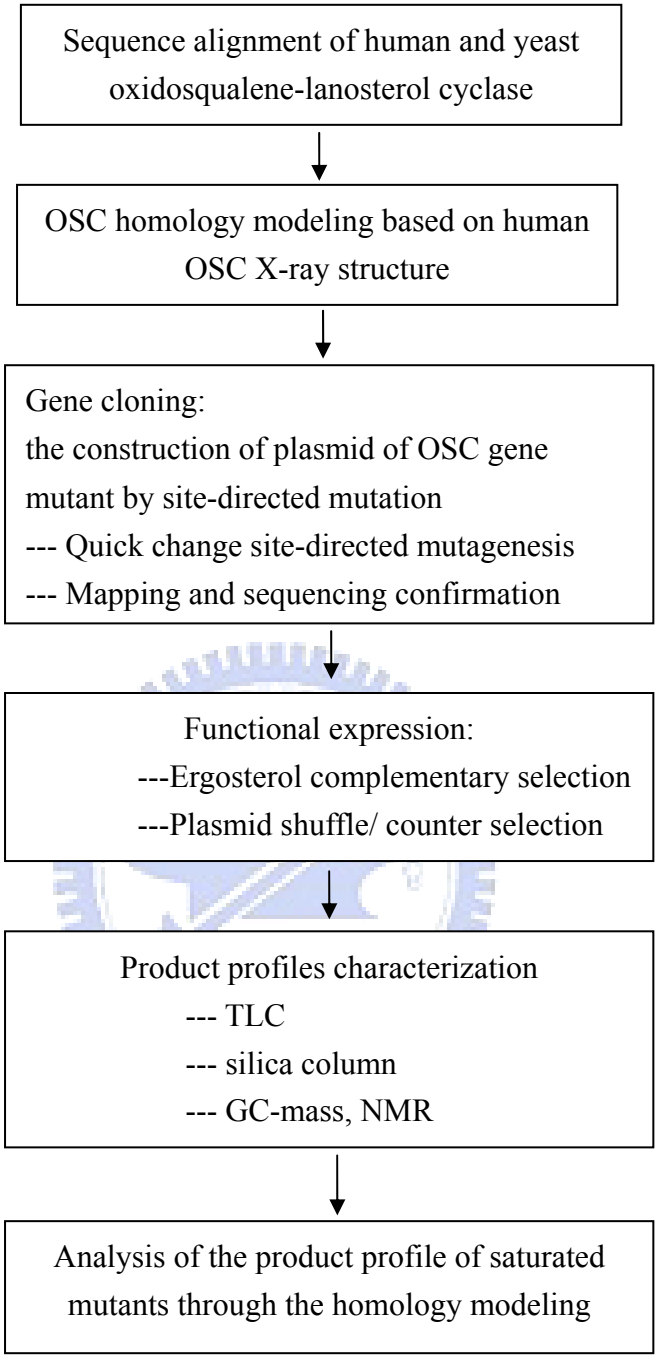

Figure 1.23 Overall experimental flowchart of this study.

Chapter2 Materials and Methods

2.1 Materials

Chemicals and reagents:

Acetic acid (Merck)
Acetic anhydride (Sigma)
Acetone (Merck)
Adenine (Sigma)
Agarose-LE (USB)
95% Alcohol (Merck)
Ampicillin sulfate (Sigma)
Anisaldehyde (Mecrk)
Bacto™Agar (DIFCO)
Bromophenol blue (USB)
Dichloromethane (Merck)
Dimethyl sulfoxide (MP Biomedicals)
DNA 10Kb Ladder (Bio Basic Inc., Tanwan)
D-Sorbitol (Sigma)
Ergosterol (Sigma)
Ethyl acetate (Merck)
Ethylenediamine-tetraacetic acid (Merck)
Ether (Merck)
G418 (Gibco)
Glycerol (Merck)
Glucose (Sigma)
Hemin Chloride (Merck)
Hexane (Merck)

Hisidine (Sigma)

LB Broth, Miller (DIFCO)

Lysine (Sigma)

Methanol (Merk)

Methioine (Sigma)

dNTP Set, 100mM Solutions (GE Healthcare)

Primers (Bio Basic Inc., Tanwan)

Potassium hydroxide (Merck)

Pyridine (Sigma)

Pyrogallol (Merck)

Restriction enzyme (New England BioLabs Inc.)

Sea sand (Merck)

Silica gel (Merck)

Silver nitrate (Merck)

Sodium sulfate (Merck)

Sulfonic Acid (Merck)

SYBR® Green I (Roche)

TLC plate (Mecrk)

Tris base (USB)

Trptophan (Sigma)

Tween 80 (Merck)

Trypton (DIFCO)

Yeast Extra (DIFCO)

Yeast Nitrogen Base w/o amino acid (DIFCO)

Uracil (Sigma)

Kits:

BigDye® Teminator v3.1 Cycle Sequencing Kit (Applied Biosystems)

GFX™ PCR DNA and Gel Band Purification Kit (GE Healthcare)

Plasmid Miniprep Purification Kit (GeneMark)

QuickChange Site-Directed Mutagenesis Kit (Stratagene Inc., La Jolla, CA)

Bacterial, yeast strains and vectors:

Escherichia coli XL-Blue (Novagen)

CBY57 (a yeast stain, MATa or MATα ERG7Δ:: LEU2 *ade*2-101 *his*3-Δ200 *leu2*-Δ1 *lys*2-801 *trp1*-Δ63 *ura3*-52 [pZS11])

TKW14C2 (a yeast stain, MATa or MATα ERG7Δ:: LEU2 *ade*2-101 *his*3-Δ200 *leu2*-Δ1 *lys*2-801 *trp1*-Δ63 *ura3*-52 *hem1*Δ::Kan^R)

Vector pRS314 (a shuttle vector with selection marker *Trp1*, New England BioLabs)

Equipments:

ABI PRISM® 3100 Genetic Analyzer (Applied Biosystems)

Allegra™ 21R Centrifuge (Beckman Coulter)

Avanti® J0E Centrifuge (Beckman Coulter)

Colling Circulator Bath Model B401L (Firstek Scientific)

Centrifuges 5415R (eppendorf)

DU 7500 UV-Vis Spectrophotometer (Beckman Coulter)

Durabath™ Water Bath (Baxter)

Electrophoresis Power Supply EPS 301 (GE healthcare)

EPSON® GT-7000 Scanner (EPSON)

GeneAmp® PCR System 9700 Thermal Cycler (Applied Biosystems)

Hoefer® HE 33 Mini Horizontal Submarine Unit (GE Healthcare)

Kodak Electrophoresis Documentation an Analysis System 120 (Kodak)

Orbital Shaking Incubator Model-S302R (Firstek Scintific)

Pulse Controller (BioRad)

Rotary Vaccum Evaporator N-N Series (EYELA)

Steritop^{TM} 0.22μm Filter Unit (Millipore)

Rotary vacuum evaporator N-N series (EYELA)

Orbital shaking incubator Model-S302R (First Scientific)

Solutions:

Ampicillin stock solution (100mg/mL)

Dissolve 1g ampicillin sulfate in 10 ml ddH_2O. Filter through 0.22μm pore size filter and stock at -20℃.

50X TAE buffer

Dissolve Tris base 242g, acetic acid 57.1 ml, and 0.5 M EDTA in 1L dH_2O and adjust to pH 8.5. Store it at room temperature. Dilute to 1X with dH_2O and adjust pH to 7.5~7.8 before use.

50X ALTHMU solution

0.2% Adeine, 0.3% Lysine, 0.2% Tryptophan, 0.2% Hisidine, 0.2% Methonine, 0.2% Uracil were dissolved in dH_2O and sterilized. Store at 4℃.

50X ALHMU solution

0.2% Adeine, 0.2% Lysine, 0.2% Hisidine, 0.2% Methonine, 0.2% Uracil was dissolved in dH_2O and sterilized. Store at 4℃.

50% Glucose solution

500g glucose was dissolved in 1L dH_2O and sterilized.

80% Glycerol solution

80 ml glycerol was added in 20 ml dH_2O and sterilized. Store at 4℃.

LB medium

25g LB Broth was dissolved in 1L dH_2O and sterilized.

LB plate

25g LB Broth and 20g Bacto^{TM} Agar was dissolved in 1L dH_2O and sterilized. The sterile LB agar was poured and dispersed in Petri dishes before it coagulates.

G418 stock solution (1g/mL)

Dissolve 500mg G418 in 500μl sterile dH_2O. Store it in darkness at 4℃.

SD medium

0.17% Yeast nitrogen base was dissolved in dH_2O and sterilized.

20% EA developing solution

Add 20ml ethyl acetate to 80ml hexane and mix it.

TLC staining solution

40ml of conc. H_2SO_4 is added (slowly!) into ethanol 800ml, followed by acetic acid 12ml and anisaldehyde 16ml.

1M sorbitol solution

182.2g D-sorbitol was dissolved in 500ml dH_2O and sterilized. Store at 4℃.

5X sequencing buffer

Dissolve 4.85g Tris base and 0.203g $MgCl_2$ in 100ml dH_2O and adjust to pH9. Store at 4℃.

10X SYBR Green solution

10000X SYBR Green was diluted to 10X with DMSO. Store it in darkness.

6X DNA loading dye

0.25% bromophenol blue and 30% glycerol were dissolved in ddH_2O. Store at -20℃.

Heme solution

0.5g hemin chloride was dissolved in 250ml 0.2N potassium hydroxide and thus mixes it with 250ml 95% alcohol in aseptic condition. Store it at room temperature in darkness.

Ergosterol supplement solution

1g Ergosterol was dissolved in 250ml 95% alcohol and thus mixes with 250ml Tween 80 in aseptic condition. Store it in darkness at room temperature.

ALHMU/Heme/Ergosterol plate

0.67g yeast nitrogen base, 2g Bacto™ Agar was dissolved in 100ml dH_2O and sterilized. Add 2ml 50X ALHMU solution, 4ml 50% glucose solution, 2ml heme solution, 2ml ergosterol supplement solution, and 100μl G148 stock solution into the sterile SD medium. Then the mixture was poured and dispersed in Petri dishes before it coagulates. All of steps are in aseptic condition and stock in darkness at 4℃.

2.2 Methods

2.2.1 The construction of recombinant plasmids:

The mutations of ERG7^{Tyr99X} and ERG7^{Trp443X} were constructed by *Site-directed mutagenesis strategies*: (Fig.2.1)

(1) **Primer design:**

YTL-OSC-Y99X-A1	P C Q X K G P I L M 5'-CCg TgT CAA NNN AAA ggg CCC ATg TTC ATg-3' *Apa I*
WSL-OSC-W443X-A1	K G A X G F S T K T E 5'-gA AAg ggg gCT NNN ggC TTC TCA ACA AAA ACC CAA ggC TAT ACA gTg g-3' *Sty* I G Y T V

Table 2.1 primer design for site-saturated mutagenesis

The gray background letters in the sequence line of primers show the target mutations, and "N" means A, T, C, G four bases, thereby 20 possible amino acids. The bold letter indicates silent mutation for *Apa* I or *Ban* I mapping analysis and construction are marked with underline. In addition, the recombination plasmids of ERG7^{Trp443X} have been constructed previously in our laboratory. In addition, the other primers for specific mutation are listed in Appendix 1.

(2) QuickChange PCR:

reagent	Volume(μl)
Template	0.4
Primer1 (1000ng/μl)	0.4
Primer2 (1000ng/μl)	0.4
10X pfu Buffer	2
dNTP (10mM)	1.4
DDW	15
Pfu polymerase	0.4

Table 2.2 QuickChange Site-Directed Mutagenesis Kit PCR composition

segment	cycles	temperature	time
1	1	95℃	2 min
2	18	95℃	30 sec
		50℃	1 min
		68℃	16min
3	1	4℃	∞

Table 2.3 QuickChange Site-Directed Mutagenesis PCR program

(3) *Dpn* I digest parental DNA template:

The digested reaction was incubated at 37℃ for 3 hours to digest the parental supercoiled DNA.

reagents	Volume (μl)
PCR products	17
10× NE Buffer 4	1
DDW	1
DpnI	1

Table 2.4 QuickChange Site-Directed Mutagenesis PCR products diegestion

(4) Transformation into XL1-Blue and enzyme mapping

The digestion of QuickChange products were added into 100μl *E. coli* XL1-Blue competent cells of each reaction and incubated on ice for 20 min. The cells were transformed by heatshock methods for 1 min at 42℃, following 1 min on ice. Then the cells were transfered to 1ml Luria-Bertani (LB) medium immediately and then shaken in 200 rpm for 1 hour at 37℃ incubator. Then, the cells were centrifuged at 8,000 rpm for 1 min and propagated on LB plate containing 100μg/ml ampicillin (LB_{amp}). Incubate these plates overnight at 37℃. Pick the colonies and culture in 3ml LB medium containing 100μg/ml ampicillin overnight at 37℃. The plasmid DNAs were isolated by Plasmid Miniprep Purification Kit, according to the manufacturer instructions. The plasmid DNAs were then digested with *Apa I* for $ERG7^{Tyr99X}$ mutants and *Ban I* for $ERG7^{Trp443X}$ mutants to confirm the presence of the mutations.

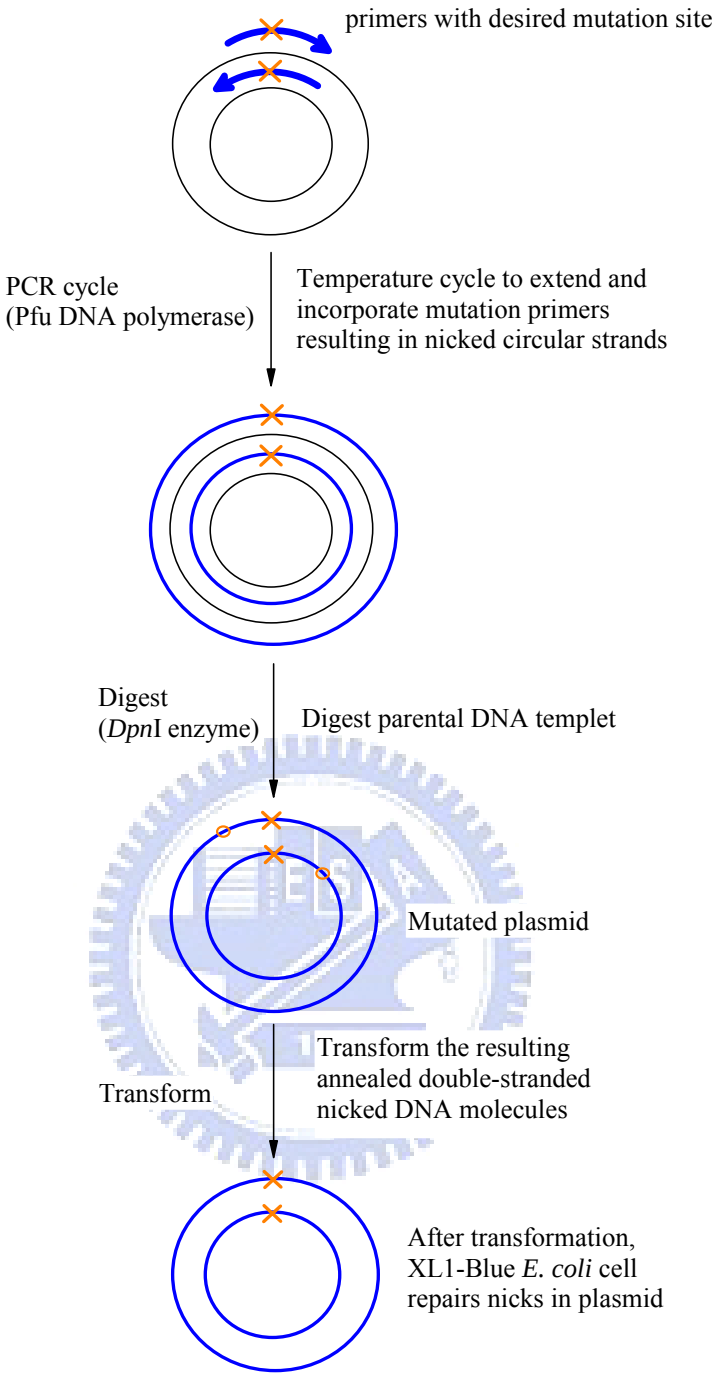

Figure 2.1 QuickChange Site-Directed Mutagenesis Kit

(5) Sequencing analysis of ERG7^{Tyr99X} and ERG7^{Trp443X} mutated genes

The exact amino acid substitution at Tyr99 and Trp443 positions were determined by sequencing of the DNA using ABI PRISM 3100 auto-sequencer. Nucleotide sequencing was performed using the dideoxynucleotide chain-termination method with only one forward of reverse primers (described on Appendix 1). Sequencing reactions were carried

out with BigDye® Terminator v3.1 Cycle Sequencing Kit, according to the manufacturer protocol. Briefly, each of sample was performed with 1μl each forward or reverse primer (Appendix 1), 2μl plasmid DNA, 3μl 5X sequencing buffer, 1μl premix and ddH_2O to create a final volume of 20μl. The each of reaction was performed on the ABI PRISM® 3100 Genetic Analyzer, following the manufacturer's guidelines.

2.2.2 Preparation of competent cell (CBY57 and TKW14C2)

Pick the yeast TKW14C2 stock into the 3ml SD medium, containing 60μl 50X ALTHMU solution, 120μl 50% Glucose solution, 60μl heme solution and 60μl ergosterol solution and then incubated at 30℃ for two to three days. Transferred the cells to 100ml SD medium with the same condition and incubated at 30℃ for 12-18 hours. After OD_{600} of yeasts reaches 1.0~1.5, the cells were centrifuged to collect at 3,000rpm, 10min at 4℃ and the supernatant was discarded. Add 35mL aseptic ddH_2O to resuspend the pellet and centrifuge it at 3000 rpm, 10min at 4℃ repeated two times. Then add 25ml 1M D-sorbitol solution to resuspend the pellet and centrifuge it at the same condition. Finally, add n*50 μL 1 M D-sorbitol into the pellet and resuspend it gentlemanly on ice for 5 min. The volume of 50μl competent cells was added into each of 1.5ml microtube with 5μl recombinant plasmids, respectively. The preparation protocol of yeast CBY57 is the same as above mention except the yeast growth medium are ALHU solution and Glucose solution.

2.2.3 Plasmid shuffle and counter selection (expression mutated ERG7 gene in yeast strain CBY57)

The pRS314-derived ERG7 mutated plasmids were electroporated into a cyclase-deficient yeast haploid strain CBY57[PZS11]. The pRS314 plasmids, TRP1 centrometric plasmids with no insert and the wild-type *S. cerevisiae* ERG7 gene, were

plated on SD+Glu+ALH+1M sorbitol medium at 30℃ for two or three days to determine the presence of both PZS11 and pRS314-derived plasmids. Individual colonies were grown in 10ml SD+Glu+ALHU liquid culture. Aliquots of 100μl of each culture were plated on the SD+Glu+ALHU and SD+Glu+ALHU+1mg/ml 5-FOA (5-fluoroorotic acid) medium and grown at 30℃ for two or three days to elucidate the complementation effect. Colonies that grew on the non-5-FOA plates, but not on 5-FOA plates, were grown separately in SD+Glu+ALHU liquid medium for mutant plasmid characterization. Expression of the pRS314 and pRS314WT (pRS314-ERG7) in the same strain were treated as negative and positive control, respectively.

2.2.4 Ergosterol complementation (expression mutated ERG7 in yeast strain TKW14C2)

The pRS314-derived plasmids were transformed into TKW14C-2 by electroporation using a GenPulser (BioRad, Hercules, CA). The pRS314 and pRS314-ERG7 gene plasmids were transformed as negative and positive controls respectively. The resulting transformants were plated onto SD+Glu+ALHMU+hemin+G418+Erg plates, and incubated at 30℃ for three to five days to select for presence of pRS314-derived plasmids. The transformants were grown overnight in 3ml SD+Glu+ALHMU+hemin+G418+Erg at 30℃. Aliquots of 100ml of each culture were plated on SD+ Glu+ALHMU+hemin+G418+Erg and the same as the front medium but without additive ergosterol solution, then both incubated at 30℃ for three to five days to confirm the complementation effect. Expression of the pRS314 and pRS314WT in the same strain were treated as negative and positive control.

2.2.5 Extracting lipids and column chromatography

In the small scale incubation, the mutant transformants were grown in the 2.5l SD liquid culture medium containing Glu+ALHMU+hemin+Erg medium at 30℃ with 220 rpm shaking for five days. The cells were harvested by centrifugation at 6000 rpm for 10 minutes. The pallets were resuspending in the solution containing 100ml ethanol, 100ml 30% KOH, 0.2g pyrogallol. This reaction was refluxed at 110℃ for 3 hours. The hydrolysate was extracted three times with total 600ml petroleum ether, the organic phase were collected and dehydrated by sodium sulfate and concentrated using a rotary evaporator. The small amount of nonsaponofiable lipid (NSL) was dissolved CH_2Cl_2 and the solutions were spotted on the thin-layer chromatography and developed with 4:1 hexane/ethyl acetate. The TLC plates were subjected to the stain buffer (5% Annisaldehyde, 5%H_2SO_4 in ethanol) and heated until the patterns appeared.

In order to fractionate the different products pattern in these mutates, 60L of mutant culture was harvested by centrifugation, washed, and saponified by refluxing them in 30%KOH and 50% ethanol for 3 hours. The petroleum extract was fractionated by silica gel column chromatography using 19:1 hexane/ethyl acetate mixture. The products were obtained that migrated between the following: oxidosqualene and lanosterol, lanosterol-positioned and ergosterol compounds. The fraction were assayed by GC-MS and examined for triterpene products with a molecule mass of m/z = 426.

2.2.6 Acetylating modification and argentic column chromatography

The acetylation modification of the triterpene alcohol fraction was performed according the previous literatures.[64] The dry triterpene alcohol fraction was first dissolved in 2ml pyridine solvent, and then excess amount of 10 mM acetic anhydride was added into solution. The solution was stirred overnight at room temperature. The acetylation reaction was monitored by TLC analysis. After 16 hours, 5ml of water was added to

terminate the reaction and three times extraction with 10ml CH_2Cl_2 were carried out. The total organic phase was collected and dried over with sodium sulfate, then evaporated in a rotary evaporator.

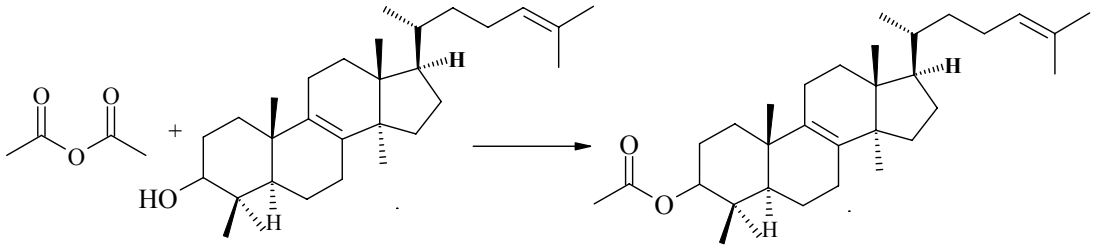

Figure 2.2 The acetylation modification

2.2.7 $AgNO_3$-impregnated silica gel chromatography

8.6g AgNO3 and 25g silica gel dissolved in 50ml water, stirred and kept them away from light in the oven under 110℃ for 16 hours. The gel was used to pack the column with hexane. The acetylated products were fractioned by AgNO3-impregnated silica gel chromatography using 3 % diethyl ether in hexane.[65-67] According to silver ion TLC (0.8g AgNO3 dissolved in methanol). The TLC were moistened by this aliquot then heated on the hot plate to dry, and repeated thrice.) and GC-MS, the single compound was collected. The products were identified using 600 MHz NMR.

2.2.8 Deacetylation reaction of the modified compounds

The dry acetylation triterpene fraction was dissolved in 10 ml methanol, and 0.5g potassium hydroxide (KOH) was added into the reaction. The reaction was performed with the closed system in the hood and stirred for 12-16 hours at room temperature. The deacetylation reaction was monitored by TLC analysis. After 16 hours, the reactant was dried by rotary evaporator and then 10 ml water was added to dissolve potassium hydroxide. The deacetylated products were thrice extracted with dichloromethane. The total organic phase was collected and dried over with anhydrous sodium sulfate (Na_2SO_4),

and then dried thoroughly in a rotary evaporator. The deacetylated products were separated by silica gel column chromatography using 19:1 hexane/ethyl acetate mixture. The structure of finally novel products were characterized and identified by NMR spectroscopy (^{1}H, ^{13}C, DEPT, COSYDEC, HSQC, HMBC, and NOE).

2.2.9 GC-MS column chromatography condition

GC analyses were performed with a Hewlett-Packard model 5890 series Ⅱ or Agilent 6890N chromatography equipped with a DB-5 column (30 m x 0.25 mm I.D., 0.25 μm film; oven gradient at 50°C for 2 min, and then 20°C per min until 300°C, held at 300°C for 20 min, 300°C injector; 250°C interface; 1/40 split ratio using helium carrier gas at 13 psi column head pressure). GC/MS was performed on a Hewlett-Packard model 5890 II GC (J & W DB-5MS column, 30 m x 0.25 mm I.D., 0.25 μm film; oven 280°C, injector 270°C, GC-MS transfer line: 280°C) coupled to a TRIO-2000 micromass spectrometer.

2.2.10 Molecular modeling

Molecular-modeling studies were using the Insight II Homology program with the X-ray structure of lanosterol-complexd human OSC as the template. The MODELER program is designed to extract spatial constraints such as stereochemistry, main-chain and side-chain conformation, distance, and dihedral angle from the template structure. The resulting structure was optimized using an objective function that included spatial constraints and a CHARMM energy function. The objective function combines free energy perturbation, correlation analysis, and combined quantum and molecular mechanics (QM/MM) to obtain a better description of molecular level structure, interactions, and energetics. The homologous model structure, with the lowest objective function, was evaluated further using the Align2D algorithm for sequence-structure alignment.[68, 69]

2.2.11 Quantum mechanical calculations protocol

The preliminary chemical structure construction was built with Chemical Office and then the G03's input file was also created. The GaussView was used to check the stereochemistry or geometry of these compound chemical structures. Geometry optimization and single point energies minimum was then calculated by Gaussian 03 at the RHF approach (quantum mechanical method). The calculation basis sets used for optimization are from HF/3-21G, B3LYP/3-21G to B3LYP/6-31G. In each basis sets, the calculation was completed until the stationary point found and the force items were converged. The positive value of individual vibration frequencies were obtained via the final basis set, b3lyp/6-31g* geom=check guess=read scf(maxcycle=999) freq(noraman) opt(maxcycle=100). These value represented the optimized structure are under the single point energies minimum. The relative energy to oxidosqualene state was measured with other chemical under energy minimum states.

Chapter3 Results and Discussion

3.1 Functional analysis of ERG7^{Tyr99} within *S. cerevisiae*

3.1.1 Generation of site-saturated mutants of ERG7^{Tyr99X}

Tyrosin99 of the *S. cerevisiae* ERG7 gene was substituted with other 19 amino acids using QuickChange site-directed mutagenesis strategy with the respective mutagenic primers. A silent mutation was concomitantly introduced to easily screen the desired mutants, according to a restriction enzyme (*Apa I*) mapping check. The positive mutants were digested into three fragments including 4.7, 2.6 and 0.57kbp comparing with the wild type plasmids pRS314OSC which was digested into two fragments 4.7kbp and 3.1kbp. The DNA agarose gel electrophoresis of the mapping results were shown in Appendix 2. The presence of the mutations was verified by sequence determination.

Following the confirmation of the amino acid substitutions at the Tyr99 position, the recombinant plasmids were transformed into yeast TKW14C2 strain (MATa or MATα ERG7Δ:: LEU2 *hem1*Δ::G418 *ade*2-101 *his*3Δ-200 *leu*2-Δ1 *lys*2-801 *trp1*-Δ63 *ura3*-52) which bears genomic HEM1 ERG7 double-knockout and eliminates the pZS11 plasmid but maintains cell viability via uptake of exogenous ergosterol from the media. Besides, the biosynthesis of methionine is blocked because of the losing *Heme* gene. So methionine was added in the media. The recombinant yeast could be viable by way of the supply with exogenous ergosterol or complement with oxidosqualene cyclase activity derived from ERG7^{Y99X}. (Fig. 3.1) The genetic selection demonstrated that TKW14C2[pERG7^{Y99X}] mutants allowed for ergosterol-independent growth, except for the Y99 deletion as well as the Y99N and Y99H mutations.(Tab. 3.1) This results indicated a functional role of Tyr99 in catalysis or structural stabilization.

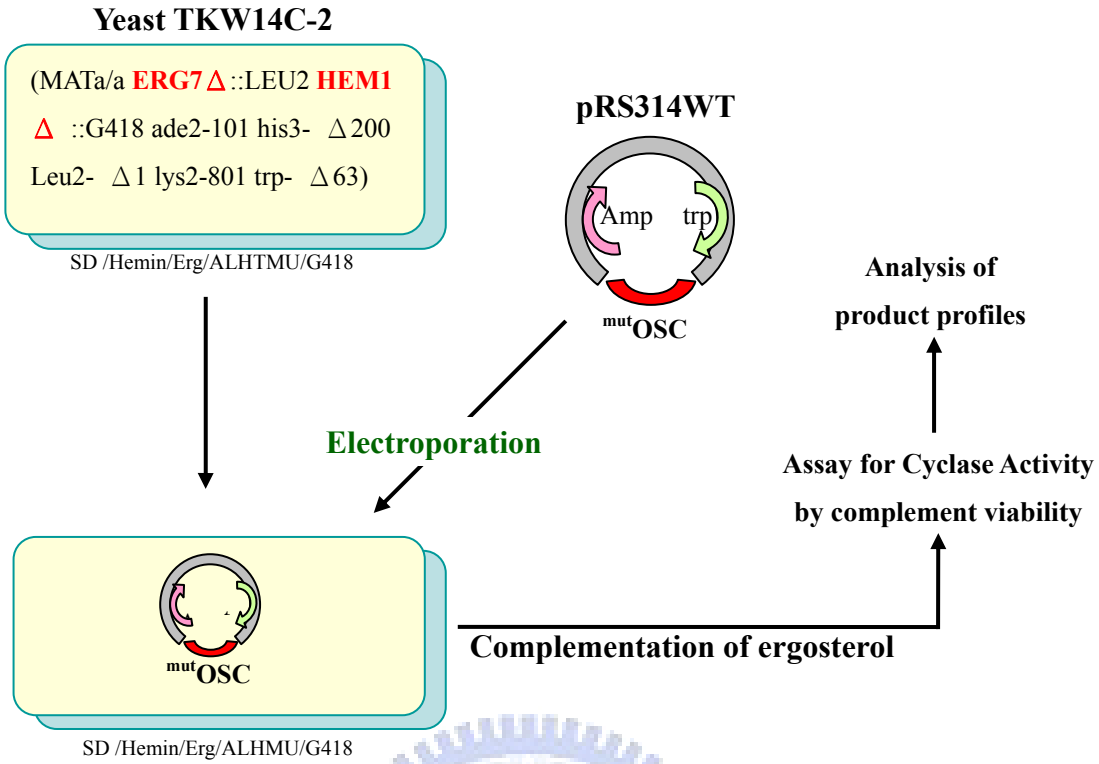

Figure 3.1 The strategy of ergosterol complement selection.

Next, each mutant, no matter the cell viability in the yeast deficient strain, was applied to the small scale liquid incubation and harvest. The small amount of recombinant yeast (2.5L culture mediums) was collected and the nonsaponifiable lipid (NSL) extract was prepared and analyzed by GC-MS. The nonsaponifiable lipid was dissolved in CH_2Cl_2 and spotted on the thin-layer chromatography developed with 20% EA/Hexane. The TLC plates were stained to observe the products pattern. The lanosterol presented in the TLC plate and oxidosqualene and ergosterol, was also observed. With silica gel chromatographic purification, the lanosterol fraction, which means the same position with lanosterol on the TLC plate, was collected following the analysis by the GC-MS and compared with those of authentic sample. Nine $ERG7^{Y99X}$ mutants including each substitution of Gly, Ala, Ile, Asp, Glu, Ser, Thr, Phe and Pro revealed and examined for three triterpenoid products with a molecule mass of *m/z* = 426: lanosterol and two novel products. (Tab.3.1)

OSC^{mut}		Enzyme mapping	Ergosterol supplement	TLC, GC-MASS analysis		
				No product	**Lanosterol**	**Novel products**
Aliphatic group	Y99**Gly** (G)	*Apa* I	+	-	V	V
	Y99**Ala** (A)		+	-	V	V
	Y99**Val** (V)		+	-	V	-
	Y99**Leu** (L)		+	-	V	-
	Y99**Ile** (I)		+	-	V	V
Acidic and amide group	Y99**Asp** (D)		+	-	V	V
	Y99**Asn** (N)		—	V	-	-
	Y99**Gln** (Q)		+	-	V	-
	Y99**Glu** (E)		+	-	V	V
Basic group	Y99**His** (H)		—	V	-	-
	Y99**Lys** (K)		+	-	V	-
	Y99**Arg** (R)		+	-	V	-
Hydroxyl-group	Y99**Ser** (S)		+	-	V	V
	Y99**Thr** (T)		+	-	V	V
Sulfur-containing	Y99**Cys** (C)		+	-	V	-
	Y99**Met** (M)		+	-	V	-
Aromatic group	Y99**Phe** (F)		+	-	V	V
	Y99**Trp** (W)		+	-	V	-
	Y99 (wild type)		+	-	V	-
Imino	Y99**Pro** (P)		+	-	V	V
Deletion Y99			—	V	-	-

Table 3.1 The results of ERG7^{Y99X} ergosterol complement selection.

3.1.2 The characterization and identification of novel products

In order to collect products for identification, 58L of mutant yeast were grown and the NSL was extracted, and the products with *m/z* = 426 were further acetylated for increasing the polarity differences between each other and spotted on the $AgNO_3$-impregenated TLC.(Fig.3.2)

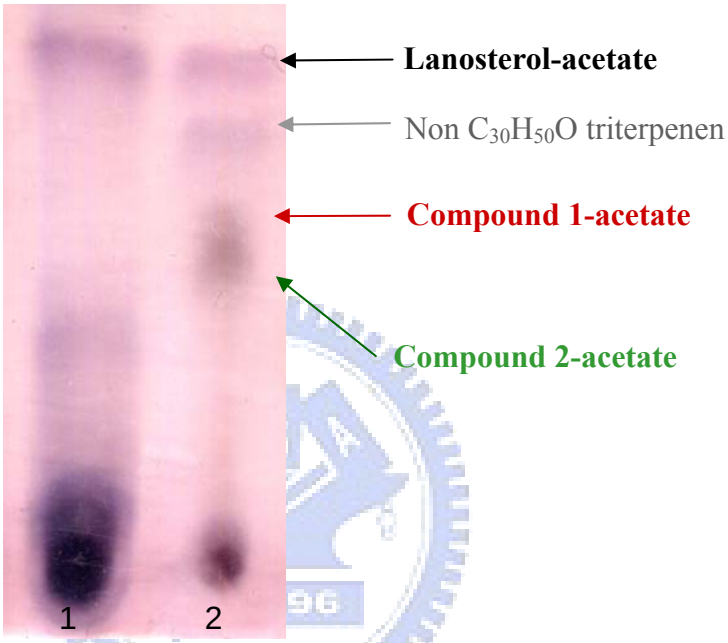

Figure 3.2 Separation of lanosterol fraction on $AgNO_3$-impregenated TLC. Lane 1 is acetylated lanosterol standard; lane 2 is the acetylation crude of lanosterol fraction.

Each single compound was isolated by $AgNO_3$-impregenated silica gel column chromatography by using 3~15% diethyl ether in hexane and subsequently applied for deacetylation as previously described (sections 2.2.7-2.2.8).

GC and GC-MS analysis

Further GC-MS-based product analysis of the lanosterol-positioned product, revealed three triterpenoid products with a molecule mass of *m/z* = 426: lanosterol and two novel products, compound 1 and 2. Compound 1 migrated on the GC column with a retention time of 0.2 min relative to compound 2. (Fig. 3.3 and Fig. 3.4)

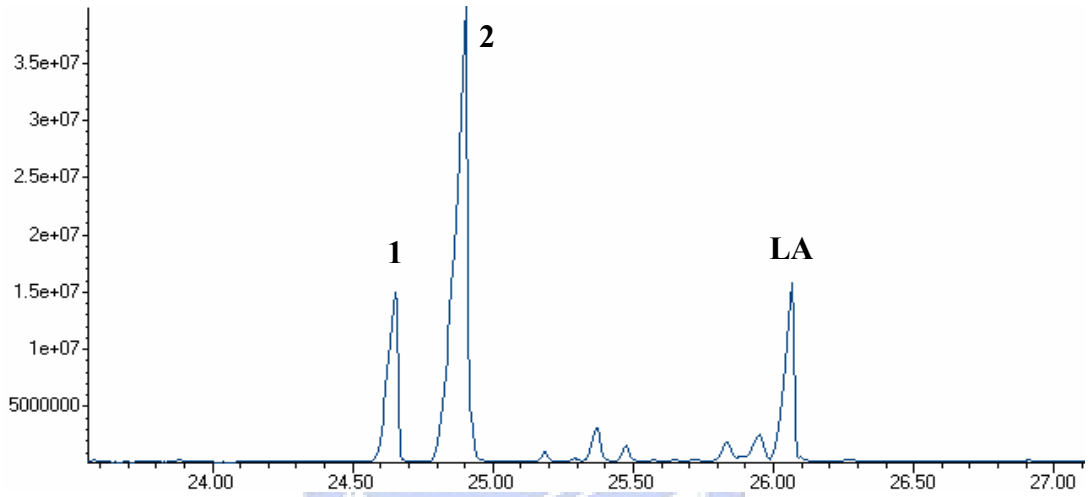

Figure 3.3 GC analysis of the NSL extracts derived from ERG7^{Y99Thr}. Peak 1 indicates compound 1; peak 2 is compound 2; LA means lanosterol. The other peaks which are not marked are not triterpenen products with *m/z* = 426.

The EI mass spectrum showed that both of novel products had the same molecular ion at *m/z* = 426 and exhibited similar fragment peaks at 357, 339, and 247, corresponding to the molecular formula $C_{30}H_{50}O$ ($[M]^+$), $[M\text{-}C_5H_9]^+$, $[M\text{-}C_5H_9\text{-}H_2O]^+$, and $[M\text{-}C_{13}H_{21}\text{-}H_2]^+$, respectively. Therefore, we suggested both of them might be mass the incompleted cyclization products. (Fig. 3.4)

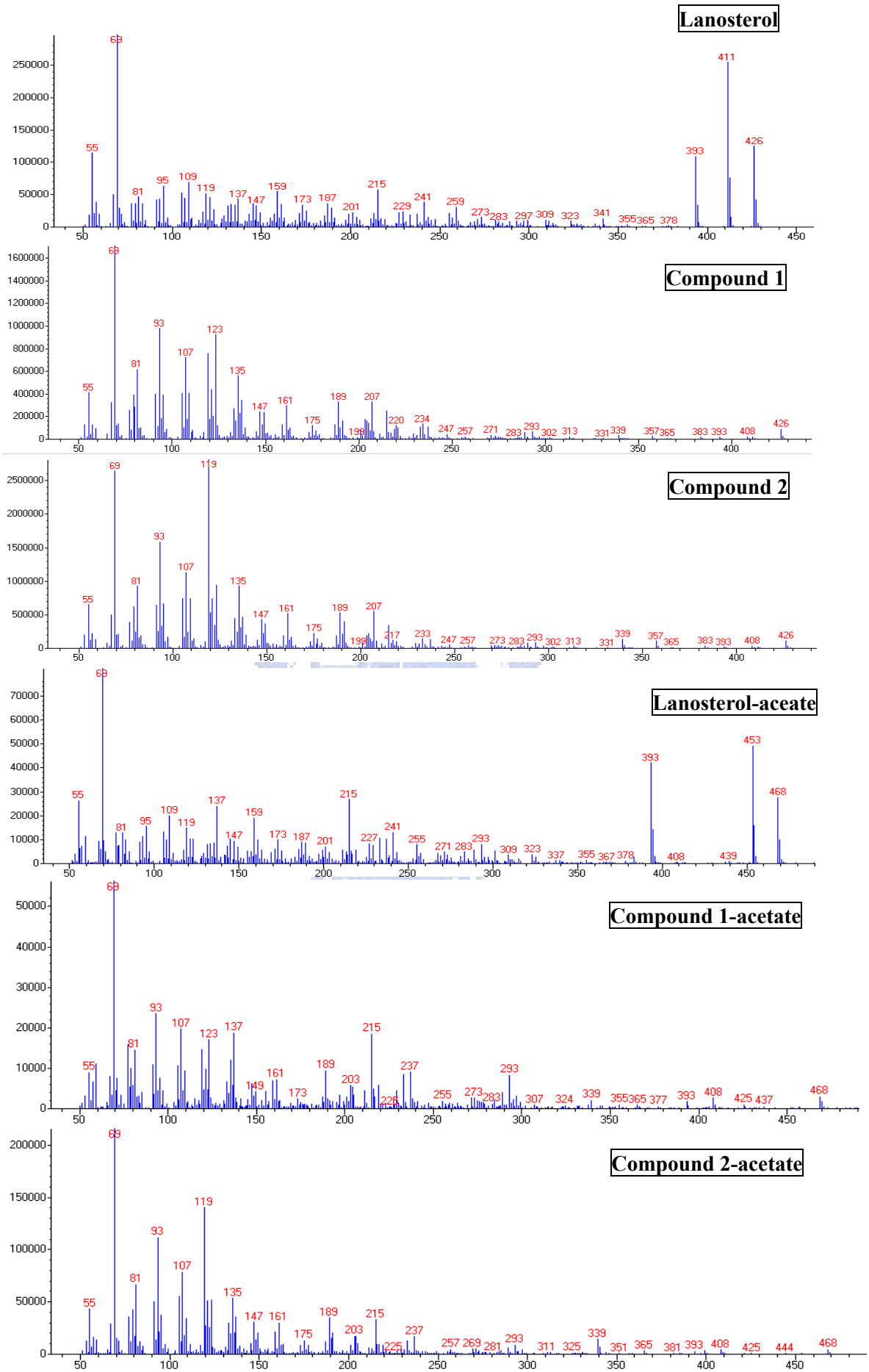

Figure 3.4 Electron-impact mass spectra of two novel products and acetylated forms derived from ERG7^{Y99Thr}.

The product profiles of each mutant are summarized in Table 3.4. No products with molecular masses of m/z = 426 were observed for inactive mutants, ERG7^{Y99N}, ERG7^{Y99H} and ERG7$^{\Delta Y99}$, consistent with the genetic selection results. On the other hand, the viable mutants produced either lanosterol alone (Y99V, Y99L, Y99Q, Y99K, Y99R, Y99C, Y99M, and Y99W) or lanosterol and two novel products (the substitutions of G, A, E, S, T, P). Additionally, the compound 2 was a major product among those ERG7^{Y99X} mutants that produced three compounds (lanosterol, compound1 and 2).

amino acids substitution	Products profile ratio (%)			
	no products	conpound 1	compound 2	lanosterol
Gly		13	58	29
Ala		17	70	13
Val				100
Leu				100
Ile		17	33	50
Asp		8	5	87
Asn	V			
Gln				100
Glu		0	44	56
His	V			
Lys				100
Arg				100
Ser		13	69	18
Thr		21	59	20
Cys				100
Met				100
Phe		6	4	90
Trp				100
Pro		28	51	21
ΔY99	V			

Table 3.2 The products profile of *S. cerevisiae* TKW14C2 expressing the ERG7^{Y99X} site-saturated mutagenesis.

NMR spectral analysis

Firstly, compound 2 was characterized to be tricyclic triterpene preliminarily through ^{1}H NMR and DEPT (Fig. 3.5); these correlations showing in the figure 3.5 suggested the involvement of a tricyclic ring skeleton. Then the structures were subsequently identified following the analysis by nuclear magnetic resonance (^{1}H, ^{13}CNMR, DEPT, ^{1}H-^{1}H COSY, HMQC, HMBC, and NOE) and comparison with those of authentic sample. All of the related NMR spectra were shown in Appendix 3.

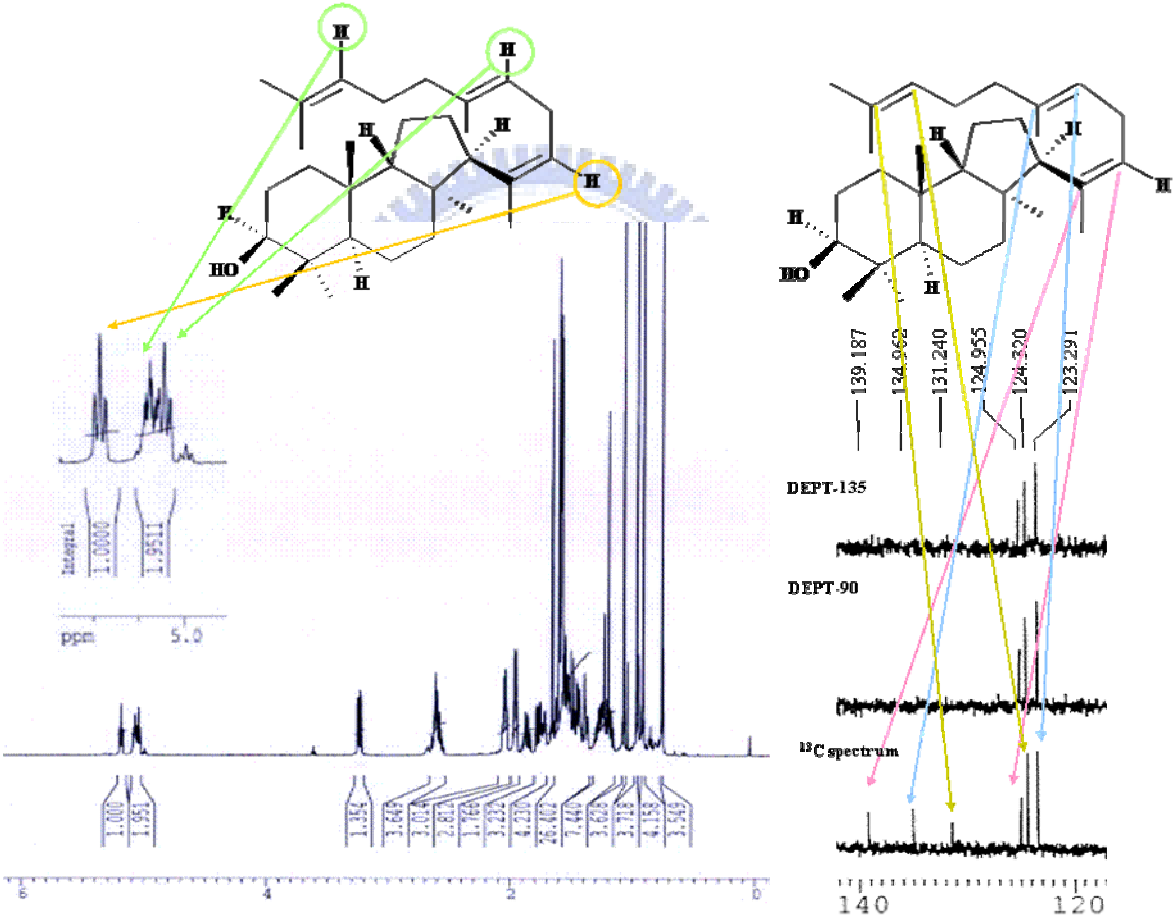

Figure 3.5 The major features of compound 2 in ^{1}H NMR and DEPT spectrum. ^{1}H NMR shows distinct chemical shifts with four vinylic methyl signals (δ 1.657, 1.600, 1.584 and 1.577), four methyl singlets (δ 1.072, 0.964, 0.918 and 0.763), and three sets of triplet alkene protons (δ 5.186, 5.076 and 5.043). DEPT revealed the presence of three tertiary-quaternary substituted double bonds (δ = 124.34-131.32, deep yellow arrows; 123.30-134.77, light blue arrows and 126.77-137.80, magenta arrows), which are characteristics of double bonds at the exocyclic hydrocarbon side chains.

Compound 2 was identified by NMR spectroscopy as (13α*H*)-isomalabarica-14*Z*, 17*E*, 21-trien-3β-ol, a chair-boat (C-B) 6-6-5 tricyclic product with trans-syn-trans stereochemistry and $\Delta^{14Z,\ 17E,\ 21}$ double bonds. (Fig.3.4, 3.5, 3.6 and Tab. 3.3)

(13α*H*)-Isomalabarica-14*Z*, 17*E*, 21-trien-3β-ol

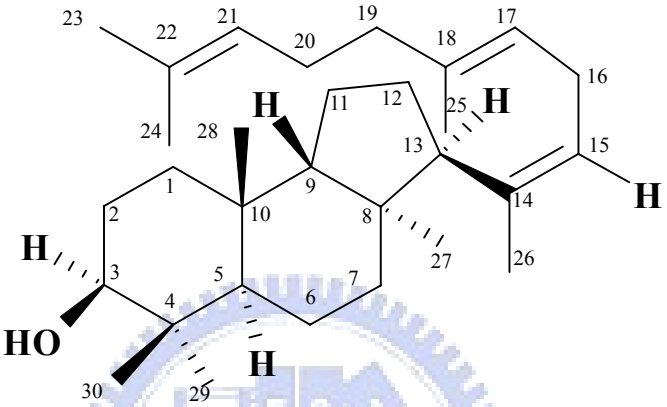

Figure 3.6 The structure of compound 2.

No.	^{13}C	^{1}H	No.	^{13}C	^{1}H	No.	^{13}C	^{1}H
1	33.82	1.45(β),1.38(α), m	11	21.17	1.56(β), 1.44(α), m	21	124.34	5.06, m
2	29.16	1.75,(α) 1.62(β), m	12	25.27	1.86(α), 1.55(β), m	22	131.32	-
3	79.53	3.20, (dd, J=11.59, 5.06Hz)	13	50.75	2.58-2.62, m	23	25.70	1.66, s
4	39.07	-	14	137.80	-	24	17.67	1.58, s
5	47.63	1.49	15	126.77	5.18, t	25	16.11	1.58, s
6	18.79	1.53(α), 1.51(β), m	16	26.92	2.58-2.62 m	26	22.21	1.60, s
7	32.50	1.75	17	123.30	5.03, m	27	29.93	1.07, s
8	44.15	-	18	134.76	-	28	23.10	0.92, s
9	54.41	1.56	19	39.66	1.97, 2.04, m	29	29.11	0.96, s
10	35.64	-	20	29.70	1.97, 2.04, m	30	15.93	0.76, s

Table 3.3 NMR assignments for (13α*H*)-isomalabarica-14*Z*, 17*E*, 21-trien-3β-ol for dilute $CDCl_3$ solution. Spectra were referenced to tetramethylsilane (TMS) at 0 ppm (^{1}H) or $CDCl_3$ at 77.0 ppm (^{13}C).

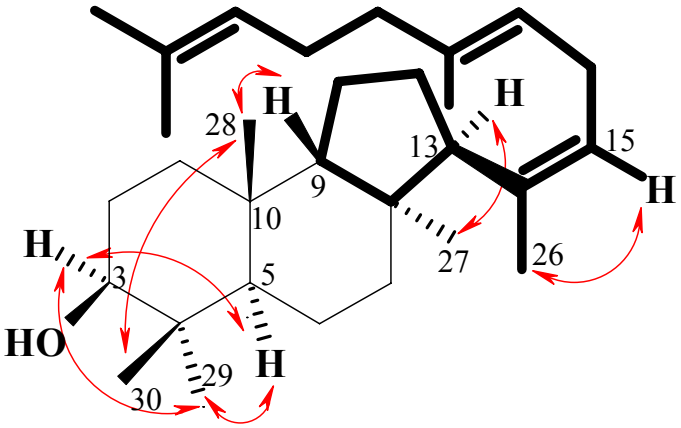

Figure 3.7 Bond connectivity and stereochemistry of (13α*H*)-isomalabarica-14*Z*, 17*E*, 21-trien-3β-olestablished by HMBC/HSQC (▬) and NOEs (⟷) spectrums.

The presence of NOEs among H-3/Me-29, Me-30/Me-28, Me-29/H-5, H-3/H-5, Me-28/H-9, H-15/Me-26, and Me-27/H-13 while the absence of NOEs among Me-27/Me-28, Me-27/H-9, H-9/H-13, Me-28/H-5, and H-13/H-5, were uniquely consistent with the stereochemistry of the C-B 6-6-5 tricyclic nucleus and the Z conformation for a double bond between C-14 and C-15. (Fig. 3.7)

It is more difficult to purify and isolate the other novel product, compound 1, because of its less quantity in the ERG7^{Y99X}. Fortunately, we found that both of compound 1 and 2 were also produced in the mutant of ERG7^{F699Met} (carried out by Hao-Yu Wen). Compound 1 exhibited similar parent peak and fragment peak patterns to the previously identified (13α*H*)-isomalabarica-14*Z*, 17*E*, 21-trien-3β-ol in EI mass. We suggested that it might be an analogous nucleus skeleton of incomplete cyclization. Furthermore, the ^{1}H-NMR spectra also showed four distinct vinylic methyl signals (δ 1.662, 1.605, 1.582 and 1.511), four methyl singlets (δ 1.044, 0.956, 0.912 and 0.756), and three alkene protons (δ 4.997, 5.081 and 5.094), supposing a tricyclic ring skeleton. (Appendix 3)

Via correlating with ^{13}C-NMR, HMQC, HMBC, 1H-1H COSY and NOE spectra, compound 1 was determined to be (13α*H*)-isomalabarica-14*E*, 17, 21-trien-3β-ol, a tricyclic product with trans-syn-trans stereochemistry and $\Delta^{14E,\ 17E,21}$ double bonds. It is structurally similar to compound 2 with differences only in the stereochemistry of the carbon double bond located at the C-14/C-15 position (Fig 3.8 and 3.9, Tab. 3.4).

(13α*H*)-isomalabarica-14*E*, 17*E*, 21-trien-3β-ol

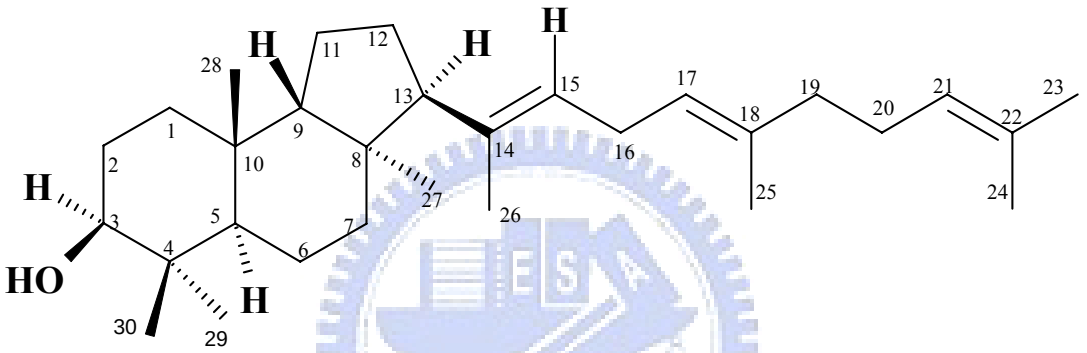

Figure 3.8 The structure of compound 1.

No.	^{13}C	^{1}H	No.	^{13}C	^{1}H	No.	^{13}C	^{1}H
1	34.11	1.37(α), 1.39(β), m	11	20.90	1.37(α), 1.53(β), m	21	124.33	5.07, m
2	29.16	1.62(β), 1.75(α), m	12	26.91	1.53(β), 1.88(α), m	22	131.29	-
3	79.52	3.23, (dd J= 11.69, 5.01 Hz)	13	59.51	2.05, m	23	25.67	1.66, s
4	39.06	-	14	139.19	-	24	17.66	1.58, s
5	47.03	1.49	15	124.96	4.99, t	25	16.09	1.60, s
6	18.62	1.21(β), 1.53(α), m	16	26.99	2.68, m	26	18.08	1.55, s
7	31.15	1.18(β), 1.62(α), m	17	123.29	5.09, m	27	29.74	1.04, s
8	44.51	-	18	134.96	-	28	23.15	0.91, s
9	52.95	1.51	19	39.66	1.96, 2.06	29	29.88	0.95, s
10	35.37	-	20	26.75	1.96, 2.06	30	15.91	0.75, s

Table 3.4 NMR assignments for (13α*H*)-isomalabarica-14*E*, 17*E*, 21-trien-3β-ol for dilute $CDCl_3$ solution. Spectra were referenced to tetramethylsilane at 0 ppm (^{1}H) or $CDCl_3$ at 77.0 ppm (^{13}C).

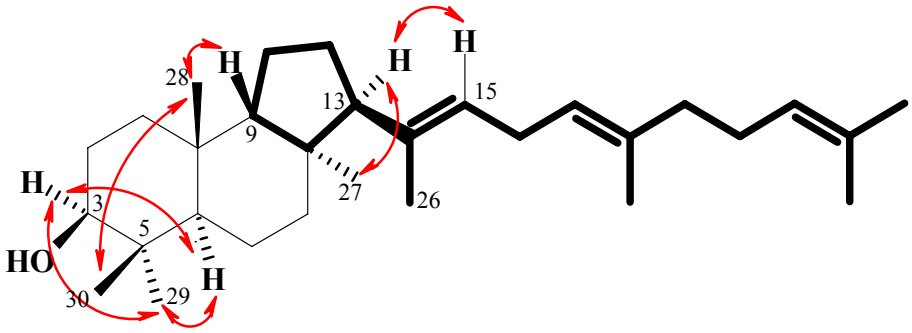

Figure 3.9 Bond connectivity and stereochemistry of (13α*H*)-isomalabarica-14*E*, 17, 21-trien-3β-ol established by HMBC/HSQC (▬) and NOEs (⟷) spectrums.

The presence of NOEs among Me-29/H-3, Me-29/H-5, Me-30/Me-28, Me-28/H-9, Me-27/H-13, and H-13/H-15, as well as the absence of NOEs between Me-30/H-3, Me-28/Me27, H-13/H-9, H-13/Me-26, and H-15/Me-26, indicate the α–orientation for H-13 and *E*-conformation for a double bond between C-14 and C-15.

These two compounds exhibited very similar structures with the previously isolated (13α*H*)-isomalabarica-14(26), 17*E*, 21-trien-3β-ol, which abstracts the C-26 proton after generating a tricyclic C-14 cation. We suggested that it resulted from a direct trapping of the common C-B 6-6-5 tricyclic Markovnikov C-14 cation but with a different deprotonation position and stereochemistry.[44,47,63]

3.1.3 Proposed cyclization/rearrangement pathways of TKW14C2 expressing ERG7^{Y99X}

Two truncated tricyclic products and the tetracyclic lanosterol were formed during the mutagenesis of Tyr99 in ERG7. In the view of the cyclization/rearrangement mechanism, the protonated epoxide of oxidosqualene initiates the formation of carbocation, following the rings annulations via cation-π interaction to a Markovnikov-favored 6-6-5 tricyclic C-14 cation without disruption at either monocyclic or bicyclic cationic location. Afterwards, the (13α*H*)-isomalabarica-trien-3β-ols form from elimination of proton at C-15 or C-26. Alternatively, C-ring has a process of ring expansion via a shift of the Markovnikov tertiary cation at the C-14 position to the anti-Markovnikov secondary cyclohexyl carbocation at the C-13 position, and then D-ring closure generates the protosteryl C-20 cation. Subsequently, a series of hydride and methyl group rearrangement generated the lanosteryl C-8/C-9 cation. Finally, a highly specific deprotonation abstracted the proton, which was either originally at C-9 or following the shift of the hydride from the C-9 to C-8 position, yields lanosterol. (Fig. 3.10)

To our surprise, none of truncated monocyclic, bicyclic intermediates, and (13α*H*)-isomalabarica-14(26),17,21-trien-3β-ol[44,47,63] were produced in the ERG7^{Y99X} mutants. The formation of the truncated cyclization intermediates by the ERG7^{Y99X} mutants implies that the Tyr99 in ERG7 plays a crucial role in the generation of tricyclic intermediates but not in promoting the boat conformation for lanosterol B-ring formation. To probe into the reactivity, Tyr99 may be involved in the stabilization of the Markovnikov tricyclic cation and/or the subsequently alternation of the deprotonation position with differential stereochemical control.

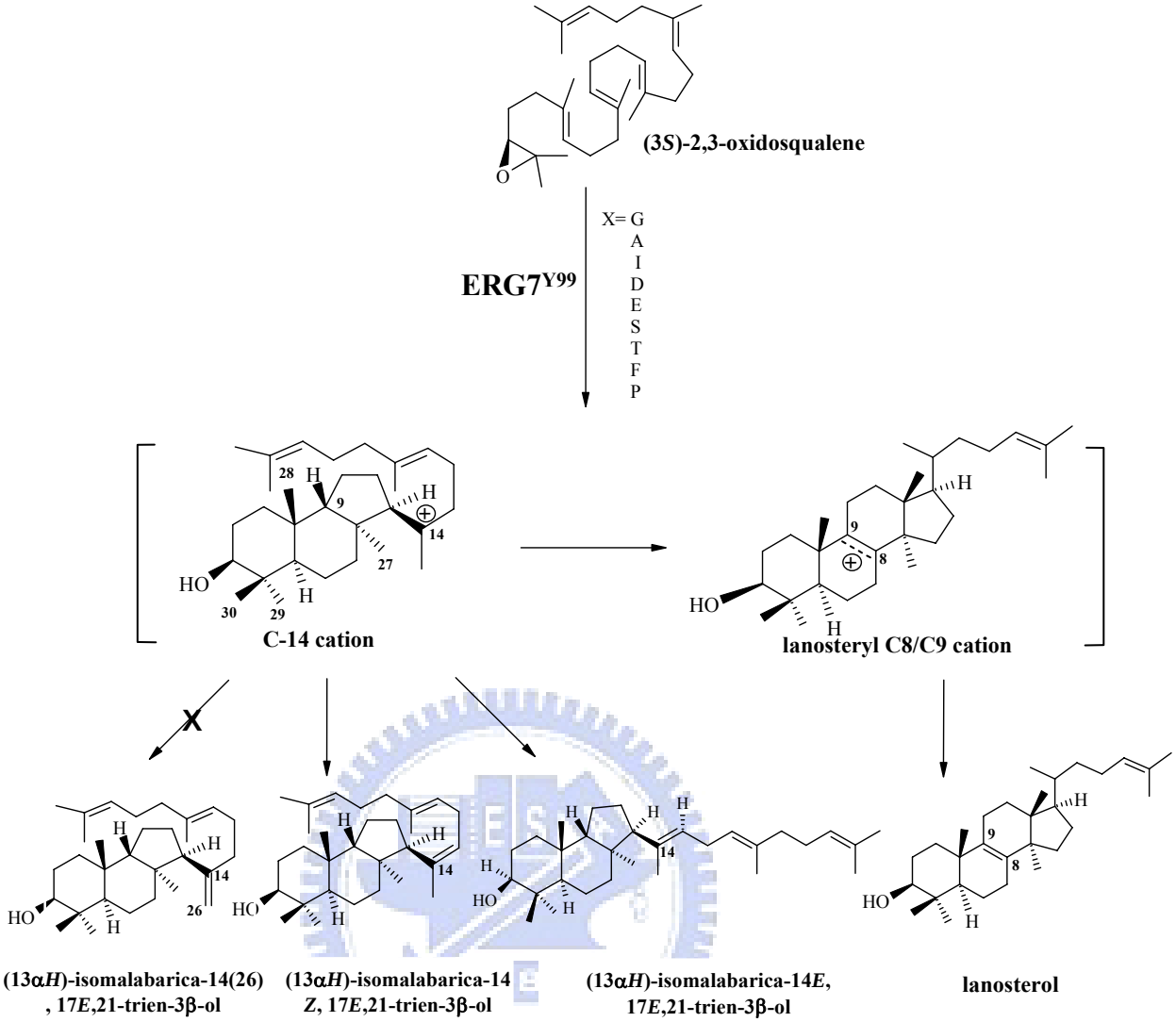

Figure 3.10 proposed cyclization/rearrangement pathway occurred in the ERG7^{Y99X} site-saturated mutants.

3.1.4 Analysis of the ERG7^{Y99X} in the OSC homology modeling

The effects of amino acid mutations on enzymatic activity, the formation of aberrant products, and relative product proportions are complicated and are only partially understood. Together with product profiles, we applied homology modeling of the *S. cerevisiae* ERG7, which was derived from the human OSC X-ray crystal structure, to provide an insight into the relationships between mutant enzyme structure and product specificity.

(A) ERG7 w/ lanosteryl C-8 cation **(B) ERG7 w/ protosteryl C-14 cation**

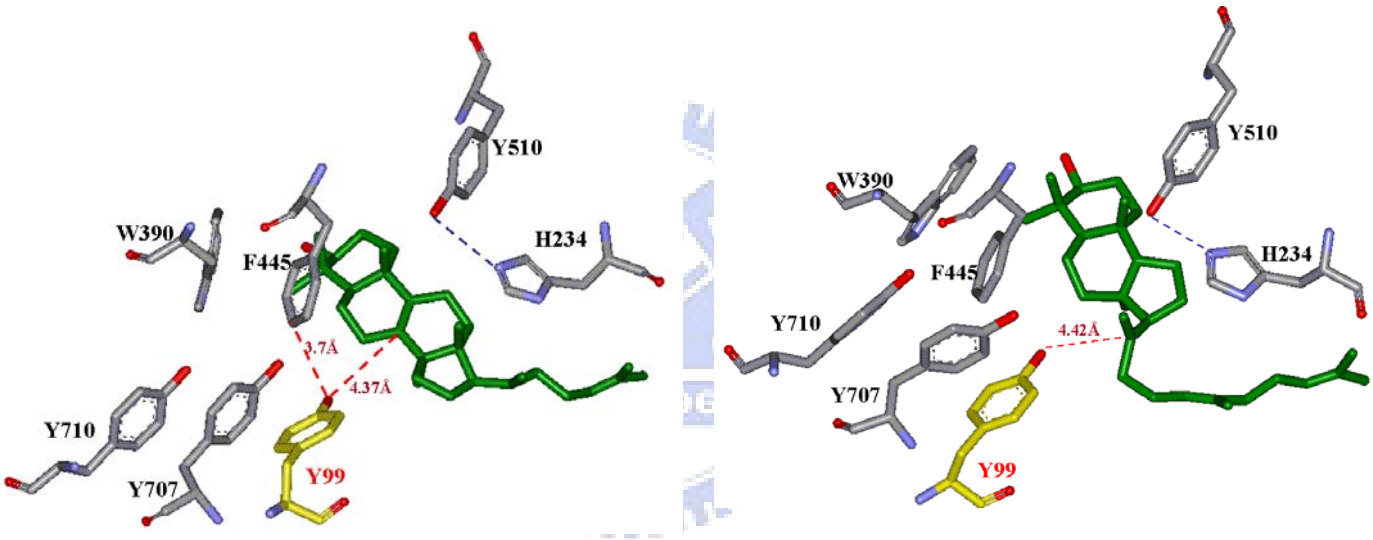

Figure 3.11 ERG7 residues form a putative π-electron pocket. These ERG7 residues interact with the (A) lanosteryl C-8 cation and (B) protosteryl C-14 cation

The previously performed site-saturated mutagenesis experiments on the His234 and Phe445 residues of ERG7 showed that both of ERG7^{F445X} and ERG7^{H234X} produced truncated tricyclic and altered deprotonation products, indicating the catalytic role of the residues in cationic stabilization at the C-14 position for the tricyclic product, and/or the C-8/C-9 position for the final deprotonation product.[42-45] In addition, a π–electron-rich pocket of aromatic residues around the Phe445 of ERG7 was suggested to be involved in substrate folding that affect either stabilizing the electron-deficient cationic intermediates

or availing against the equilibrium shift toward the lanosteryl C-8/C-9 cation during the rearrangement process for the formation of lanosterol. [33,45] Among these aromatic residues, His234 of ERG7 is hydrogen bonded to Tyr510 and located near the ceiling of the active site cavity, proximally to the B/C ring fusion and the C-8 and C-14 positions. Tyr99 is located at a distance of approximately 3.7 Å to interact with the Phe445 residue and close to the C/D ring of the substrate. (Fig. 3.11)

Scrutiny of the model suggests that Tyr99 residue is positioned in the middle side wall of the active site cavity by interacting with the C-ring, with the phenolic hydroxyl side chain pointed towards the substrate. The C-14 cation was found at a distance of approximately 4.4Å to the observed phenolic oxygen of Tyr99, a distance within the range needed to stabilize the dipole of Tyr99. (Fig. 3.11)

It is comprehensible that changes at Tyr99 strongly affect the orientation or electrostatic interaction of the phenolic oxygen of Tyr99 that is originally positioned to stabilize the C-14 cation for C-ring expansion and further D-ring closure. Perhaps some additional space for the free rotation of the hydrocarbon side chain moiety is offered through mutations at this position, resulting in abstracting protons from different position and/or orientations.

Alternatively, it is possible that mutations at Tyr99 generate a new base that leads to the Markovnikov C-B 6-6-5 cation and subsequent disproportional formation of (13α*H*)-isomalabarica-14*E*, 17, 21-trien-3β-ol and (13α*H*)-isomalabarica-14*Z*, 17, 21-trien-3β-ol (compound 1 and 2). On the other hand, a deletion at Tyr99 position may lead to a local main chain adjustment in the mutant compared with the wild type, obstructing the substrate binding and subsequent catalysis. Therefore, no product could be obtained from the ERG7^{Y99} deletion mutant.

Some mutants, such as Y99Gly, Y99Ala, Y99Ser, Y99Thr and Y99Pro, which led to produce more truncated tricyclic products than the wide type product lanosterol may cause

from that the shortened reactive distance or the lost of π-electrons is insufficient for destabilization of the Markovnikov tertiary cation created at C-14 during the C-ring formation. Either a distance variation between the functional side chain of the substitution amino acid and C-14 cation, or a electrostatic change of the replaced residues may be in proportion to the products yielding ratio.

3.1.5 The analysis of product energy profile

Quantum mechanical calculations were performed mainly with Gaussian 03 for modeling the folding pathway to get an optimal stabilization of the chemicals which was in the lowest energy states. Herein we diagramed the calculation results to show the relative energy profiles among substrate and products as well as various tricyclic intermediate conformers. (Fig. 3.12)

The results are consistent with the previous results of Matsuda that showed that progressive reaction energy release was primary observed during the A, B, and C-ring formation but much less energetic for D-ring closure in neglecting the role of the enzyme.[70]

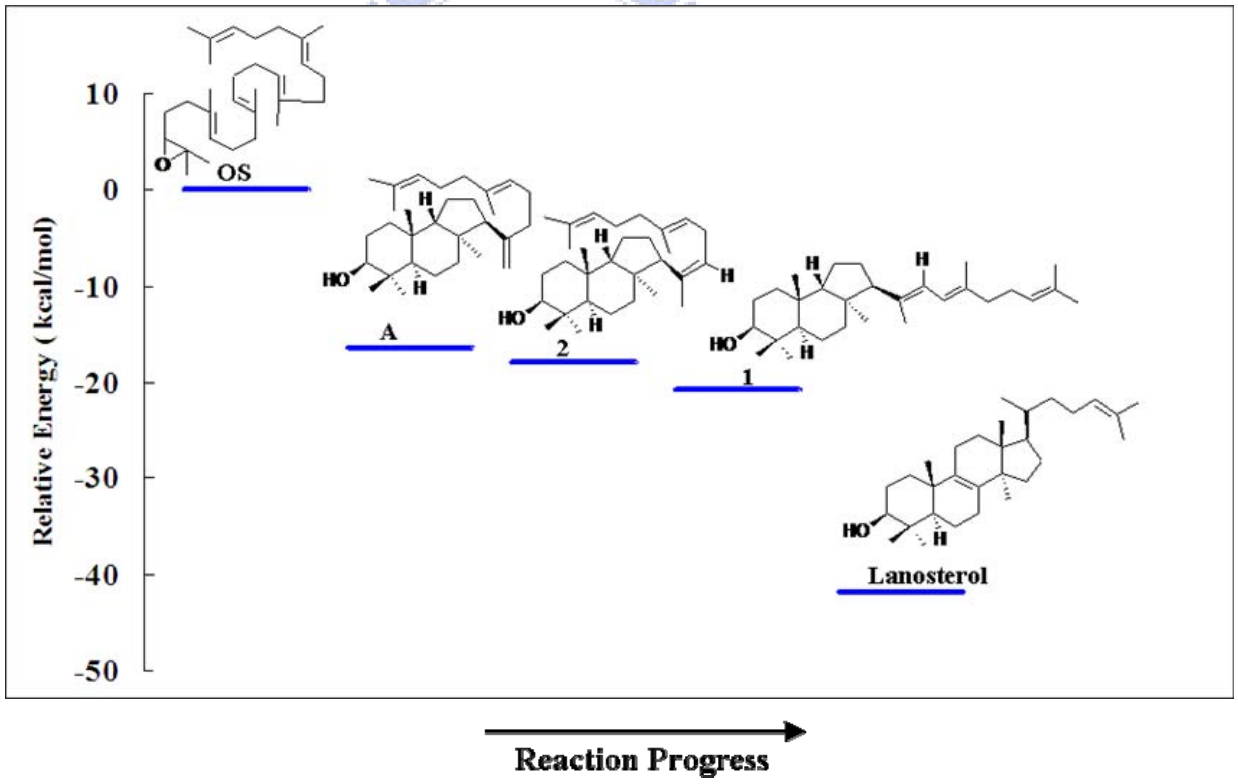

Figure 3.12 The product energy profile from quantum mechanical calculations. The relatively energetic states of compounds A [(13α*H*)-isomalabarica-14(26), 17E, 21-trien-3β-ol], 2 [(13α*H*)-isomalabarica-14*Z*, 17*E*, 21-trien-3β-ol], 1 [(13α*H*)-isomalabarica-14*E*, 17*E*, 21-trien-3β-ol], and lanosterol were measure under the minimum energy states and comprised with the substrate of the enzymatic cyclization, oxidosqualene. The resulting data provided by Cheng-Hsiang Chang.

Comparing energies among various tricyclic conformers showed energy levels down from compounds A to 1 to 2. Little influence of the enzymatic effect was observed when the tricyclic cation was converted into the tetracyclic intermediate. However, the substitution of amino acid residues at different spatial positions may alter a kinetically favored double-quaternary double bond deprotonation that produces the thermodynamically favored tertiary-quaternary double bond products. Notably, the differences in energies of various tricyclic intermediate conformers could be compensated by the amino acid residues in the stabilization of the Markovnikov tricyclic cation and/or the subsequently alteration of the deprotonation position with differential stereochemical control, with compound 2 in favor of compound 1.

3.2 Functional analysis of ERG7^{W443} within *S. cerevisiae*

A series of amino acids residues, sequences ^{441}GAWGFSTKTQGYT^{453} within *S. cerevisiae* ERG7, were subjected to both alanine-scanning mutagenesis and plasmid shuffle selection for the identification of possible residues involved in the complementation of cyclase-deficient yeast strain CBY57.[62] One of the three inactive mutations is Trp443Ala mutation, which failed to complement the cyclase deficiency. In my thesis, I genetically selected Trp443 site-saturated mutants (W443X) and characterized each of mutants for determination of the functional role of W443 and to investigate the effects of substitutions of this residue on other proteinogenic amino acids in terms of catalysis and product specificity.

3.2.1 Generation of site-saturated mutants of ERG7^{W443X}

Tryptophan 443 of the *S. cerevisiae* ERG7 gene was substituted with other 18 amino acids (W443Ala has been analyzed before.[63]) by using QuickChange site-directed mutagenesis strategy with the respective mutagenic primers. A silent mutation was concomitantly introduced to easily screen the desired mutants, according to a restriction enzyme (*Sty* I/ *Xho* I) mapping confirm. The positive mutants were digested into five fragments including 5.5Kb, 0.89Kb, 0.59Kb, 0.2Kb and 0.021Kb (unapparent) comparing with the wild type plasmids pRS314OSC which was digested into four fragments 5.5Kb, 1.1Kb, 0.59Kb and 0.021Kb (unapparent). The DNA agarose gel electrophoresis of the mapping results were shown in Appendix 2. The presence of the mutations was verified by sequence determination.

The recombinant plasmids were confirmed and transformed into TKW14C2 by the same strategies as previously described in section 3.1.1. The genetic selection of the TKW14C2[pERG7^{W443X}] mutants were shown in Table 3.5. The genetic selection results showed that only six mutants including W443Val, W443Leu, W443His, W443Cys,

W443Met, and W443Phe which allowed for ergosterol-independent growth. These results indicated that this position is decisive for the catalytic function of the OSC.

OSC^{mut}		**Enzyme mapping**	**Sequence confirmation**	**Ergosterol supplement (complement with TKW14C2)**
Aliphatic group	W443**Gly** (G)	*Sty* I/ *Xho* I	V	—
	W443**Ala** (A)		V	—
	W443**Val** (V)		V	+
	W443**Leu** (L)		V	+
	W443**Ile** (I)		V	—
Acidic and amide group	W443**Asp** (D)		V	—
	W443**Asn** (N)		V	—
	W443**Gln** (Q)		V	—
	W443**Glu** (E)		V	—
Basic group	W443**His** (H)		V	+
	W443**Lys** (K)		V	—
	W443**Arg** (R)		V	—
Hydroxyl-group	W443**Ser** (S)		V	—
	W443**Thr** (T)		V	—
Sulfur-containing	W443**Cys** (C)		V	+
	W443**Met** (M)		V	+
Aromatic group	W443**Phe** (F)		V	+
	W443**Tyr** (Y)		V	—
	W443 (wild type)		V	+
Imino	W443**Pro** (P)		V	—

Table 3.5 The genetic selection results of *S. cerevisiae* TKW14C2 expressing the $ERG7^{W443X}$ site-saturated mutagenesis.

3.2.2 Lipid extraction, column chromatography and product characterization

Each kind of recombinant yeast was incubated in 2.5L culture mediums and harvested by centrifugation. The collection and analytic protocols of NSL extract is similar to the analysis of TKW14C2[pERG7^{Y99X}] mutants (section 3.1.1). Four of six viable TKW14C2[pERG7^{W443X}] mutants including W443Val, W443His, W443Cys and W443Met yielded lanosterol as the only product with molecular mass of *m/z*=426. The other two viable TKW14C2[pERG7^{W443X}] mutants, W443Ala (according to previous analysis[63]) and W443Lys revealed two monocyclic triterpenoid products with a molecule mass of *m/z* = 426: achilleol A and camelliol C comparing with the authentic sample. (Fig.3.13) The product profiles of each mutant are summarized in Table 3.6.

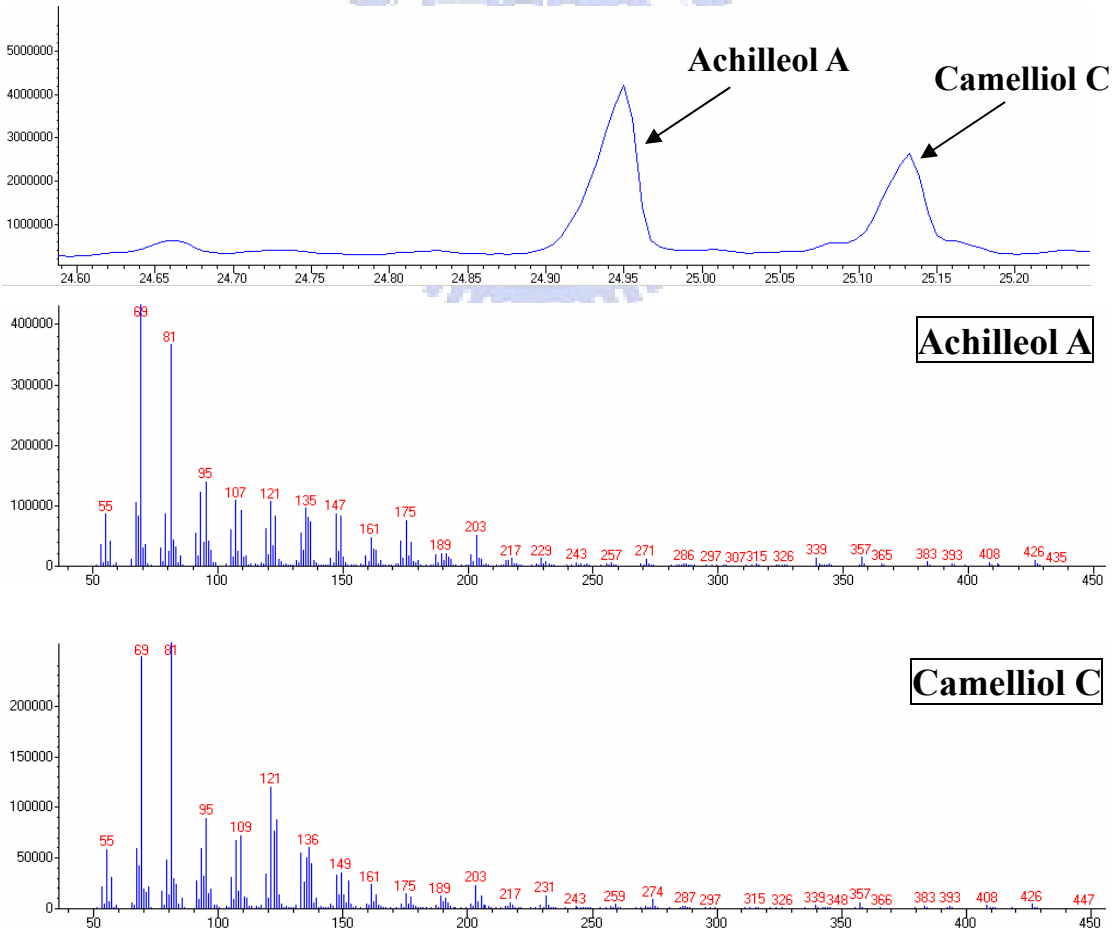

Figure 3.13 Electron-impact mass spectra of two monocyclic triterpenoid products derived from ERG7W^{443Lys}.

amino acids substitution	Ergosterol supplement	Products profile ratio (%)			
		no products	**Lanosterol**	**Achilleol A**	**Camelliol C**
Gly	—	V	-	-	-
Ala	—	-	0	68	32
Val	+	-	100	-	-
Leu	+	-	100	-	-
Ile	—	V	-	-	-
Asp	—	V	-	-	-
Asn	—	V	-	-	-
Gln	—	V	-	-	-
Glu	—	V	-		-
His	+	-	100	-	-
Lys	—	-	0	56	44
Arg	—	V	-	-	-
Ser	—	V	-	-	-
Thr	—	V	-	-	-
Cys	+	-	100	-	-
Met	+	-	100	-	-
Phe	+	-	100	-	-
Tyr	—	V	-	-	-
Pro	—	V	-	-	-
Wild type	+	-	100	-	-

Table 3.6 The products profile of *S. cerevisiae* TKW14C2 expressing the ERG7^{W443X} site-saturated mutagenesis.

3.2.3 Proposed cyclization/rearrangement pathways of TKW14C2 expressing ERG7^{W443X}

The first report site-directed mutant that can produce both monocyclic achilleol A and camelliol C, the formation of various incomplete cyclization products was found in ERG7^{Tyr510X}. The position of Tyr510 was supposed to be involved in the stabilization of cationic intermediates during the exposide protonation and A-ring cyclization.[46-47] The formation of achilleol A and camelliol C were identified as evidence for premature truncation of C-10 cationic intermediates formation following the proton abstraction from Me-25 or C-1 position. (Fig. 3.14)

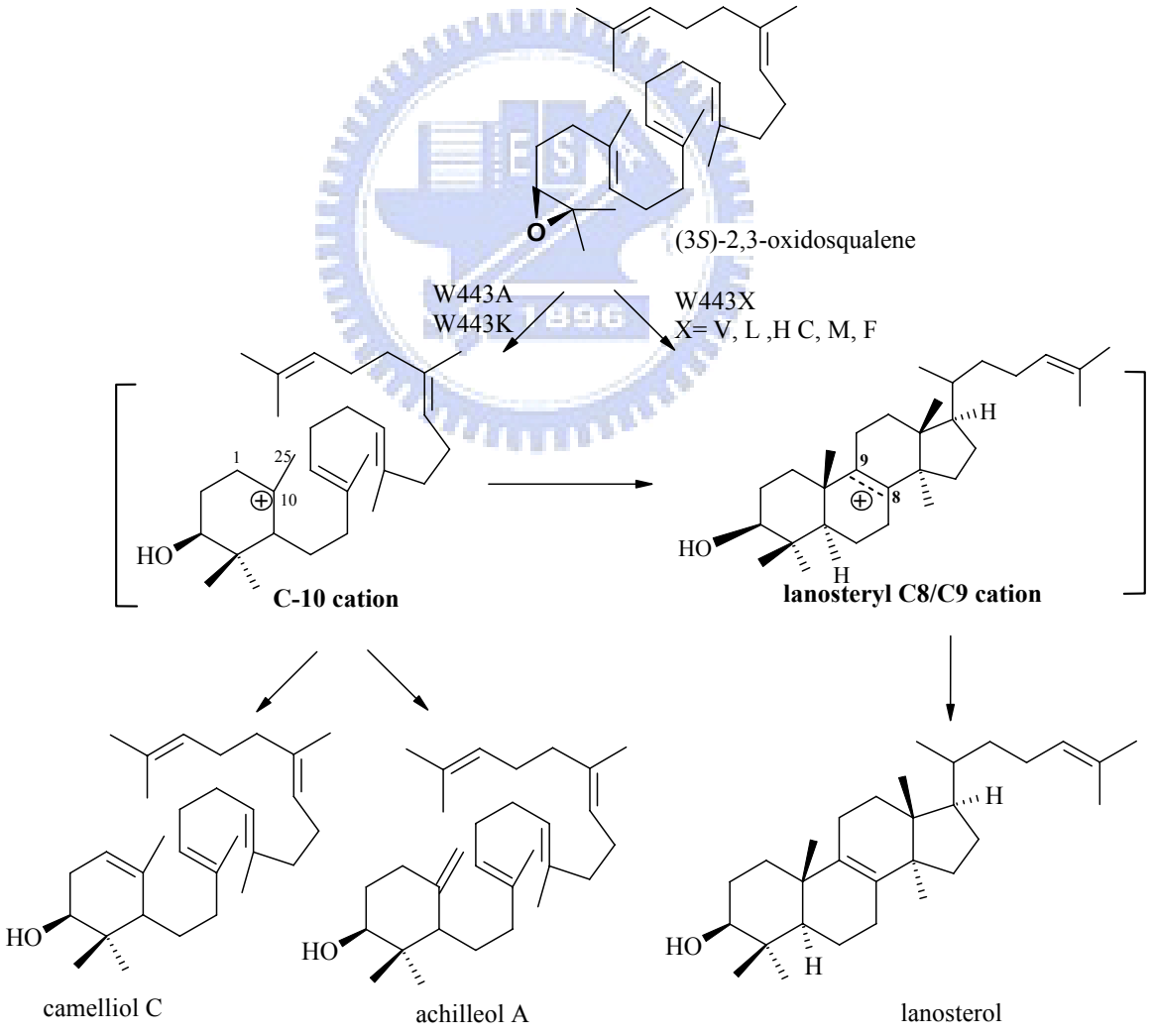

Figure 3.14 *S. cerevisiae* OSC ERG7^{W443X} mutants convert oxidosqualene to monocyclic triterpenoid products: Camelliol C and Achilleol A.

3.2.4 Analysis of the ERG7^{W443X} in the OSC homology modeling

The multiple sequence alignment analysis showed that the Trp443 was highly conserved in most cyclase, the Trp443 of *S. cerevisiae* ERG7 corresponds to F363 in *A. acidocaldarius* SHC and to W470 in *A.thaliana CAS*. These three residues are all aromatic amino acids; however their functional role analysis during catalytic cyclization mechanism has not been suggested and reported before.

According to the previous studies, the achilleol A and camelliol C were also produced from the other cyclase-inactive mutants, Lys448Ala which were previously identified from the region upstream of the putate active site in our laboratory by ergosterol complement experiment. Lys448 are located at the flexible loop region opposite to the position of the essential Asp456 and displayed interactions to hold the correct conformation in dimeric association with two amino acids, Phe426 and Asn332. Replacing Lys448 with Ala was supposed to disrupt the electrostatic interaction between subunits or held the cyclization/rearrangement cascade at the intermediate stage, thus forming only the initially cyclized A-ring.[62-63]

In the previous homology model studies, the Trp443 was supposed to be positioned spatially opposite to the Asp456, below the molecular plain and close to the high-energy C-10 (lanosterol numbering) cationic intermediate. The Trp443 was suggested to be at the nearest neighbor to the active site residues and thereby stabilize the high-energy C-10 cation intermediate during the concerted process of epoxide opening and A-ring formation. Substitution of Trp with Ala might disrupt the steric or cation- electronic effect between substrate and enzyme; elongation of the cyclization cascade would thus be inhibited and the reaction be held at monocyclic triterpenes.[62-63] However, in my homology modeling analysis, the Trp443 is positioned spatially above to the Asp456 and the molecular plain whereas it seems to be far from substrate (10.28Å between oxygen of Trp and C-10 of lanosterol; 10.1Å between oxygen of Trp and C-2 of lanosterol). (Fig. 3.15)

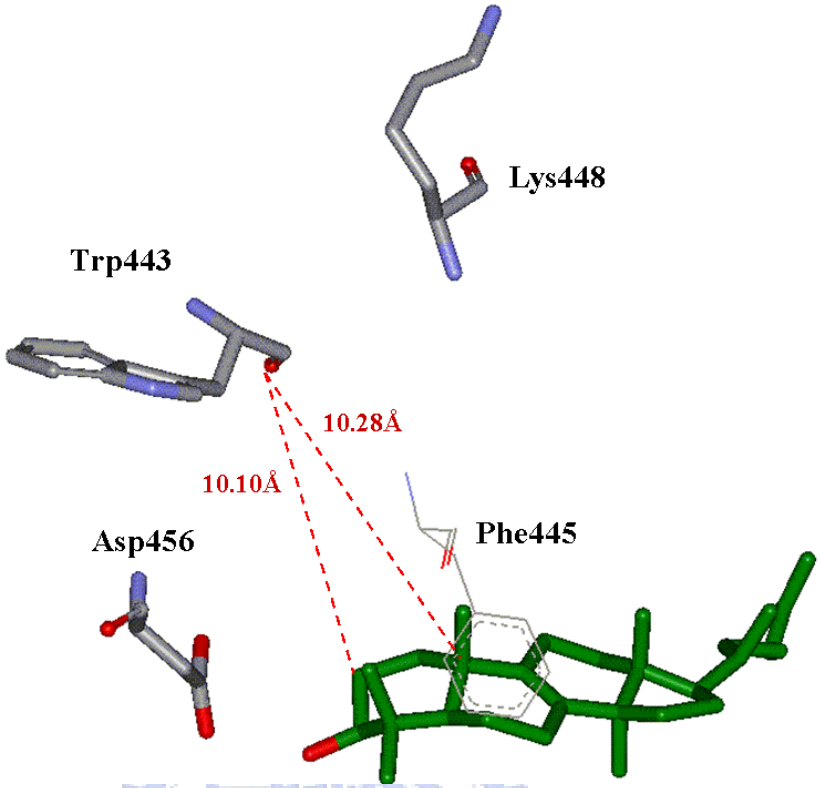

Figure 3.15 Local views of the homology modeled Asp456, Trp443, Lay448, and Phe445 positions in S. cerevisiae ERG7 structure based on the X-ray structure of lanosterol-complexed human OSC and determined by using the Insight II Homology program.

Obviously, Trp443 is not located in the putative π–electron pocket; however the site-saturated mutagenesis results showed that only W443Val, W443Leu (aliphatic residues), W443Cys, W443Met (sulfur-containing residues), W443Phe (aromatic residue) and His (basic residue) were able to complement to the OSC deficient strain and yield lanosterol. This observation revealed that W443 position is indispensable; changes of the side chain at W443 position may influence the interactive distances for the proper substrate binding and subsequent catalysis. On the other hand, two inactive mutants, W443A (aliphatic residue) and W443K (basic residue) produced achilleol A as a major product and camelliol C as a minor product. The formation of the truncated monocyclic intermediated suggested that Trp residue may also play an crucial role both in influencing the substrate

prefolding and stabilizing the epoxide protonation and inducing A-ring formation via the generation of the C-10 cation.

Moreover, the exact reason for the higher accumulation of achilleol A over that of camelliol C, and the production of achilleol A whenever camelliol C is produced, remain unclear. Furthermore, whether the Trp443 interact with the substrate directly or via the other residues in the active site pocket, needs more mutagenesis at neighboring residues and homology modeling of the W443X mutants, in order to clarify the functional roles of Trp443.

Chapter4 Conclusions

Site-directed mutagenesis is a molecular biology technique in which a mutation is created at a defined site in a DNA molecule, and site-saturated mutagenesis means the substitution of specific sites with other 19 proteinogenic amino acids. This technique was applied to obtain a detailed understanding of structure-function relationships for the putative active sites in the enzyme.

In our studies, site-saturated mutagenesis coupled with product isolation and characterization of the mutations at Tyr99 and Trp443 position of OSC ERG7 within *S. cerevisias* revealed their catalytic function in affecting the cyclization/rearrangement mechanism. Both of these two residues were suggested play crucial roles in enzyme catalytic cyclization/rearrangement. Herein we summarize several important conclusions of our studies:

4.1 The functional analysis of TKW14C2[pERG7^{Tyr99X}]

(1) The TKW14C2[pERG7^{Tyr99X}] expressed ERG7^{Tyr99X} as its sole oxidosqualene cyclase. The genetic selection results showed that several Tyr99X mutants could complement to ergosterol-deficient growth except the deletion of Tyr99 as well as the mutation of Y99N, Y99H in ERG7.

(2) Several mutants including Y99A, Y99G, Y99I, Y99D, Y99S, Y99T, Y99F, and Y99P produced two novel products with a molecular mass of m/z = 426 except lanosterol, which are both truncated tricyclic triterpenoid products (13α*H*)-isomalabarica-14*Z*, 17*E*, 21-trien-3β-ol and (13α*H*)-isomalabarica-14*E*, 17*E*, 21-trien-3β-ol, identified by ^{1}H and ^{13}C NMR for the first time. The product profile of ERG7^{Y99X} demonstrates the truncation of the cyclization/rearrangement cascade at chair-boat 6-6-5 tricyclic Markovnikov cation, at the C-14 position, and subsequent abstraction of protons at

C-15 position with different stereochemical preferences.

(3) The functional role of ERG7^{Y99} is suggested to affect both chair-boat 6-6-5 tricyclic Markovnikov cation stabilization and the stereochemistry of the protons at the C-15 position for subsequent deprotonation, but not to enforce the boat conformation for lanosterol B-ring formation.

(4) In homology modeling analysis, the phenolic oxygen of Tyr99 residue is at a distance of approximately 4.4Å from the C-14 cation, and its location is differently in space from that to His234 and Phe445 to the common C-14 cation which affects the orientation or electrostatic interaction between the enzyme and its cationic intermediate, and results in the abstraction of a proton form a different position or orientation. Therefore, changes at Tyr99 or a deletion of this position may strongly impact the structure and lead to an adjustment of the active site and result in obstruction of substrate binding and catalysis.

(5) The product energy profile from quantum mechanical calculations suggested that the energetics of stereochemical control during the tricyclic Markovnikov cation deprotonation step could be affected by the inclusion of these enzymatic effects. It may be the reason why the (13α*H*)-isomalabarica-14*Z*, 17*E*, 21-trien-3β-ol was produced as a major product in Y99Gly, Y99Ala, Y99Ser, Y99Thr and Y99Pro mutants.

4.2 The functional analysis of TKW14C2[pERG7^{Trp443X}]

(1) In the previous alanine-scanning mutagenesis and plasmid shuffle selection of the ^{441}GAWGFSTKTQGYT^{453} within this of *S. cerevisiae* ERG7, Trp443Ala was one of the inactive mutants. The following ergosterol complementation experiment uncovered that ERG7^{Trp443Ala} produced two monocyclic triterpenen products concomitantly, achilleol A and camelliol C.

(2) The genetic selection demonstrated that only six mutants including Trp443Val, Trp443Leu, Trp443His, Trp443Cys, Trp443Met, and Trp443Phe which allowed for ergosterol-independent growth and yielded lanosterol as an only product with molecular mass of *m/z*=426. Whereas one of inactive mutant, Trp443Lys, revealed two monocyclic triterpenoid products with a molecule mass of *m/z* = 426: achilleol A and camelliol C, as well as the observation in the ERG7^{W443A} mutant.

(3) The formation of achilleol A and camelliol C were identified as evidence for premature truncation of C-10 cationic intermediates following the proton abstraction from Me-25 or C-1 position. This finding suggested that Trp residue may also play a crucial role both in influencing the substrate prefolding and stabilizing the epoxide protonation and A-ring formation to generate C-10 cation. However, the exact reason for the higher accumulation of achilleol A over that of camelliol C, and the production of achilleol A whenever camelliol C is produced, remain unclear.

(4) Although Trp443 is not located in the putative π–electron pocket and positioned spatially far from A-ring of lanosterol, it might provide an interaction with the neighboring residues to stabilize the carbocationic intermediates produced during protonation of epoxide and subsequent A-ring formation.

Chapter 5 Future Works

For the Tyr99 functional analysis, our results showed that how the structure-function relationships of the OSC via the expression of $ERG7^{Y99X}$ site-saturated mutants in *S. cerevisiae*. However, our substantiation of Tyr99 functional role contradicted the supposition, which Tyr98 of human OSC is spatially positioned to enforce the energetically unfavorable boat conformation of OS for lanosterol B-ring formation via pushing the methyl group at C-8 (lanosterol numbering) below the molecular plane. The expression of site-directed mutants of $Tyr98X^{hOSC}$ will be carried out to identify the function of this conserved residue.

Furthermore, the HEM1 ERG7 ERG1 triple knockout mutant which is the yeast strain with the deletion of both oxidosqualene cyclase (ERG7) and squalene epoxidase (ERG1). This triple knockout strain will be developed for the *in vitro* analysis of the mutated oxidosqualene cyclase via the addition of the substrates. This oxidosqualene free strain will prevent the interference due to the downstream enzymes and consequently ensure the more detailed understanding for the catalytic function of the putative active-sites.

Chapter6 References

1. I. Abe, M. Rohmer, G. D. Prestwich *Chem. Rev.* **93**, 2189(1993)
2. K. U. Wendt, G. E. Schulz, E. J. Corey, D. R. Liu *Angew. Chem. Int. Ed.* **39**, 2812(2000).
3. R. Xu, G. C. Fazio, S. P. T. Matsuda *Phytochemistry* **65**, 261(2004).
4. I. Abe, Y. F. Zheng, G. D. Prestwich *Biochemistry* **37**, 5779(1998).
5. T. Dang, I. Abe, Y. F. Zheng, G. D Prestwich *Chem. & Bio.* **6,** 333(1999).
6. M. J. R. Segura, B. E. Jackson, S P. T. Matsuda *Nat. Prod. Rep.* **20**, 304(2003).
7. T. Schulz–Gasch, M. Stahl *J. Comput. Chem.* **24**, 741(2003).
8. E. J. Corey, S. C. Virgil *J. Am. Chem. Soc*. **112**, 6429(1990).
9. E. J. Corey, S. C. Virgil *J. Am. Chem. Soc*. **113**, 4025(1991).
10. E. J. Corey, S. C. Virgil, S. Sarshar *J. Am. Chem. Soc*. **113**, 8171(1991).
11. E. J. Corey, S. C. Virgil, R. Liu, S. Sarshar *J. Am. Chem. Soc*. **114**, 1524(1992).
12. E. E. van Tamelen *J. Am. Chem. Soc*. **104**, 6480(1982).
13. D. Rittenberg, R. Schoenheimer *J. Bio. Chem.* 235(1937).
14. K. Bloch, D. Rittenberg *J. Bio. Chem.* 625(1942).
15. R. B. Woodward, K. Bloch *J. Am. Chem. Soc*. **75**, 2024(1953).
16. R. K. Maudgal, T. T. Tchen, K. Bloch *J. Am. Chem. Soc*. **80**, 2589(1958).
17. J. W. Cornforth, R. H. Cornforth, C. Donninger, G. Popják, Y. Shimizu, S. Ichii, E. Forchielli, E. Caspi *J. Am. Chem. Soc*. **87**, 3224(1965).
18. E. J. Corey, W. E. Russey, P. R. Ortiz de Montellano *J. Am. Chem. Soc*. **88**, 4750(1966).
19. E. E. van Tamelen, J. D. Willett, R. B. Clayton, K. E. Lord *J. Am. Chem. Soc*. **88**, 4752(1966).
20. J. D. Willett, K. B. Sharpless, K. E. Lord, E. E. van Tamelen, R. B. Clayton *J. Biol.*

Chem. **242**, 4182(1967).

21. D. H. R. Barton, T. R. Jarman, K. C. Watson, D. A. Widdowson, R. B. Boar, K. Damps *Perkin Trans.* **1**, 1134(1975).
22. G. Ourisson, M. Rohmer, K. Poralla *Annu. Rev. Microbiol.* **41**, 301(1987).
23. G. Ourisson, M. Rohmer, R. Anton *Recent. Adv. Phytochem*. **13**, 131(1979).
24. M. Rohmer, P. Bouvier, G. Ourisson *Proc. Nadl. Acad. Sci.* **76**, 847(1979)
25. W. S. Johnson, S. J. Telfer, S. Cheng, U. Schubert *J. Am. Chem. Soc*. **109**, 2517(1987).
26. W. S. Johnson, S. D. Lindell, J. Steele *J. Am. Chem. Soc*. **109**, 5852(1987).
27. C. J. Buntel, J. H. Griffin *J. Am. Chem. Soc*. **114**, 9771(1992).
28. Z. Shi, C. J. Buntel, J. H. Griffin *Proc. Nadl. Acad. Sci.* **91**, 7370(1994).
29. R. Kelly, S. M. Miller, M. H. Lai, D. R. Kirsch *Gene* **87**, 177(1990).
30. K.U. Wendt *Angew. Chem. Int. Ed.* **44**, 3966(2005).
31. K.U. Wendt, K. Poralla, G.E. Schulz, *Science* **277**, 1811(1997).
32. K.U. Wendt, A. Lenhart, G.E. Schulz, *J. Mol. Biol.* **286**, 175 (1999).
33. R. Thoma, T. Schulz-Gasch, B. D'Acry, J. Benz, J. Aebi, H. Dehmlow, M. Hennig, M. Stihle, A. Ruf *Nature* **432**, 118(2004).
34. E. J. Corey, H. Cheng, C. H. Baker, S. P. T. Matsuda, D. Li, X. Song *J. Am. Chem. Soc*. **119**, 1277(1997).
35. E. J. Corey, H. Cheng, C. H. Baker, S. P. T. Matsuda, D. Li, X. Song *J. Am. Chem. Soc*. **119**, 1289(1997).
36. E. J. Corey, D. D. Staas *J. Am. Chem. Soc*. **120**, 3526(1998).
37. C. Jenson, W. L. Joergensen *J. Am. Chem. Soc*. **119**, 10846(1997).
38. B. A. Hess *Org. Lett.* **5**, 165(2003).
39. B. A. Hess *J. Am. Chem. Soc*. **124**, 10286(2002).
40. D. Gao, Y.-K. Pan, K. Byun, J. Gao *J. Am. Chem. Soc*. **120**, 4045(1998).

41. B. M. Joubert, L. Hua, S. P. T. Matsuda *Org. Lett.* **2**, 339(2000).

42. T. K. Wu, Y. T. Liu, F. H. Chiu, C. H. Chang *Org. Lett.* **21**, 4691(2006).

43. E. J. Corey, S. C. Virgil, H. Cheng, C. H. Baker, S. P. T. Matsuda, V. Sigh, S. Sarshar *J. Am. Chem. Soc*. **117**,11819(1995).

44. T. K. Wu, Y. T. Liu, C. H. Chang *ChemBioChem* **6**, 1177(2005).

45. T. K. Wu, Y. T. Liu, C. H. Chang, M. T. Yu, H. J. Wang *J. Am. Chem. Soc*. **128**,6414(2006).

46. T. K. Wu, C. H. Chang *ChemBioChem* **5**, 1712(2004).

47. S. Lodeiro, W. K. Wilson, H. Shan, S. P. T. Matsuda *Org. Lett.* **8**, 439(2006).

48. T. K. Wu, M. T. Yu, Y. T. Liu, C. H. Chang, H. J. Wang, E. W. G. Diau *Org. Lett.* **8**, 1319(2006).

49. E. A. Hart, L. Hua, L. B. Darr, W. K. Wilson, J. Pang and S. P. T. Matsuda *J. Am. Chem. Soc*. **121**,9887(1999).

50. J. B. R. Herrera, W. K. Wilson, S. P. T. Matsuda *J. Am. Chem. Soc*. **122**,6765(2000).

51. S. Lodeiro, M. J. R. Segura, M. Stahl, T.Schulz-Gasch, S. P. T. Matsuda *ChemBioChem* **5**, 1581(2004).

52. S. Lodeiro, T.Schulz-Gasch, S. P. T. Matsuda *J. Am. Chem. Soc*. **127**, 14132(2005).

53. T. Hoshino, T. Sato *Chem.Commun.* 291(2002).

54. T. Merkofer, C. Pale-Grosdemange, K. U. Wendt, M. Rohmer, K. Poralla *Tetra. Lett.* **40**, 2121(1999).

55. K. U. Wendt, A. Lenhart, G. E. Schulz *J. Mol. Biol.* **286**, 175(1999).

56. C. Feil, R. Su¨ssmuth, G. Jung, K. Poralla *Eur. J. Biochem.* **242**, 51(1996).

57. D. W. Christianson *Chem. Rev.* **106**, 3412(2006).

58. D. J. Reinert, G. Balliano, G. E. Schulz *Chem. Biol.* **11**, 121(2004).

59. K. Poralla, A. Hewelt, G. D. Prestwich, I. Abe, I. Reipen, G. Sprenger *Trends Biochem. Sci.* **19**, 157(1994).

60. K. Poralla *Bioorg. Med. Chem. Lett.* **4**, 285(1994).

61. T. K. Wu, J. H. Griffin *Biochemistry* **41**, 8238(2002).

62. 邱逢旋， 利用定點突變研究酵母菌中氧化鯊烯-羊毛硬脂醇環化酶結構與反應機制間的關係，國立交通大學生物科技研究所，碩士論文，中華民國八十九年。

63. 張程翔, Mutagenesis approaches, inhibition studies, and SELEX technology to investigate product specificity and cataqalytic activity of oxidosqualene cyclase,國立交通大學生物科技研究所，博士資格考，中華民國九十年

64. S. Freimund, S. Kopper *Carbohydr. Res.* **308**, 195(1998).

65. S. Freimund, S. Kopper *Carbohydr. Res.* **339**, 217(2004).

66. H. E. Vroman, A. F. J. Cohen *Lipid Res.* **8**, 150(1967).

67. R. A. J. Pascal, C. L. Farris, G. J. Schroepfer *J. Anal. Biochem.* **101**, 15 (1980).

68. A. Sali, T. L. Blundell *J. Mol. Biol.* **212**, 403(1990).

69. A. Sali, T. L. Blundell *J. Mol. Biol.* **234**, 779(1993).

70. S. P. T Matsuda, W. K. Wilson, Q. Xiong *Org. Biomol. Chem.* **4**, 530(2006).

Appendix 1

Primers used in this thesis

Mutagenesis

WSL-OSC-Y99SMC-1	5'-CCg TgT CAA (A/T)(T/g)(g/T) AAA ggg CCC ATg TTC ATg-3'
WSL-OSC-Y99SMC-2	5'-CAT gAA CAT ggg CCC TTT (C/A)(C/A)(T/A) TTg ACA Cgg-3'
WSL-OSC-Y99EVQ-1	5'-CCg TgT CAA (C/g)(A/T)(g) AAA ggg CCC ATg TTC ATg-3'
WSL-OSC-Y99EVQ-2	5'-CAT gAA CAT ggg CCC TTT (C)(T/A)(C/g) TTg ACA Cgg-3'
WSL-OSC-delY99-1	5'-CCg TgT CAA AAA ggg CCC ATg TTC ATg-3'
WSL-OSC-delY99-2	5'-CAT gAA CAT ggg CCC TTT TTg ACA Cgg-3'
FHC-W443A	5'-gA AAg ggg gCT ATg ggC TTC TCA ACA AAA ACC CAA ggC TAT ACA gTg g -3'
WSL-OSC-W443M-1	5'-gA AAg ggg gCT ATg ggC TTC TCA ACA AAA ACC CAA ggC TAT ACA gTg g-3'
WSL-OSC-W443M-2	5'-C CAC TgT ATA gCC TTg ggT TTT TgT TgA gAA gCC CAT AgC CCC CTT T C-3'
HJW-W443IMK	5'-TTT AAT TgC TTC TgC AgT gCA ATC TgC CAC TgT ATA gCC TTg ggT TTT TgT TgA gAA gCC (C/T)(A/T)T AgC CCC CTT TC-3'
HJW-W443VDEG	5'-TTT AAT TgC TTC TgC AgT gCA ATC TgC CAC TgT ATA gCC TTg ggT TTT TgT TgA gAA gCC (g/T)(A/C/T)C AgC CCC CTT TC-3'
HJW-W443FC	5'-TTT AAT TgC TTC TgC AgT gCA ATC TgC CAC TgT ATA gCC TTg ggT TTT TgT TgA gAA gCC g(A/C)A AgC CCC CTT TC-3'
HJW-W443Q	5'-TTT AAT TgC TTC TgC AgT gCA ATC TgC CAC TgT ATA gCC TTg ggT TTT TgT TgA gAA gCC CTg AgC CCC CTT TC-3'

Sequencing

HJW-L158-A2	5'-gAT TAC ATA gTT CgC TAC ggT Acc AAA CAC-3'
YTL-OSCW390X-1	5'-CCA TTA Tgg gTA CCA Atg gTg TgC AAA CCN NNg ATT gTg Cg-3'

Appendix 2

DNA electrophoresis of site-directed mutagenesis

(a)

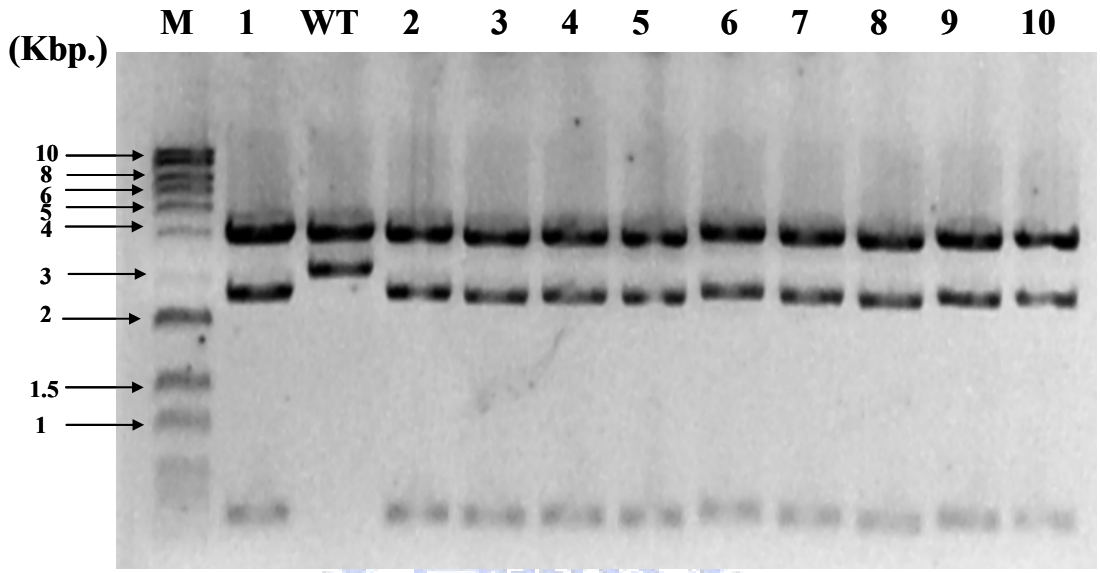

(b)

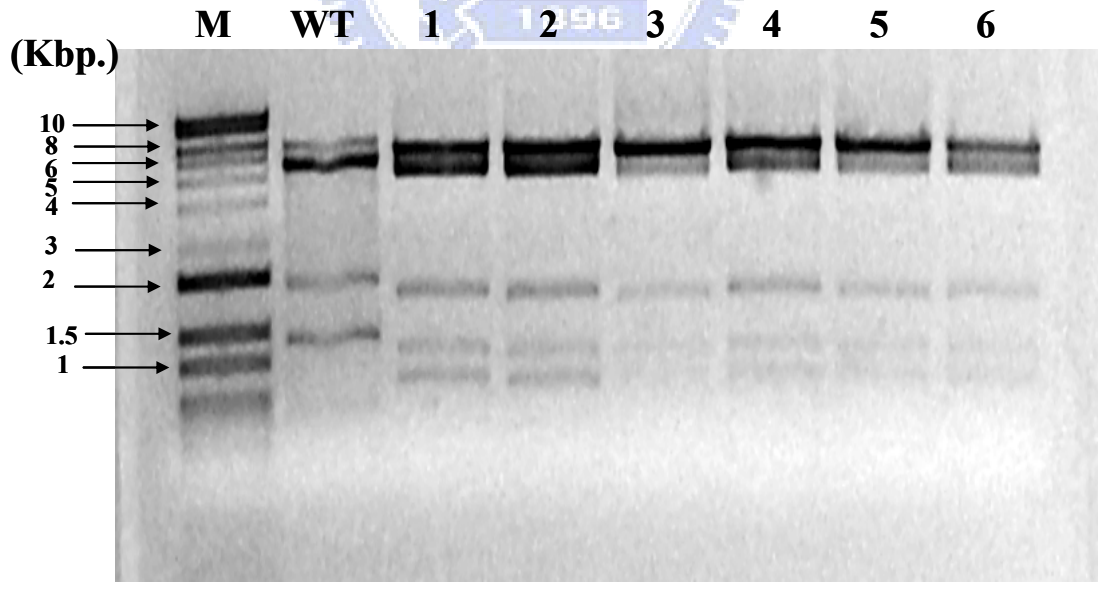

Appendix 2. DNA agarose gel electrophoresis of site-directed mutated plasmid checked by restriction enzymes. Lane M, 10-100 bp. DNA marker. Lane WT, pRS314+ERG7. (a) Lane 1-10 pRS314+ERG7Y99X. (b) Lane 1-6 pRS314+ERG7W443X.

Appendix 3

^{1}H NMR of (13α*H*)-isomalabarica-14*Z*,17*E*,21-trien-3β-ol

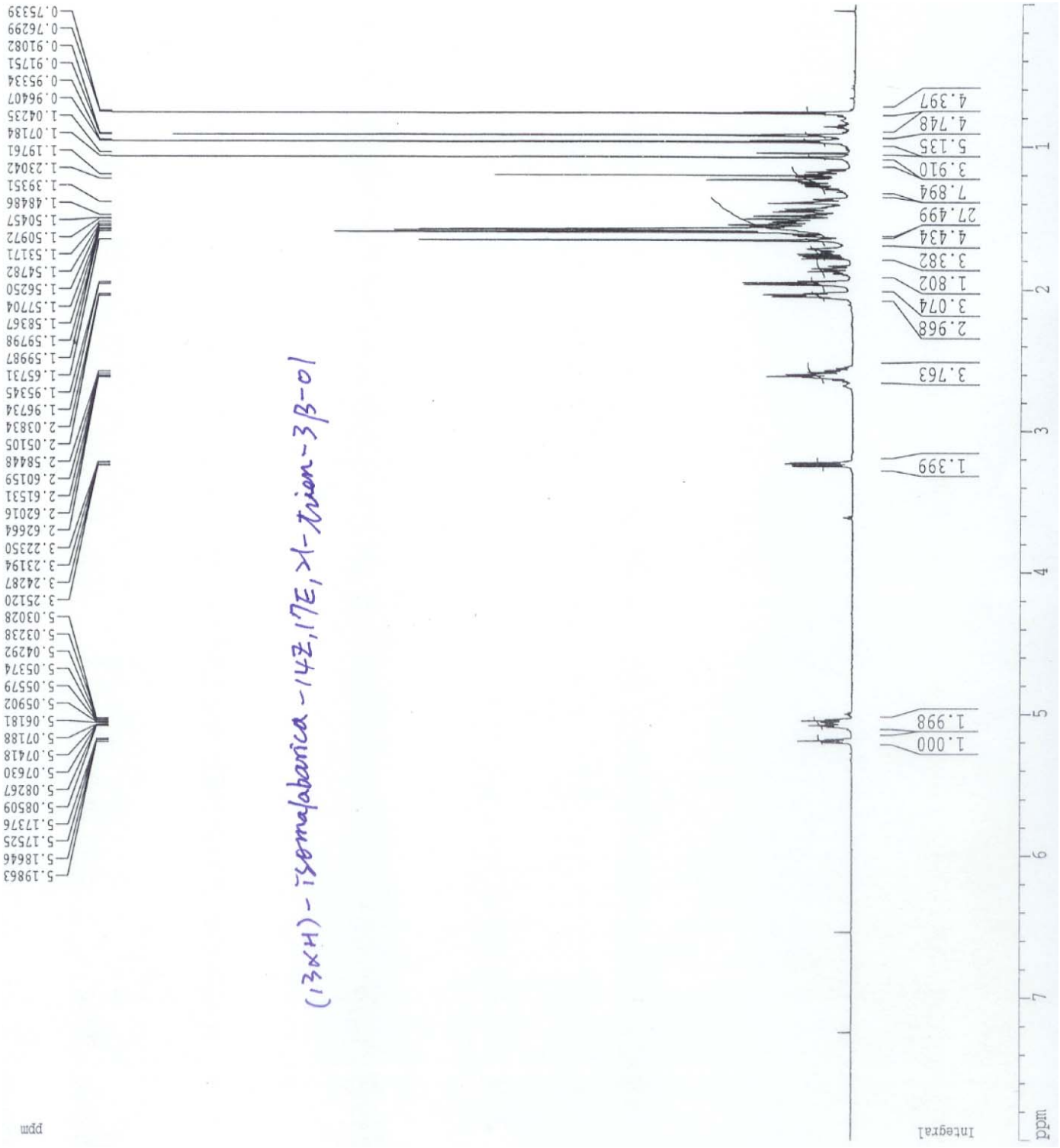

^{13}C NMR of (13α*H*)-isomalabarica-14*Z*,17*E*,21-trien-3β-ol

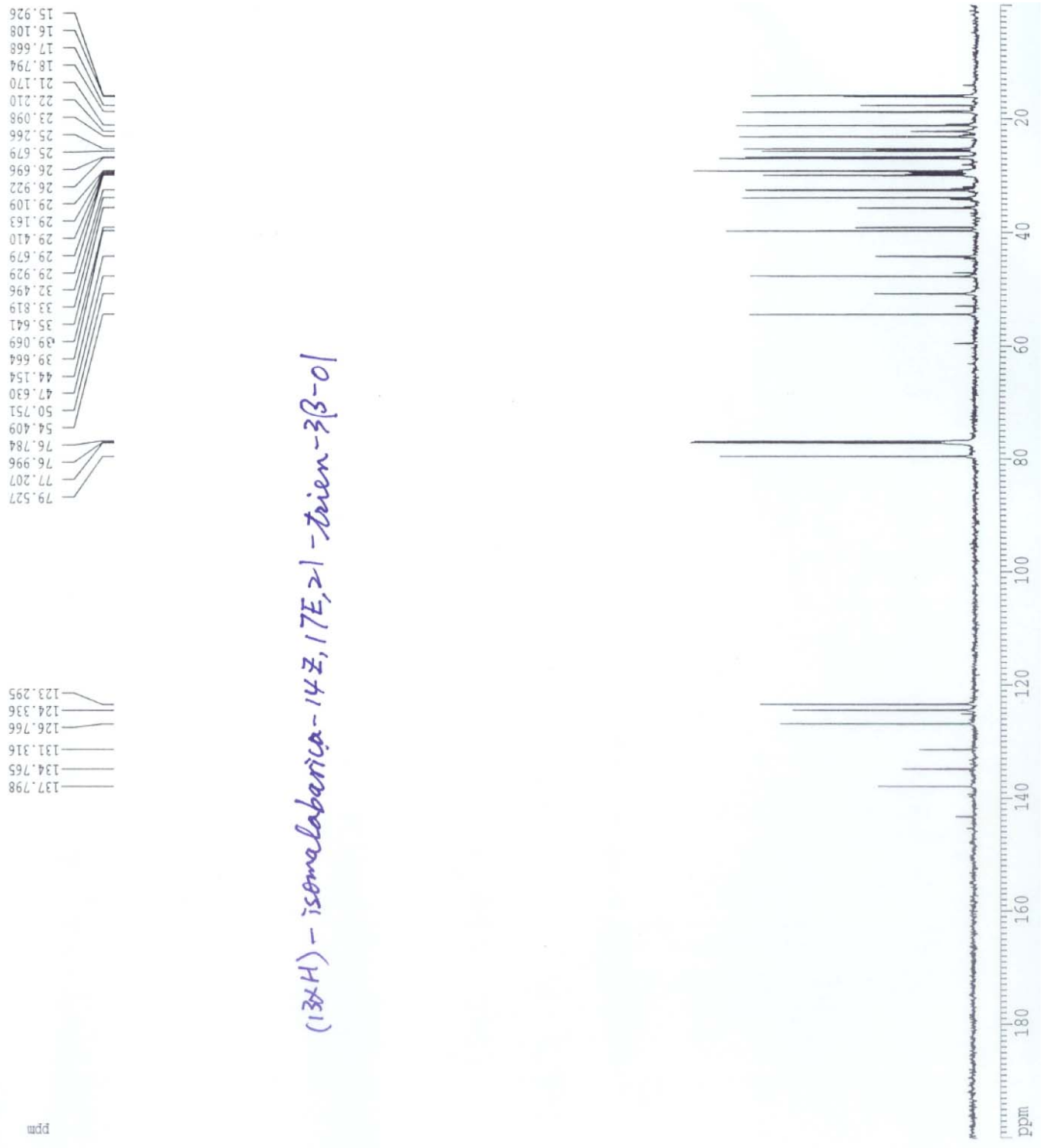

DEPT of (13α*H*)-isomalabarica-14*Z*,17*E*,21-trien-3β-ol

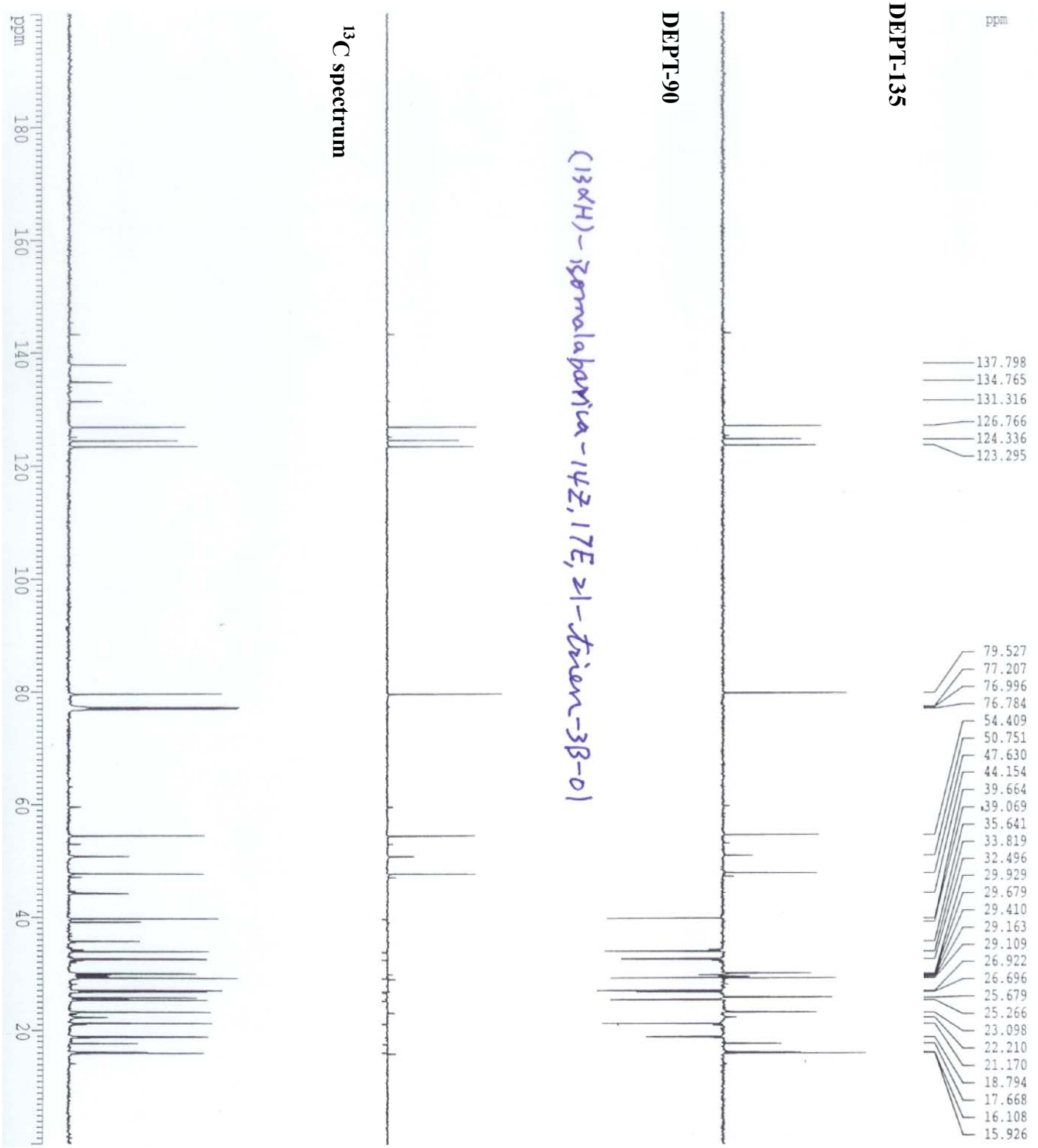

HMQC of (13α*H*)-isomalabarica-14*Z*,17*E*,21-trien-3β-ol

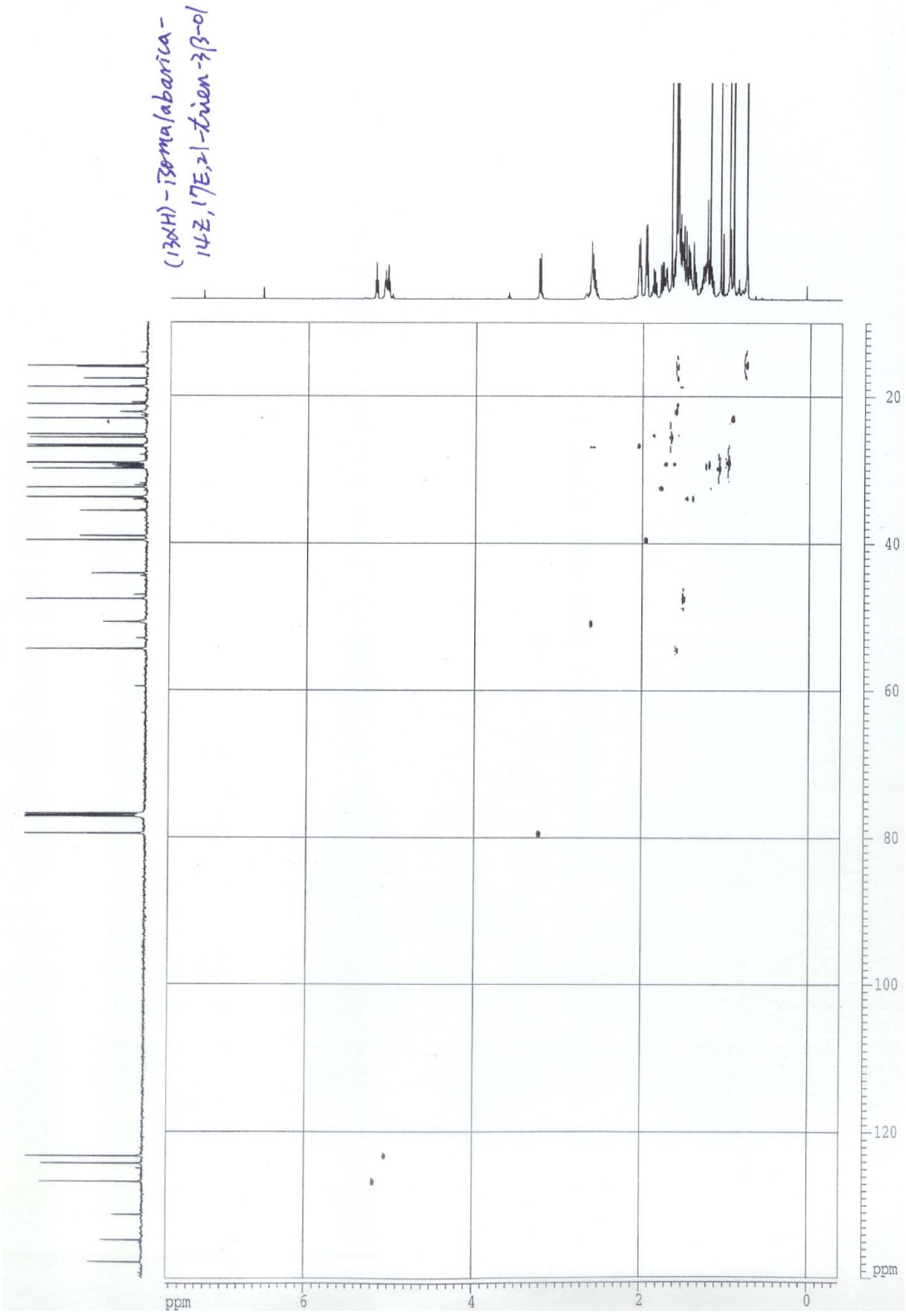

HMBC of (13α*H*)-isomalabarica-14*Z*,17*E*,21-trien-3β-ol

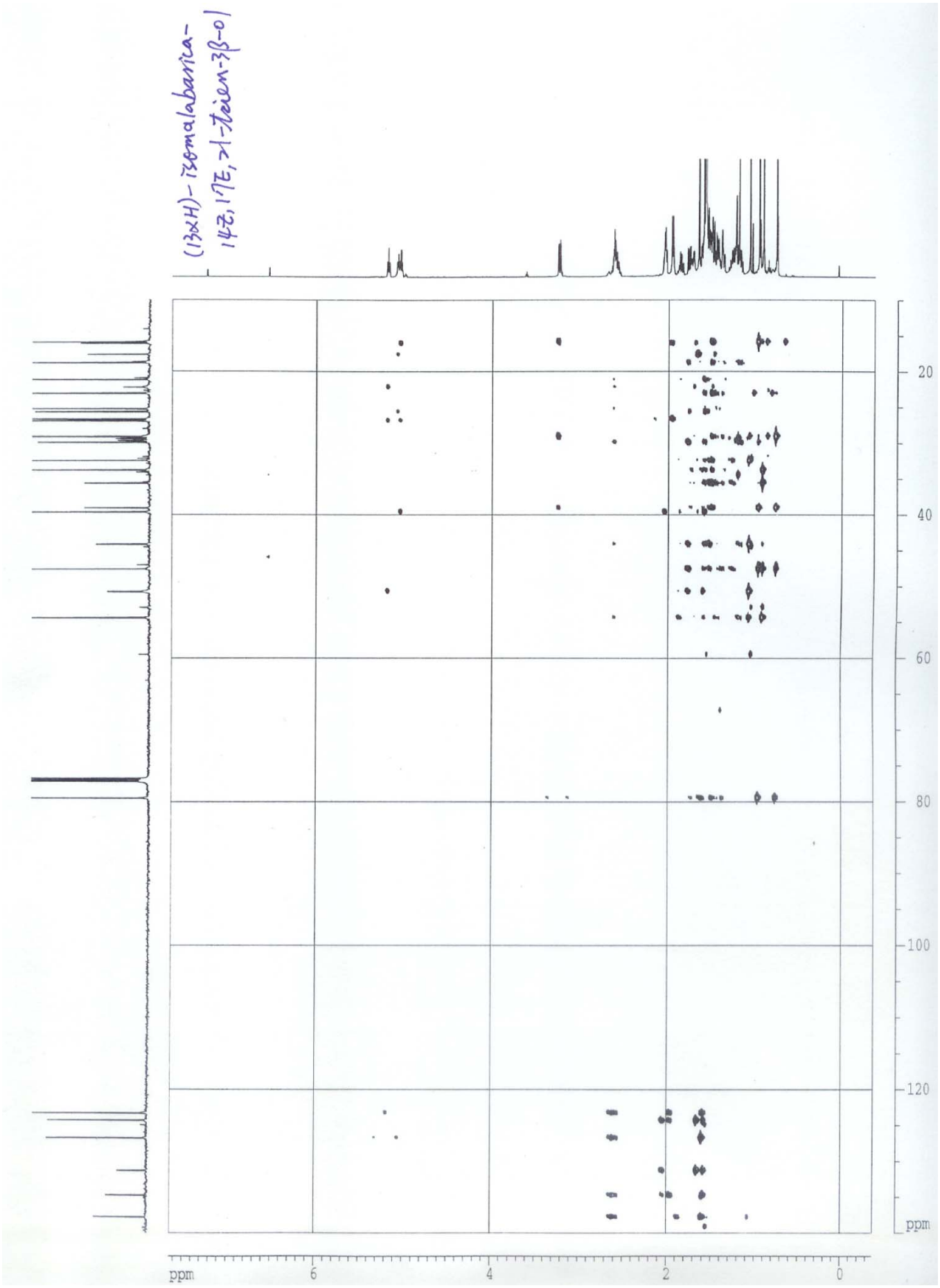

^{1}H-^{1}H COSY of (13α*H*)-isomalabarica-14*Z*,17*E*,21-trien-3β-ol

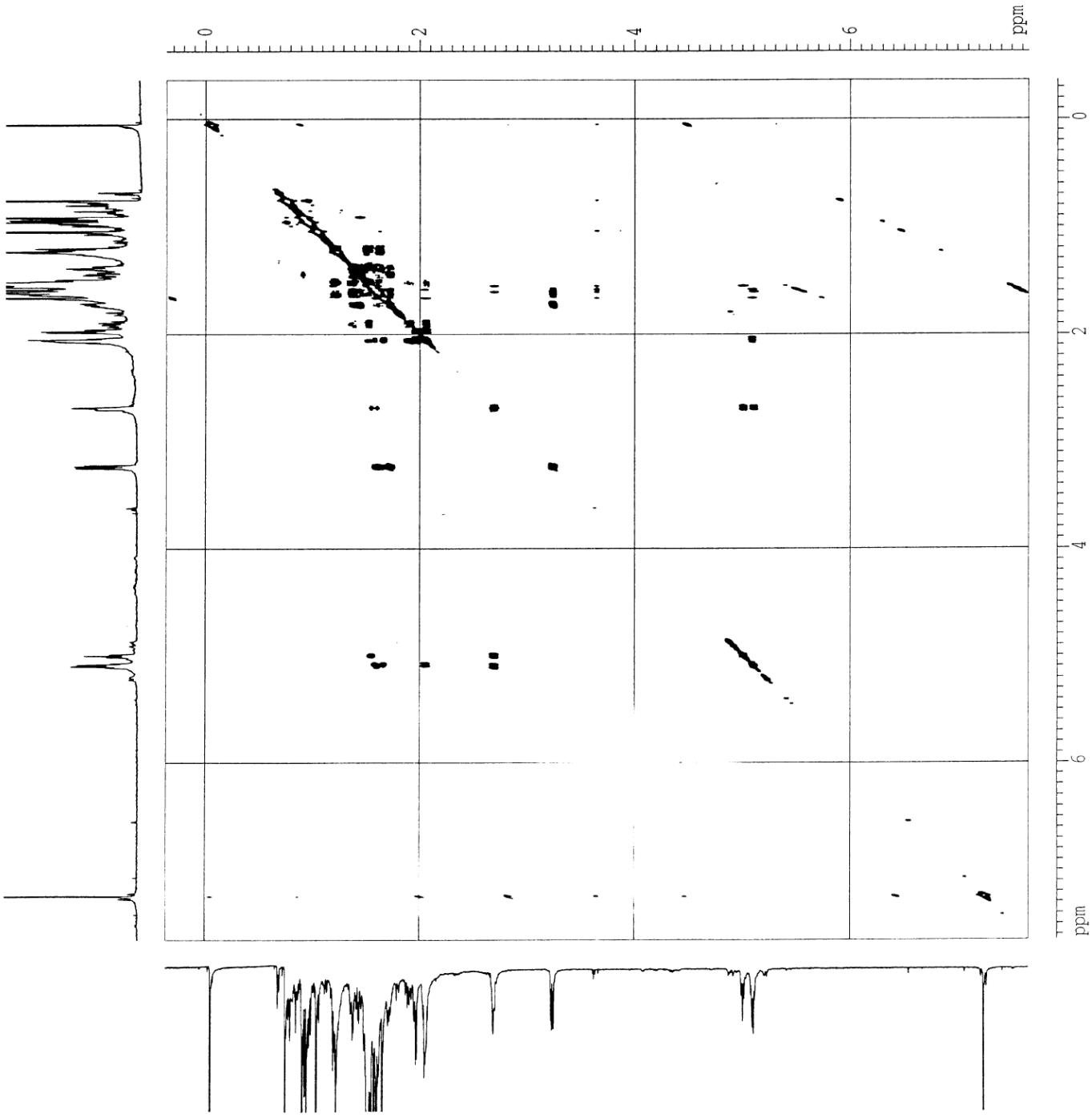

Appendix 4

^{1}H NMR of (13α*H*)-isomalabarica-14*E*,17*E*,21-trien-3β-ol

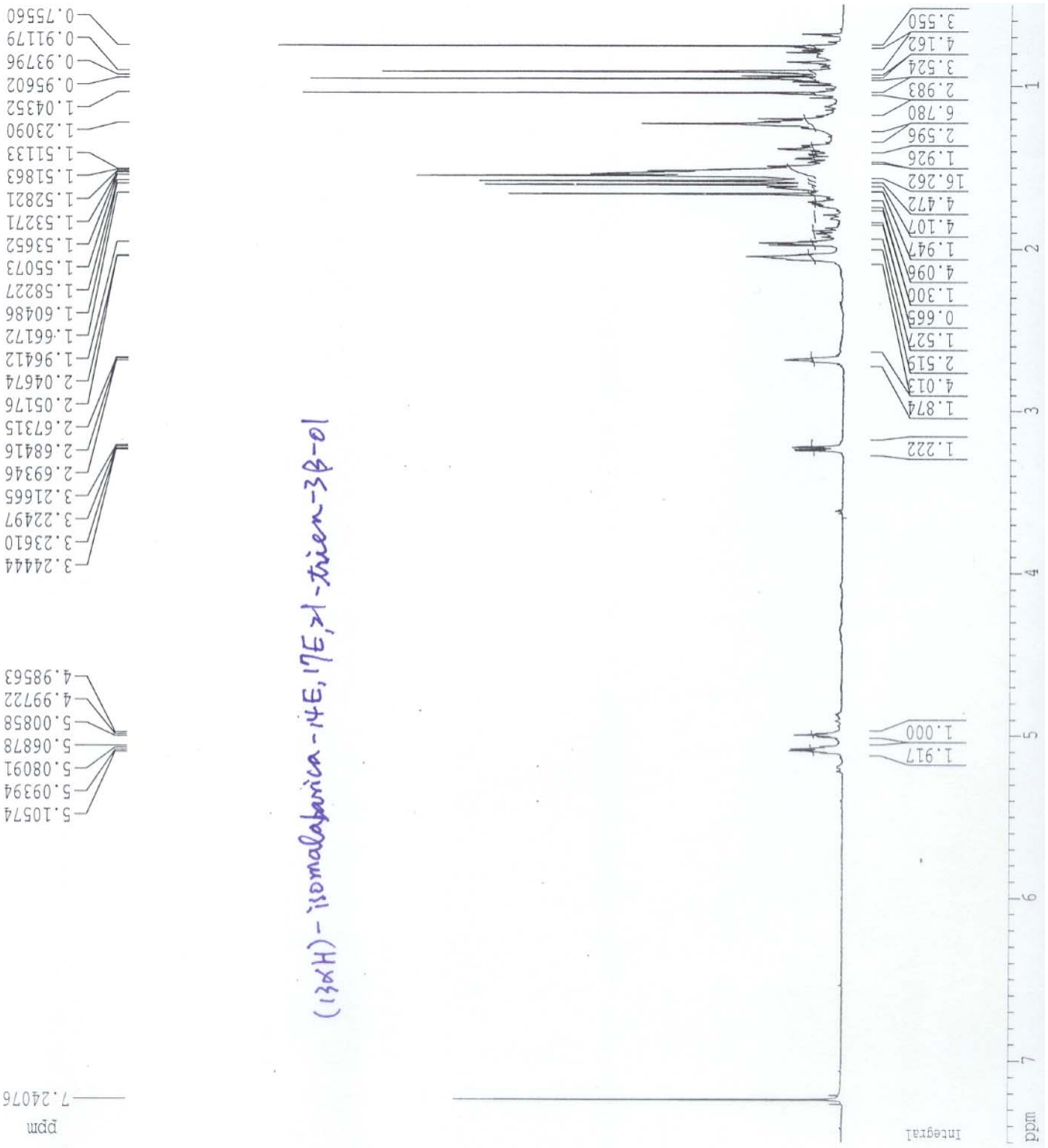

^{13}C NMR of (13α*H*)-isomalabarica-14*E*,17*E*,21-trien-3β-ol

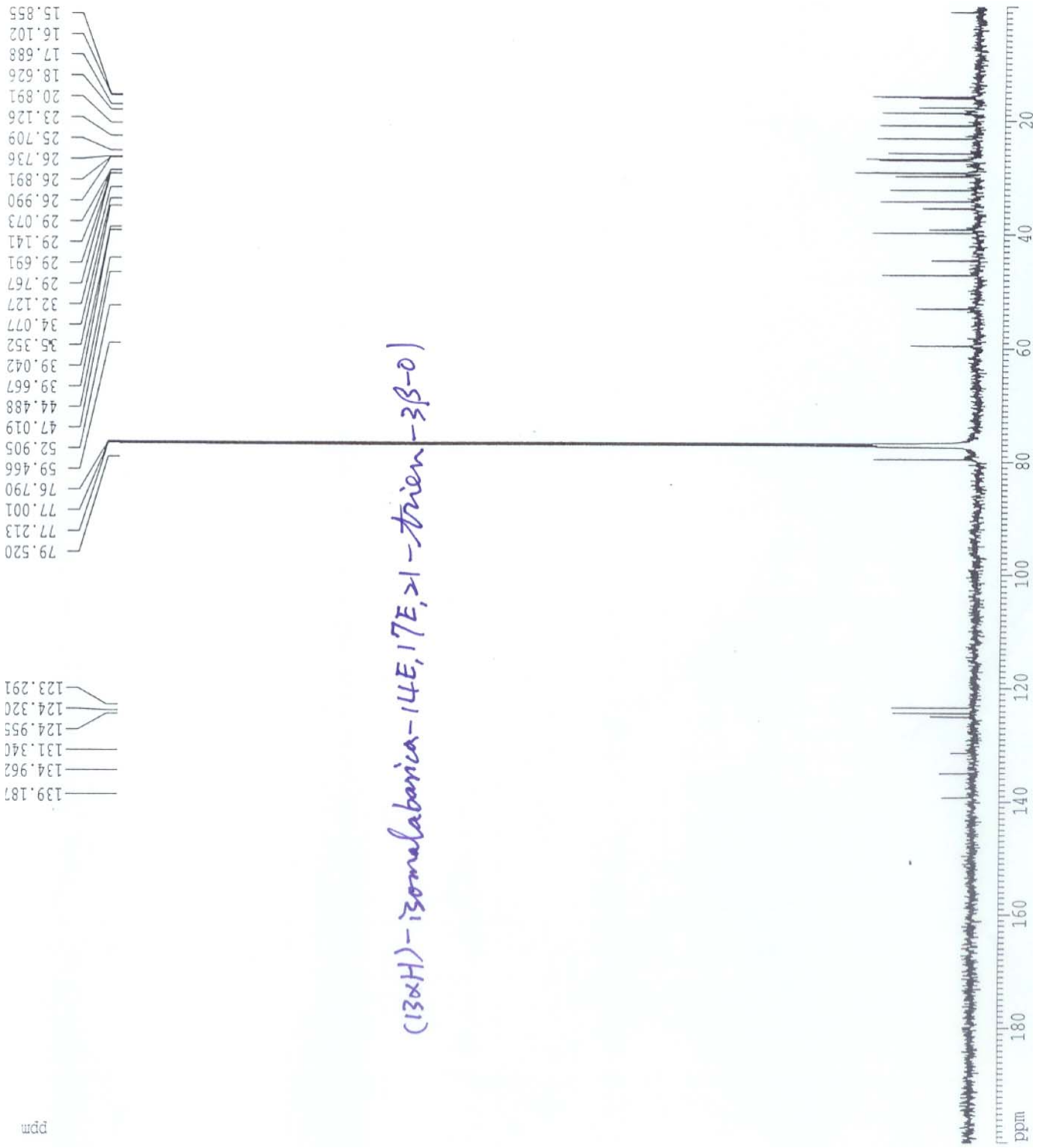

DEPT of (13α*H*)-isomalabarica-14*E*,17*E*,21-trien-3β-ol

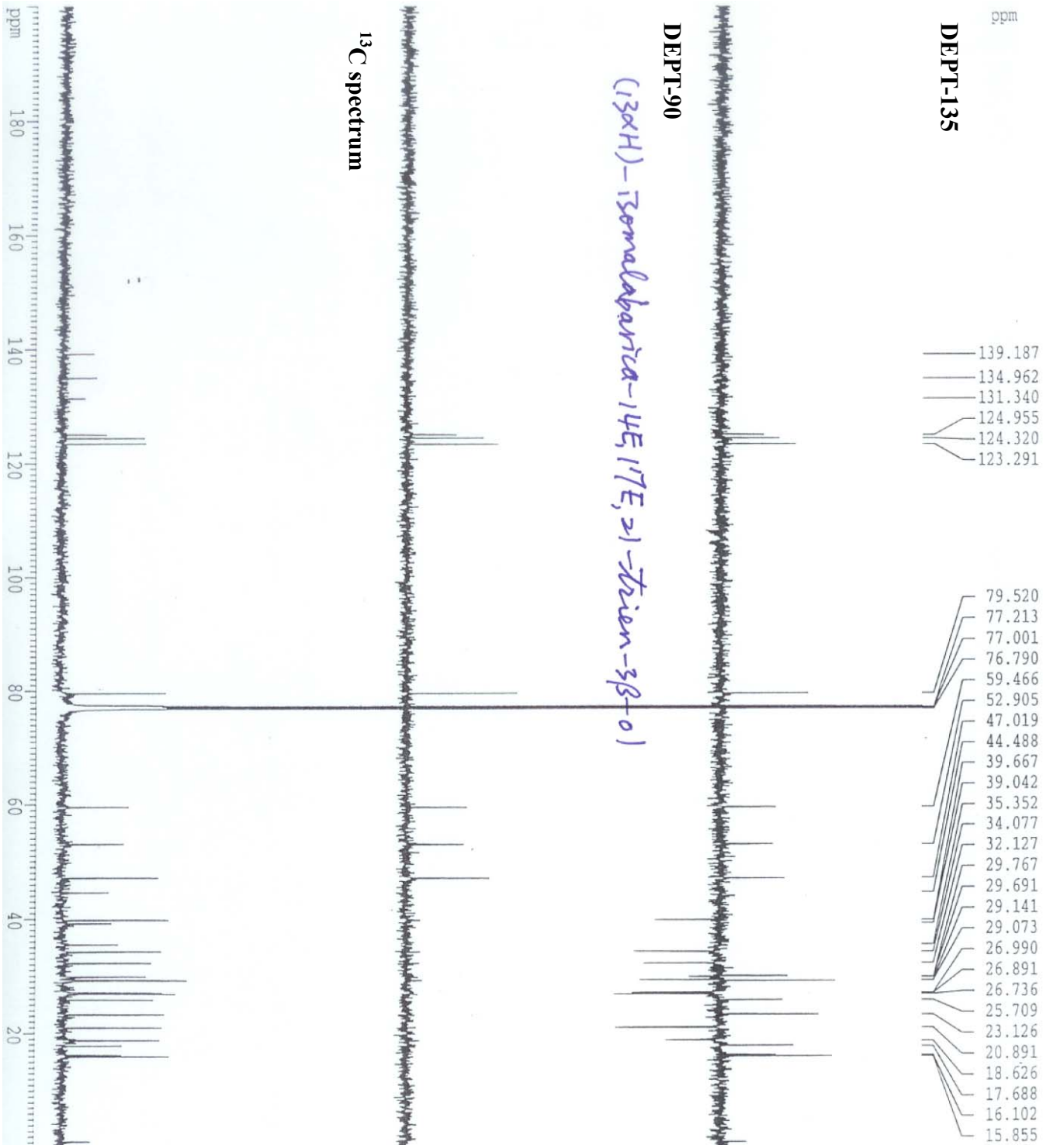

HMQC of (13α*H*)-isomalabarica-14*E*,17*E*,21-trien-3β-ol

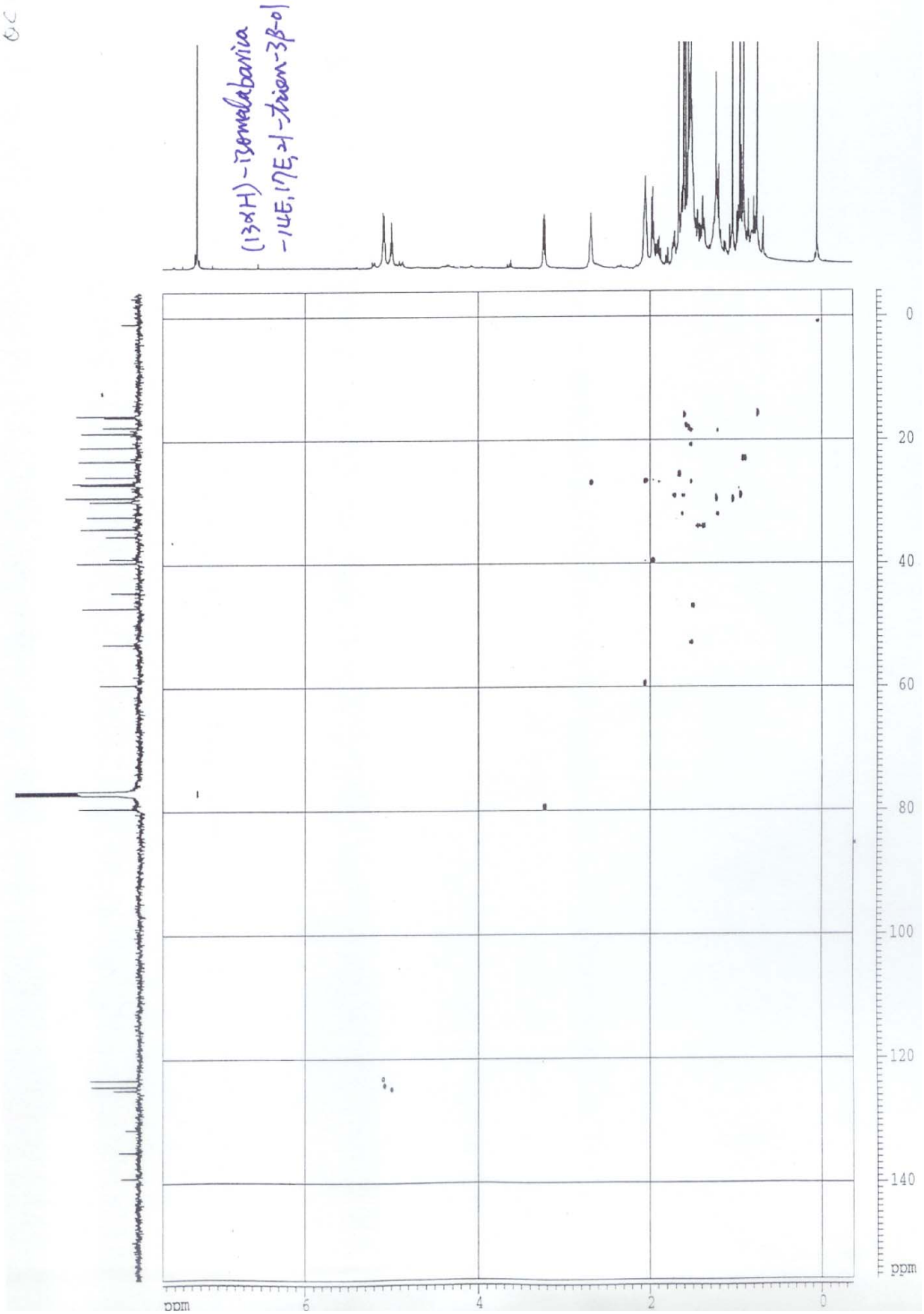

HMBC of (13α*H*)-isomalabarica-14*E*,17*E*,21-trien-3β-ol

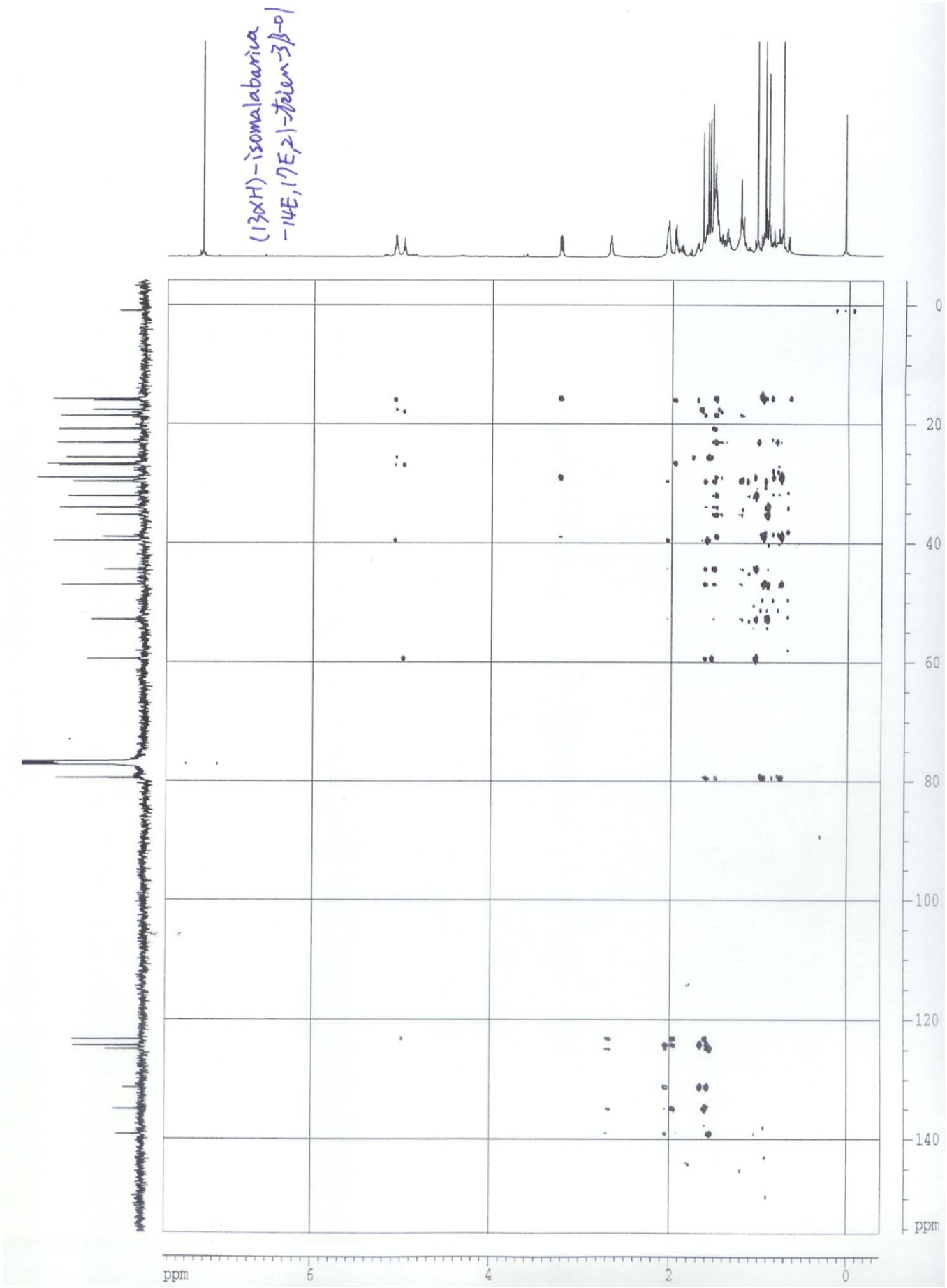

^{1}H-^{1}H COSY of (13α*H*)-isomalabarica-14*E*,17*E*,21-trien-3β-ol